Molecular beam epitaxy and optical performance in group IV and group III-V semiconductors for photonic applications

Ph.D. Dissertation Defense

Rigo Alberto Carrasco

Co-advisors: Dr. Preston Webster and Dr. Stefan Zollner

Department of Physics
New Mexico State University
November 5, 2021

Investments in space

- In 2020 and 2021 alone, 2823 satellites have been launched into space, that's 24% of the 11858 satellites ever launched since 1957

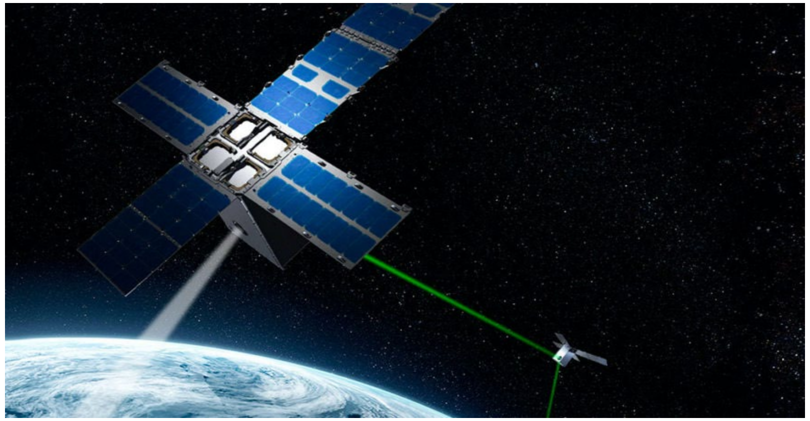

Optical inter-satellite links concept
Spacenews June 8 2020

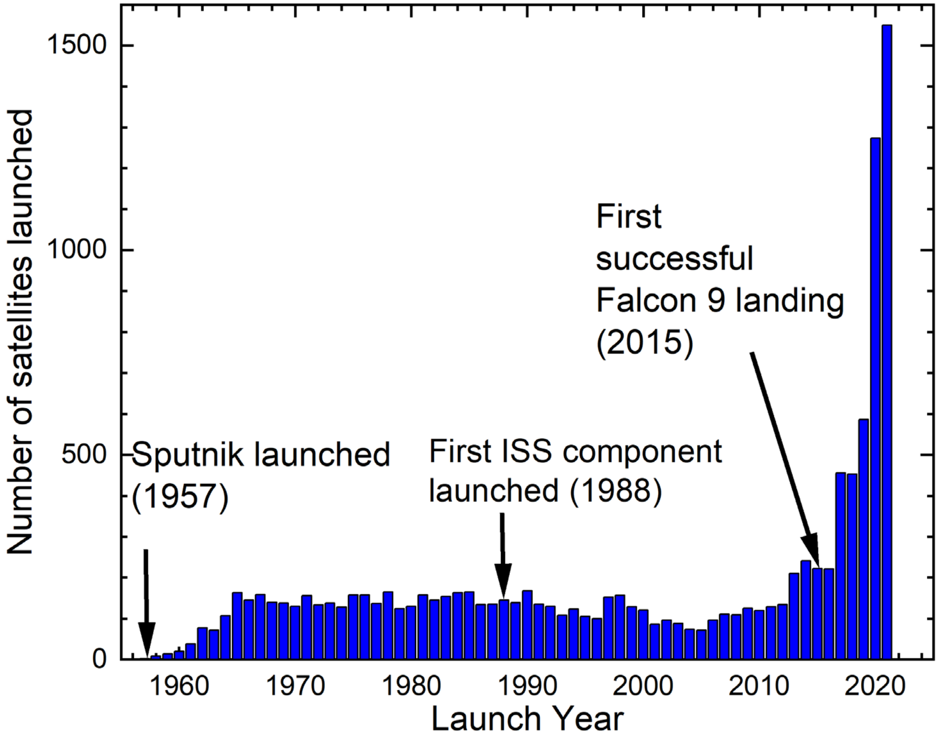

Data from Unoosa.org

Investments in space

- In 2020 and 2021 alone, 2823 satellites have been launched into space, that’s 24% of the 11858 satellites ever launched since 1957
- Declining launch and technology costs → LEO satellite mega constellation
  - **Missile warning**, satellite-satellite communication, real-time warfighter communication

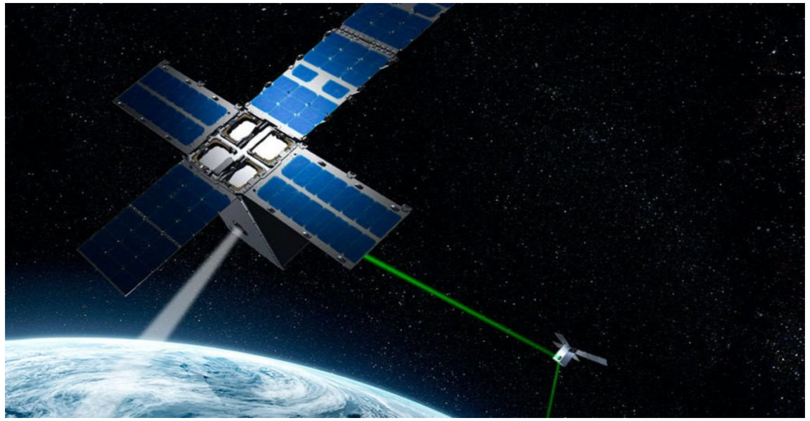

Optical inter-satellite links concept
Spacenews June 8 2020

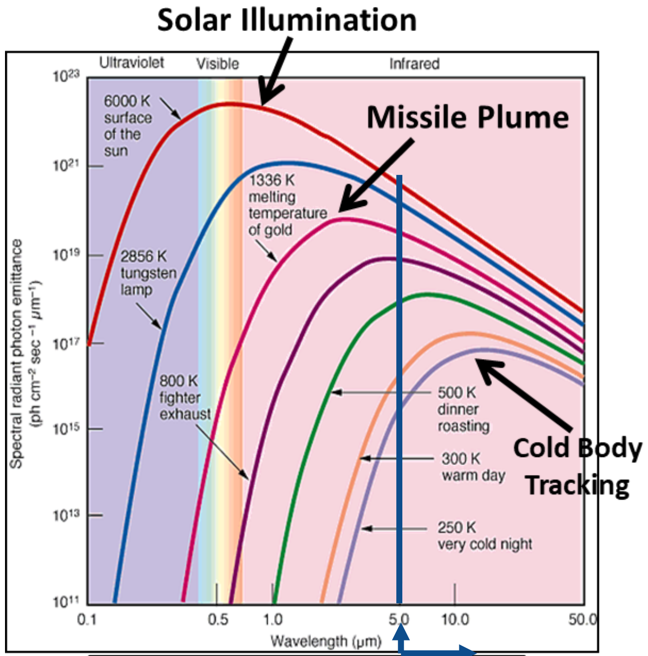

Diverse Spectral Signatures

Investments in space

- In 2020 and 2021 alone, 2823 satellites have been launched into space, that’s 24% of the 11858 satellites ever launched since 1957
- Declining launch and technology costs → LEO satellite mega constellation
  - ➢ **Missile warning**, satellite-satellite communication, real-time warfighter communication
- Mid-wave infrared sensor technology is a long-standing need for missile warning

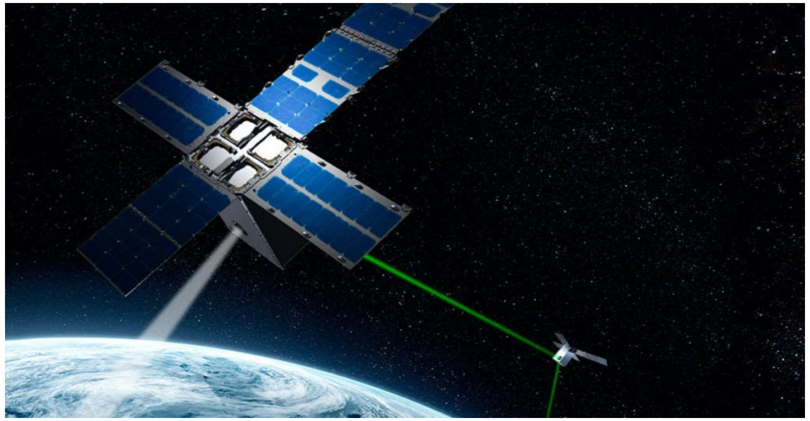

Optical inter-satellite links concept
Spacenews June 8 2020

Solar Illumination

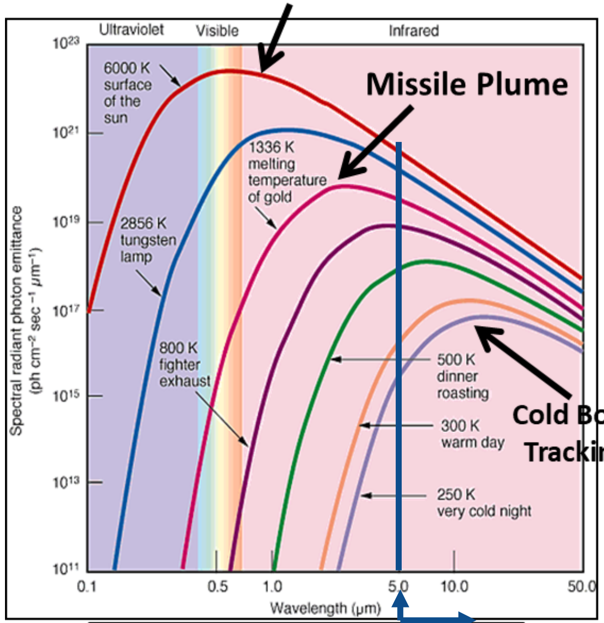

Missile Plume

Cold Body Tracking

Diverse Spectral Signatures

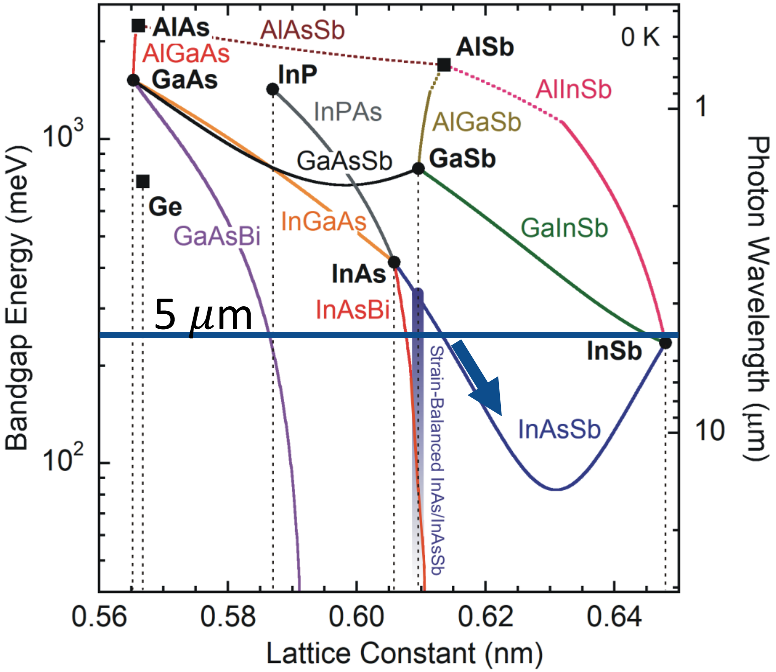

Investments in space

- In 2020 and 2021 alone, 2823 satellites have been launched into space, that's 24% of the 11858 satellites ever launched since 1957
- Declining launch and technology costs → LEO satellite mega constellation
  - **Missile warning**, satellite-satellite communication, real-time warfighter communication
- Mid-wave infrared sensor technology is a long-standing need for missile warning
- **Low-cost, high yield material solutions needed to satisfy satellite-based sensing**

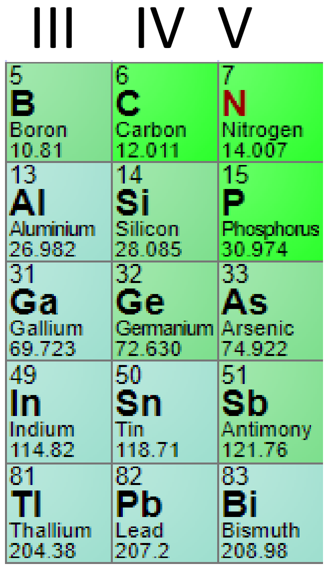

III	IV	V
5 **B** Boron 10.81	6 **C** Carbon 12.011	7 **N** Nitrogen 14.007
13 **Al** Aluminium 26.982	14 **Si** Silicon 28.085	15 **P** Phosphorus 30.974
31 **Ga** Gallium 69.723	32 **Ge** Germanium 72.630	33 **As** Arsenic 74.922
49 **In** Indium 114.82	50 **Sn** Tin 118.71	51 **Sb** Antimony 121.76
81 **Tl** Thallium 204.38	82 **Pb** Lead 207.2	83 **Bi** Bismuth 208.98

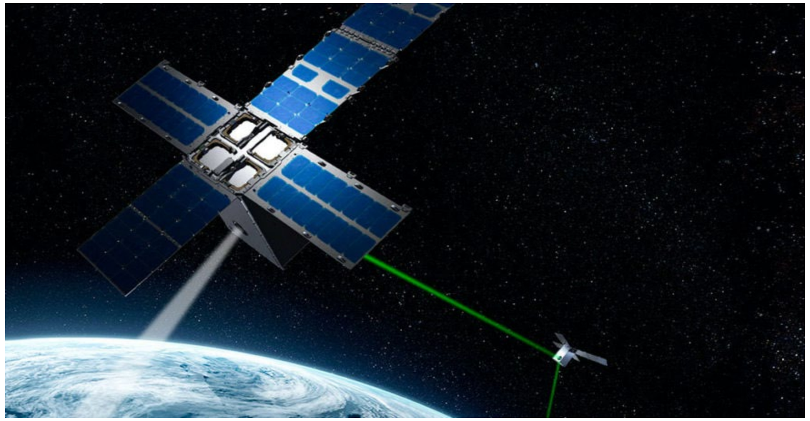

Optical inter-satellite links concept
Spacenews June 8 2020

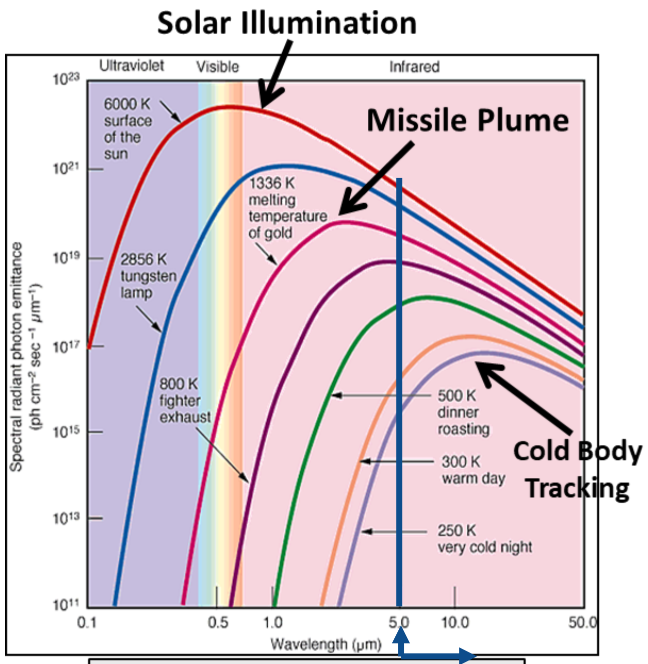

Diverse Spectral Signatures

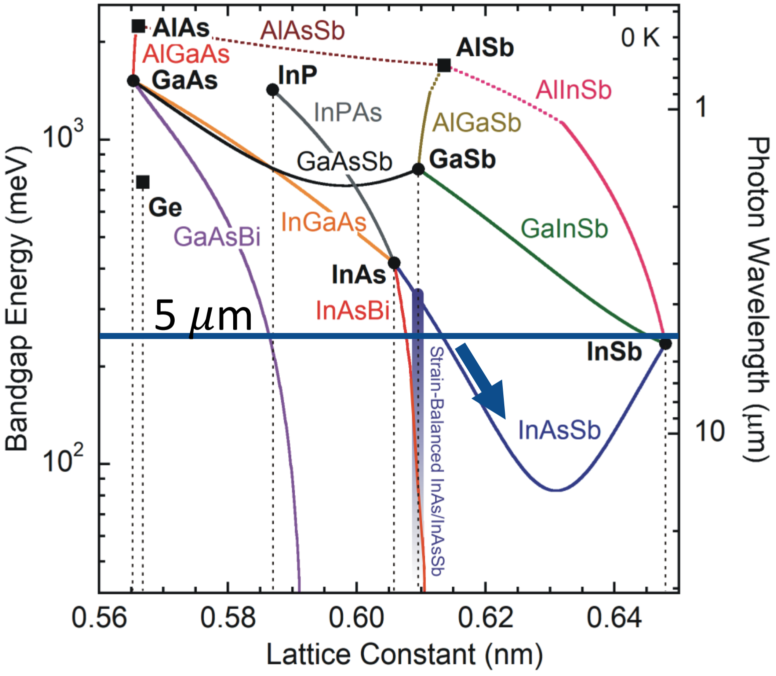

Low-cost, high yield material solutions needed to satisfy satellite-based sensing

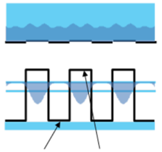

- **A III-V superlattice solution to mid-wave infrared sensing**
  - In(Ga)As/InAsSb superlattice for mid-wave detection
- **Sample growth and characterization methods**
  - Molecular beam epitaxy of superlattices
  - Steady-state photoluminescence and time-resolved photoluminescence for optical performance characterization
  - Dark-current and quantum efficiency for device performance
- **Results**
  - Recombination rate analysis and radiation hardness of InGaAs/InAsSb superlattices

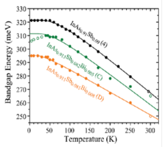

- **A bulk III-V solution to mid-wave infrared sensing**

- **A group IV solution to mid-wave sensing**

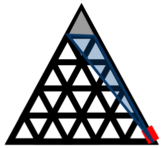

- **Beyond mid-wave materials and toward topological quantum materials**

A III-V superlattice solution

- Strain-balancing InAs/InAsSb type-II superlattices allows for bandgap engineering in a high optoelectronic quality material system
  - ➢ Strain-balancing leads to *asymmetric* layer thickness

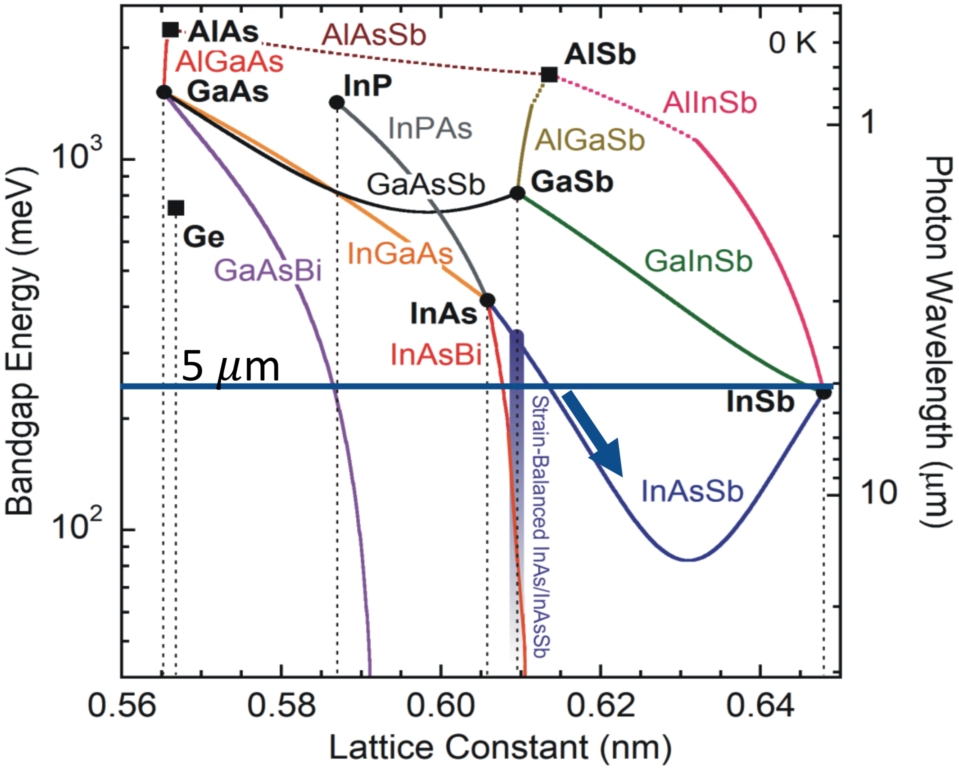

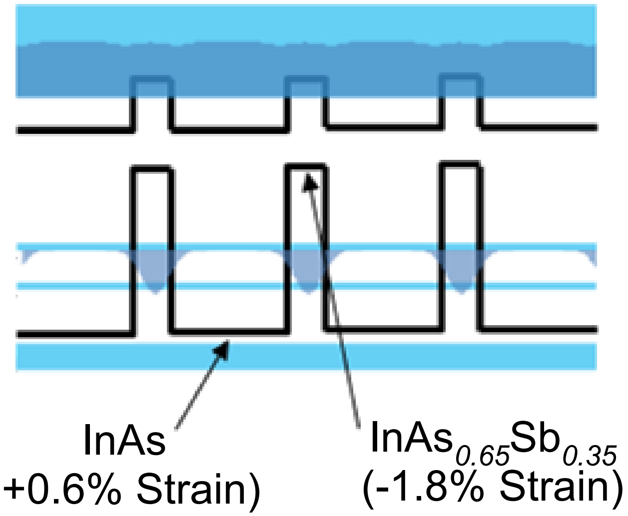

Compare thicknesses

InAs/InAsSb

$$d_{InAs} = 3\times d_{InAsSb}$$

A III-V superlattice solution

- Strain-balancing InAs/InAsSb type-II superlattices allows for bandgap engineering in a high optoelectronic quality material system
  - ➢ Strain-balancing leads to *asymmetric* layer thickness
- Incorporation of Ga in In(Ga)As/InAsSb type-II superlattices provides a new design parameter to optimize wavefunction overlap

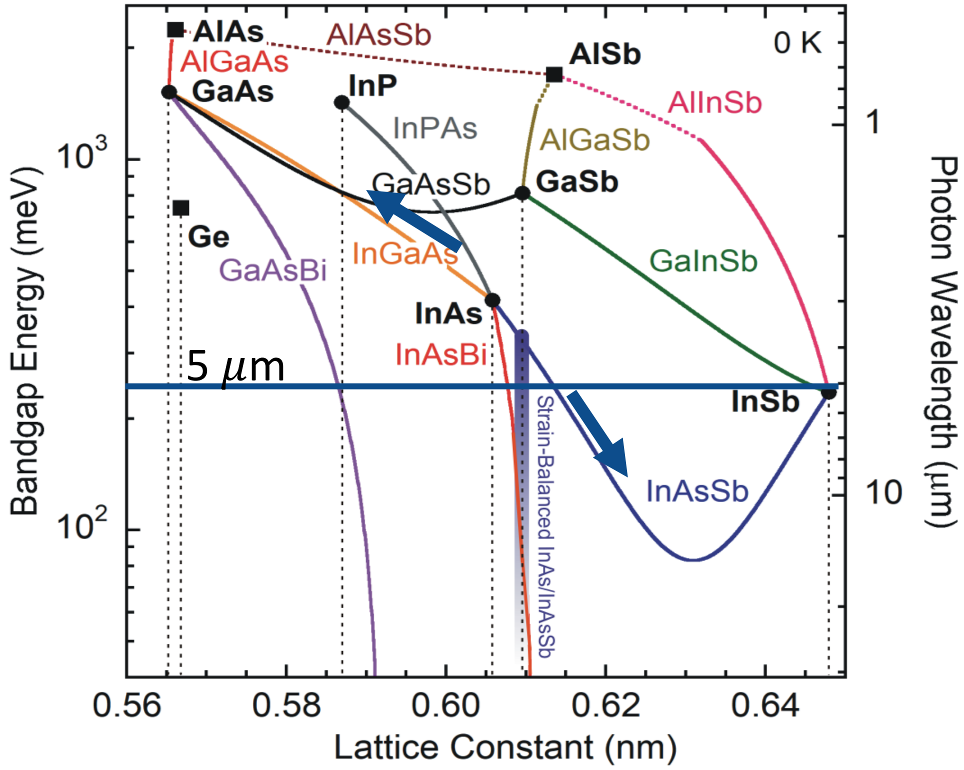

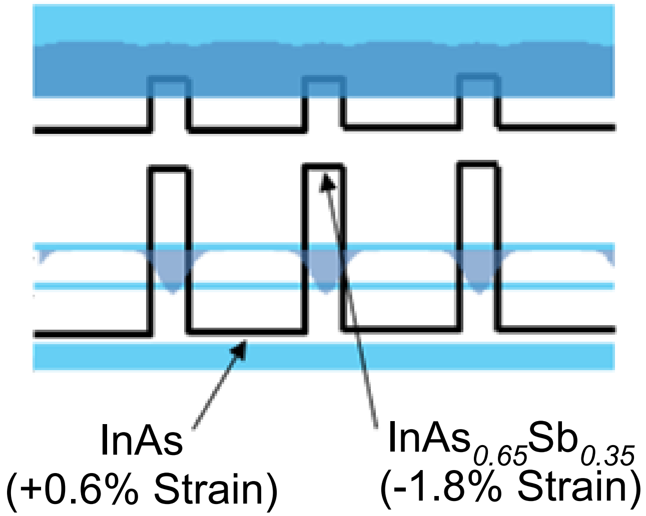

Compare thicknesses

InAs/InAsSb

$$d_{InAs} = 3 \times d_{InAsSb}$$

A III-V superlattice solution

- Strain-balancing InAs/InAsSb type-II superlattices allows for bandgap engineering in a high optoelectronic quality material system
  - ➢ Strain-balancing leads to *asymmetric* layer thickness
- Incorporation of Ga in In(Ga)As/InAsSb type-II superlattices provides a new design parameter to optimize wavefunction overlap
  - ➢ Allows for *symmetric* layer thickness
  - ➢ How do you grow a superlattice?

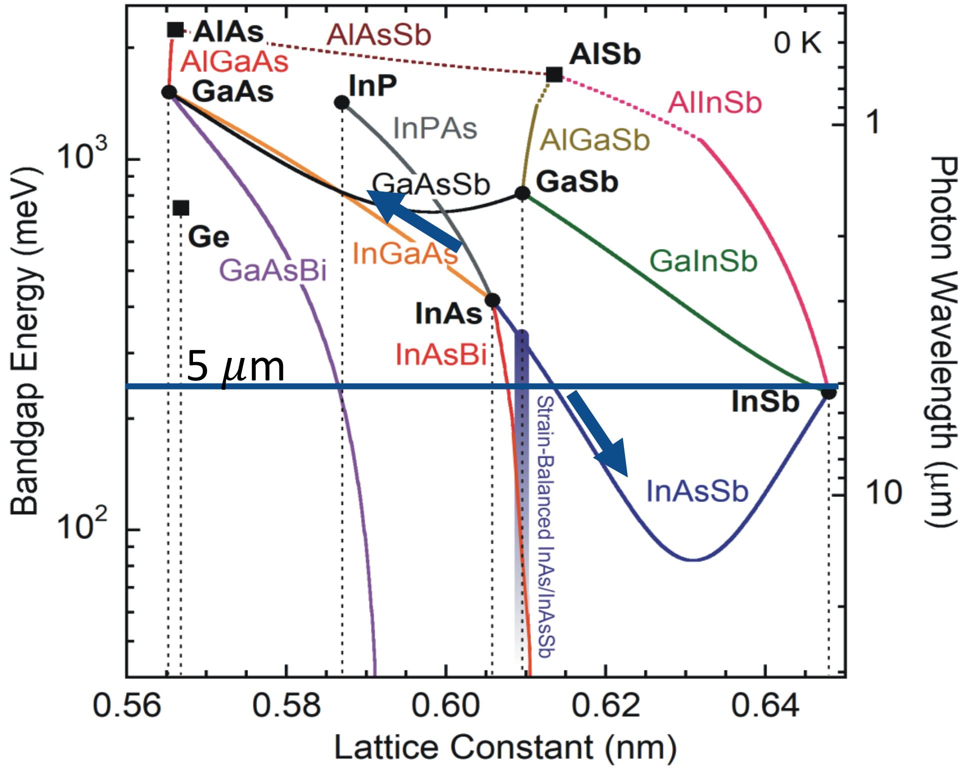

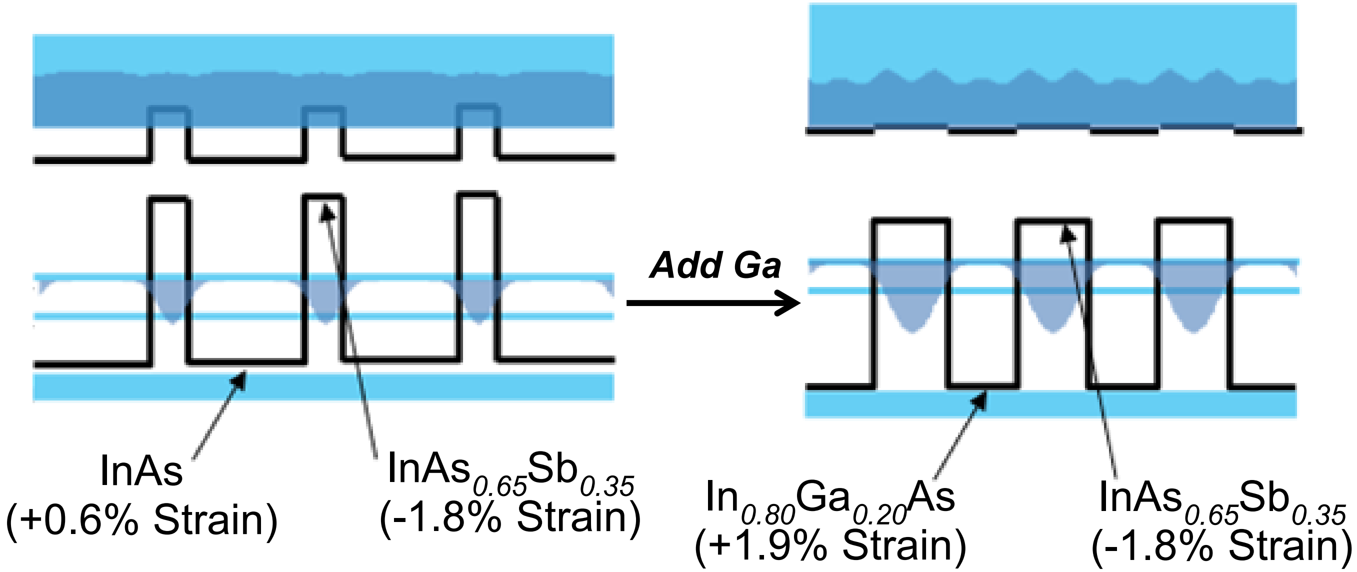

Compare thicknesses

InAs/InAsSb	**InGaAs/InAsSb**
$d_{InAs} = 3 \times d_{InAsSb}$	$d_{InGaAs} = 0.9 \times d_{InAsSb}$

Sample growth: molecular beam epitaxy (MBE)

- Ultra-high purity materials are heated to vapor phase to impinge substrate
  - Solid-source MBE
- Source shutters and valves allow for sub-nanometer tunability

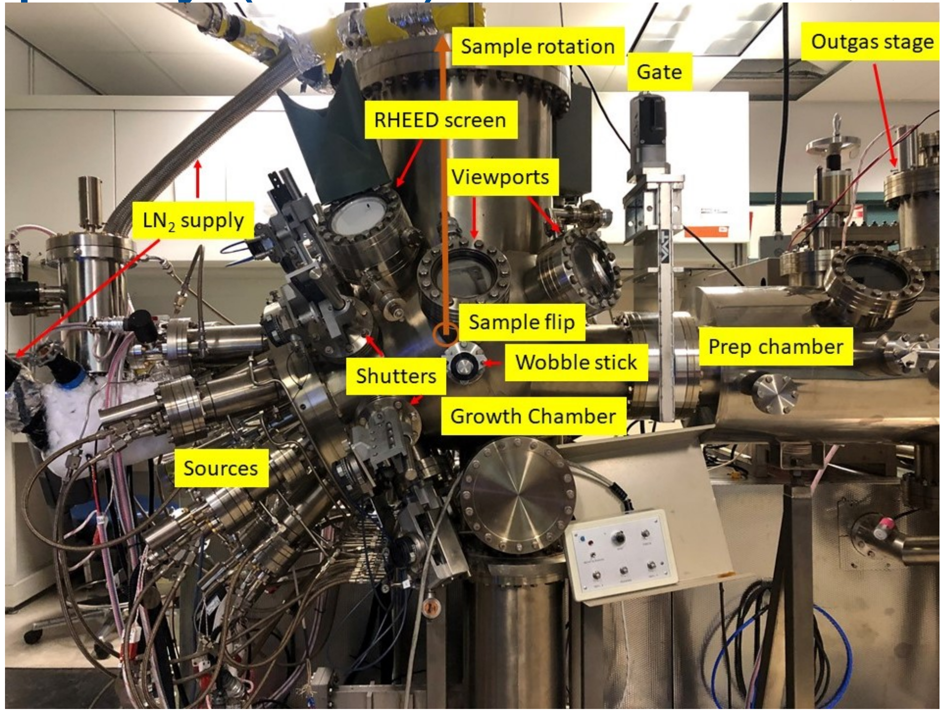

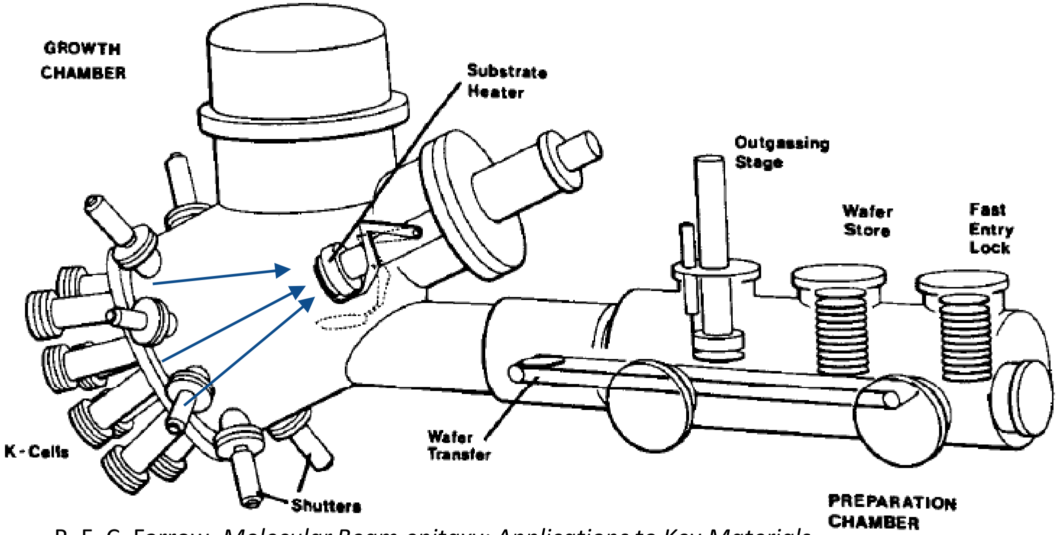

R. F. C. Farrow, *Molecular Beam epitaxy: Applications to Key Materials*

Sample growth: molecular beam epitaxy (MBE)

- Ultra-high purity materials are heated to vapor phase to impinge substrate
  - ➢ Solid-source MBE
- Source shutters and valves allow for sub-nanometer tunability
  - ➢ Engineer superlattices, quantum wells

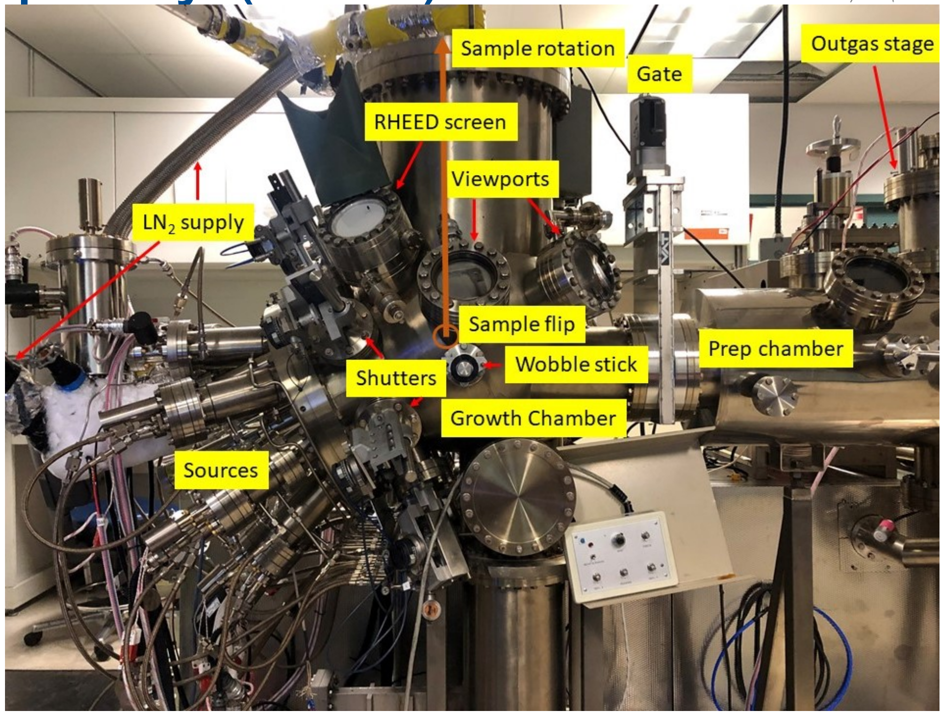

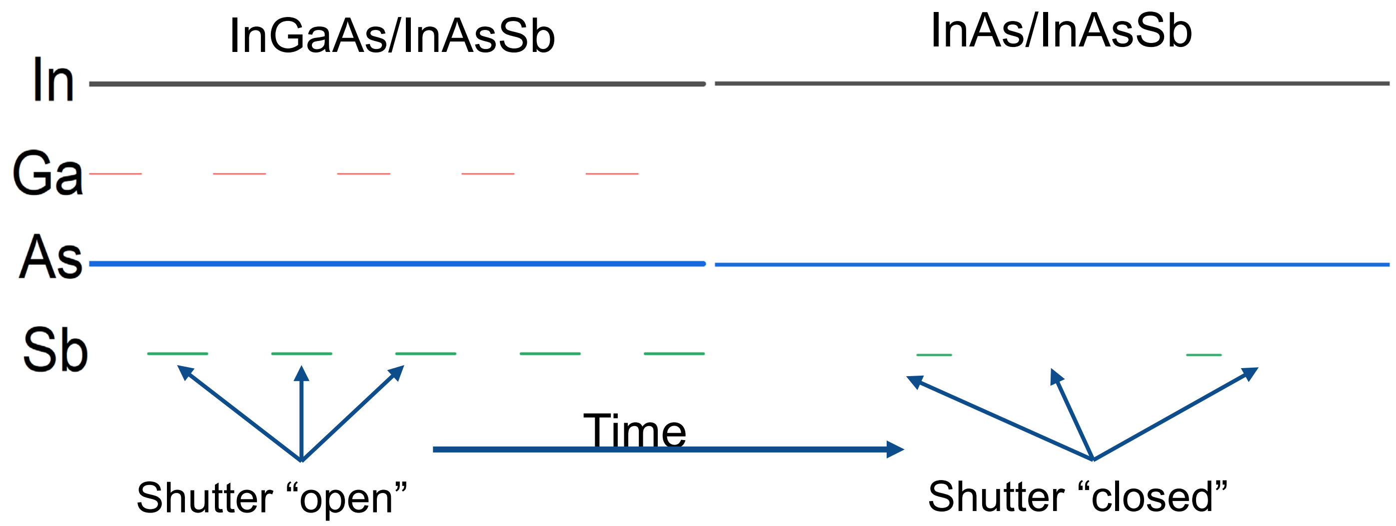

InGaAs/InAsSb

$$d_{InGaAs} = 0.9\times d_{InAsSb}$$

InAs/InAsSb

$$d_{InAs} = 3\times d_{InAsSb}$$

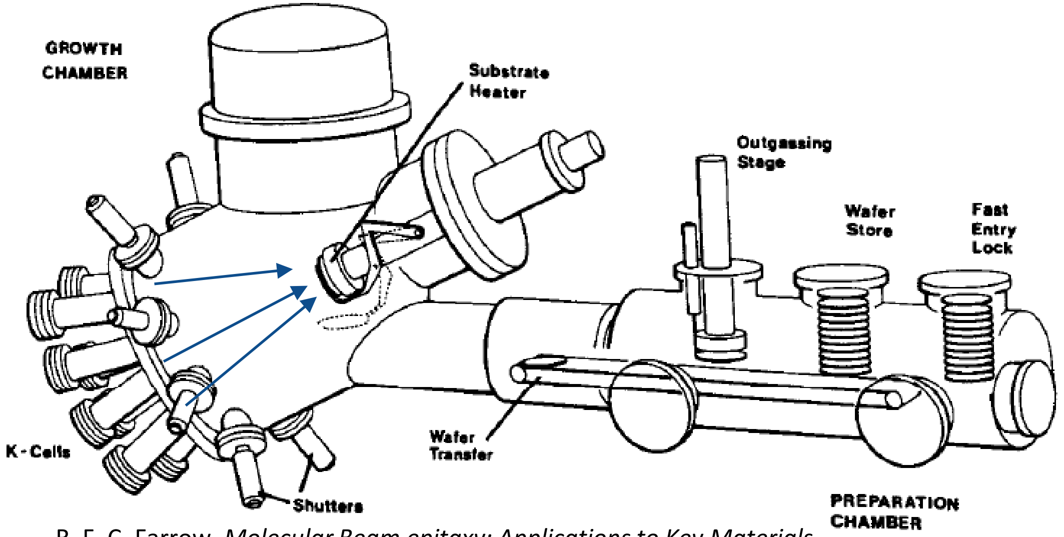

R. F. C. Farrow, *Molecular Beam epitaxy: Applications to Key Materials*

Sample growth: molecular beam epitaxy (MBE)

- Ultra-high purity materials are heated to vapor phase to impinge substrate
  - ➢ Solid-source MBE
- Source shutters and valves allow for sub-nanometer tunability
  - ➢ Engineer superlattices, quantum wells

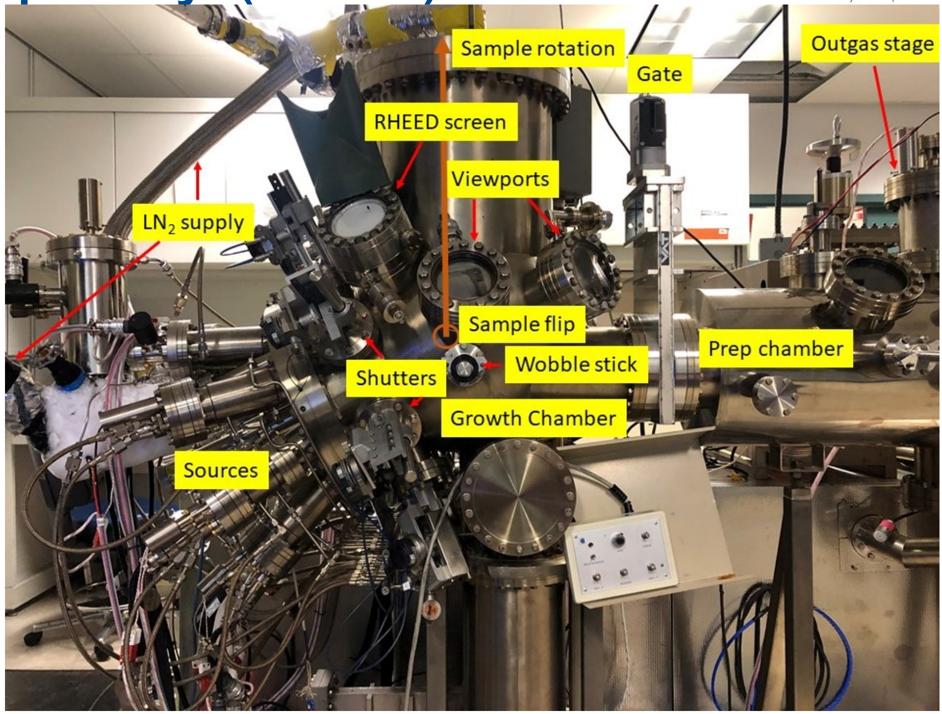

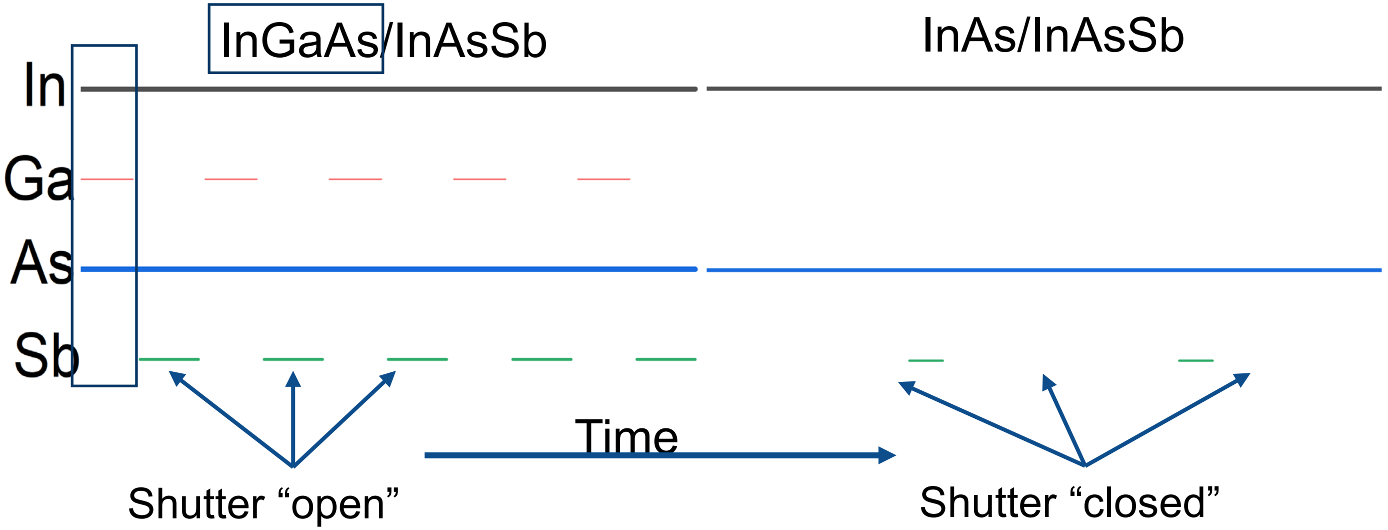

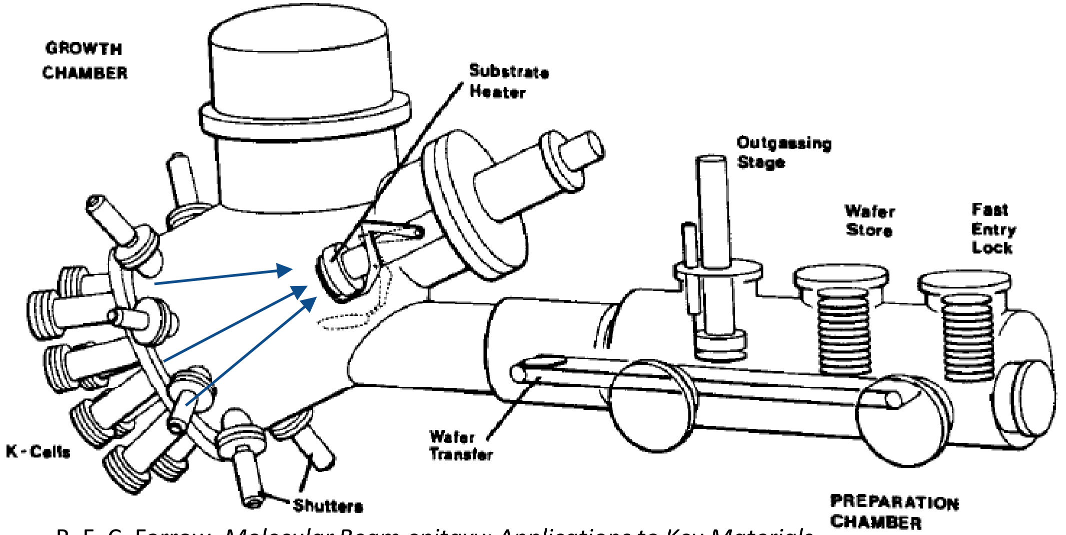

R. F. C. Farrow, *Molecular Beam epitaxy: Applications to Key Materials*

InGaAs/InAsSb

$$d_{InGaAs} = 0.9 \times d_{InAsSb}$$

InAs/InAsSb

$$d_{InAs} = 3 \times d_{InAsSb}$$

Sample growth: molecular beam epitaxy (MBE)

- Ultra-high purity materials are heated to vapor phase to impinge substrate
  - ➢ Solid-source MBE
- Source shutters and valves allow for sub-nanometer tunability
  - ➢ Engineer superlattices, quantum wells

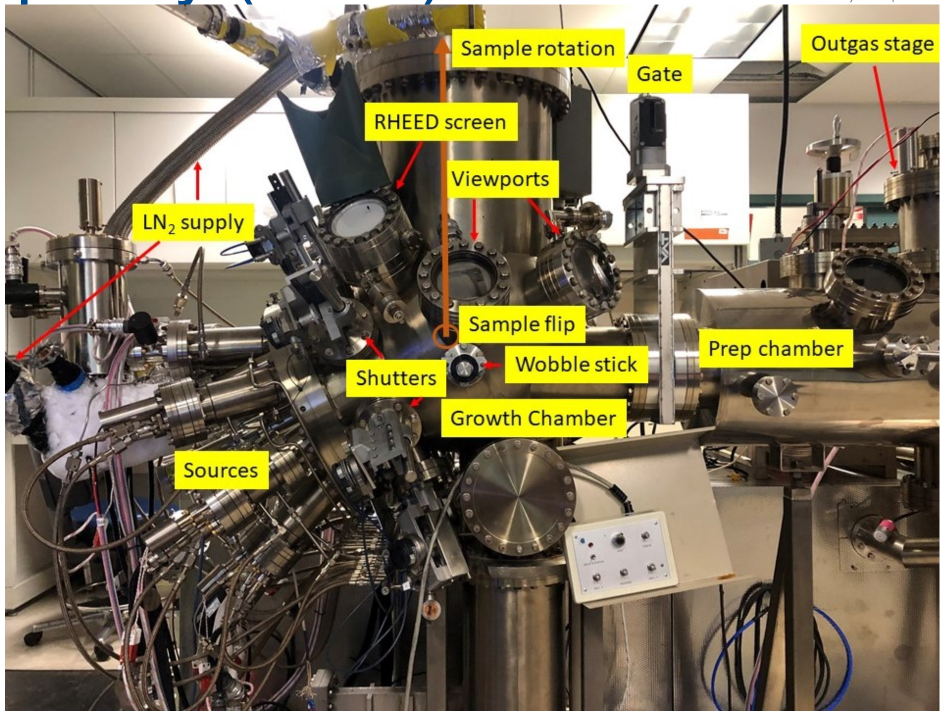

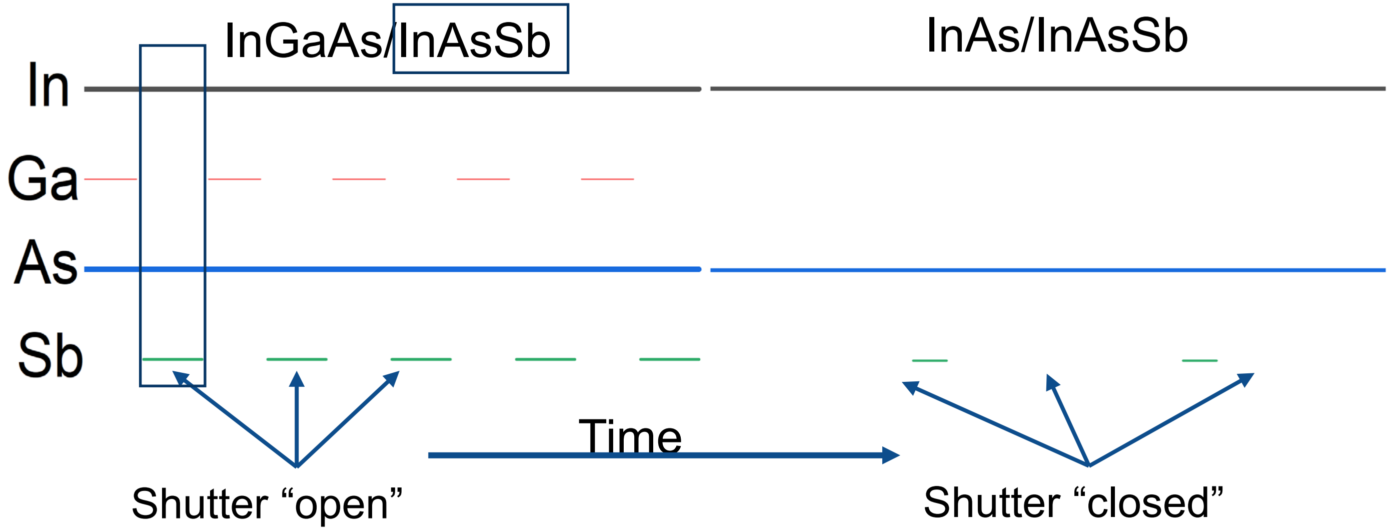

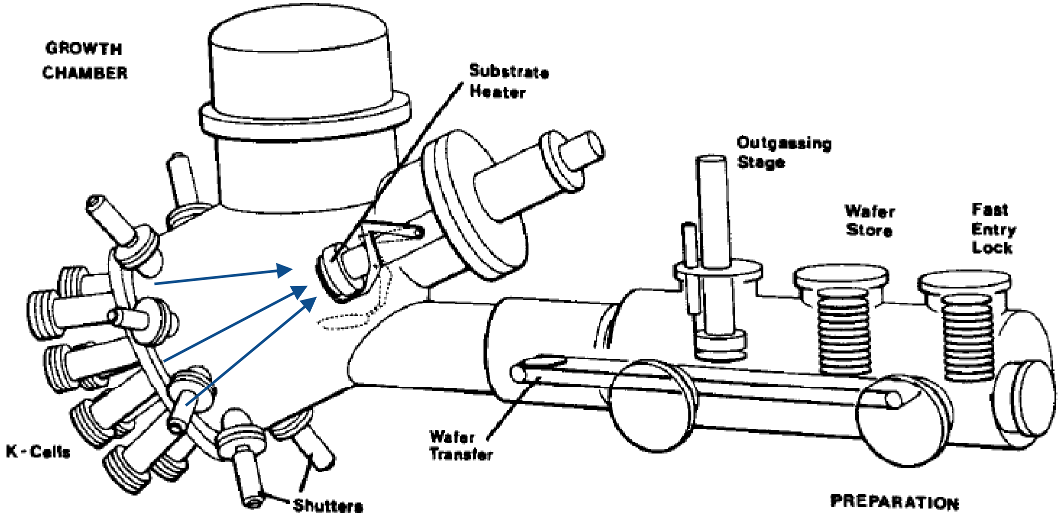

R. F. C. Farrow, *Molecular Beam epitaxy: Applications to Key Materials*

InGaAs/InAsSb

$d_{InGaAs} = 0.9\times d_{InAsSb}$

InAs/InAsSb

$d_{InAs} = 3\times d_{InAsSb}$

Sample growth: molecular beam epitaxy (MBE)

- Ultra-high purity materials are heated to vapor phase to impinge substrate
  - ➢ Solid-source MBE
- Source shutters and valves allow for sub-nanometer tunability
  - ➢ Engineer superlattices, quantum wells
- Chamber under ultra-high vacuum (UHV) conditions ($\leq 5 \times 10^{-10}\ torr$)
  - ➢ ~100x pressure in space ($1 \times 10^{-12}\ torr$)
  - ➢ $1\ atm = 760\ torr$
- After growth, optical characterization required

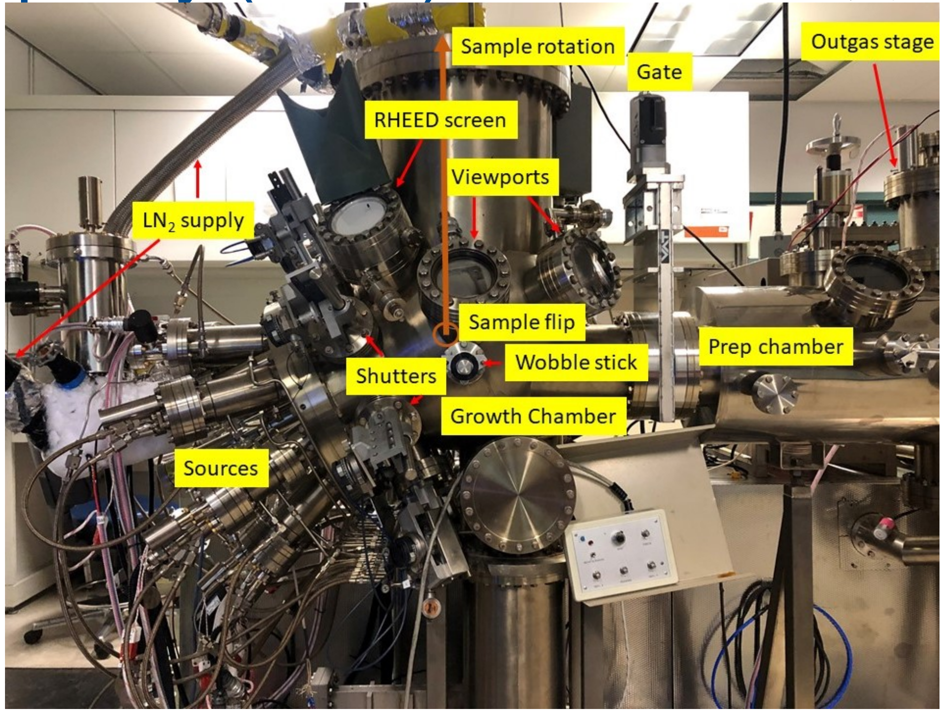

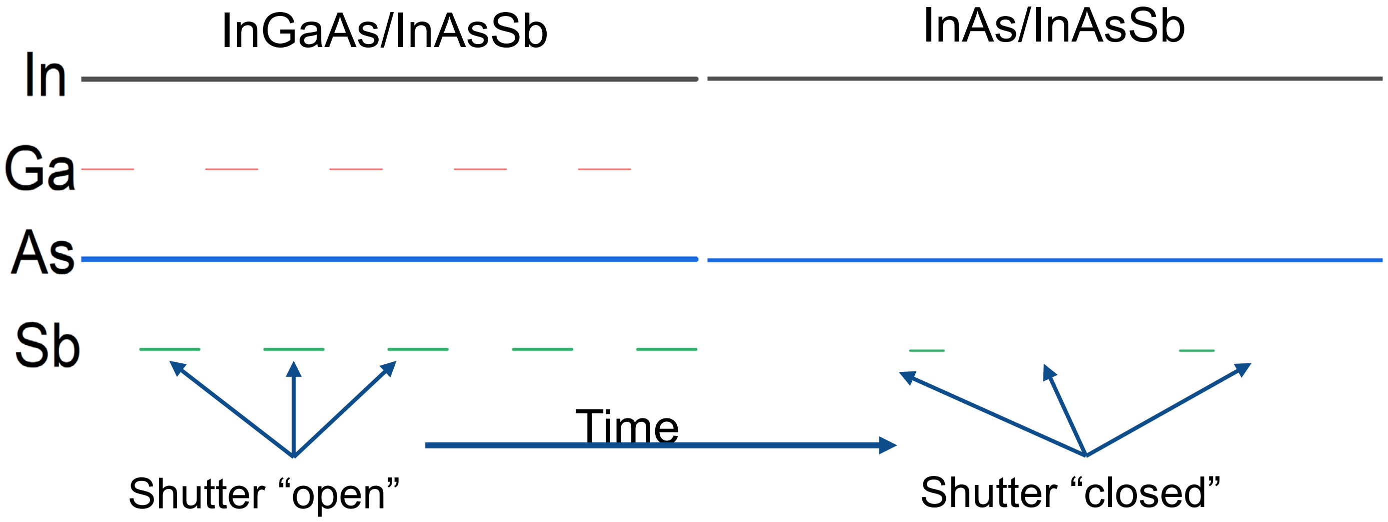
InGaAs/InAsSb

InAs/InAsSb

In

Ga

As

Sb

Time

Shutter "open"

Shutter "closed"

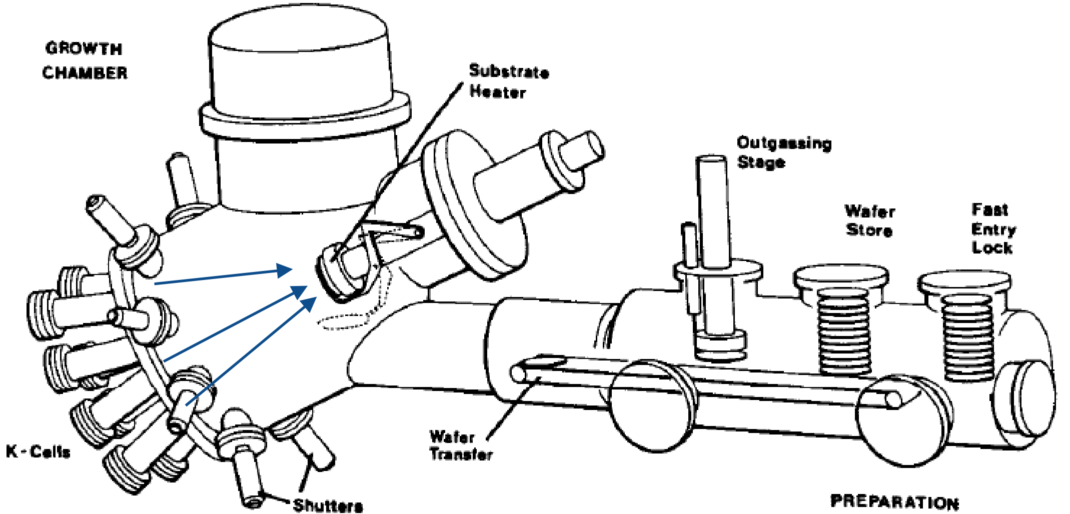

R. F. C. Farrow, *Molecular Beam epitaxy: Applications to Key Materials*

InGaAs/InAsSb

$d_{InGaAs} = 0.9 \times d_{InAsSb}$

InAs/InAsSb

$d_{InAs} = 3 \times d_{InAsSb}$

Characterization: steady-state photoluminescence

- Excite material with light $\left(h\nu_L > h\nu_g\right)$

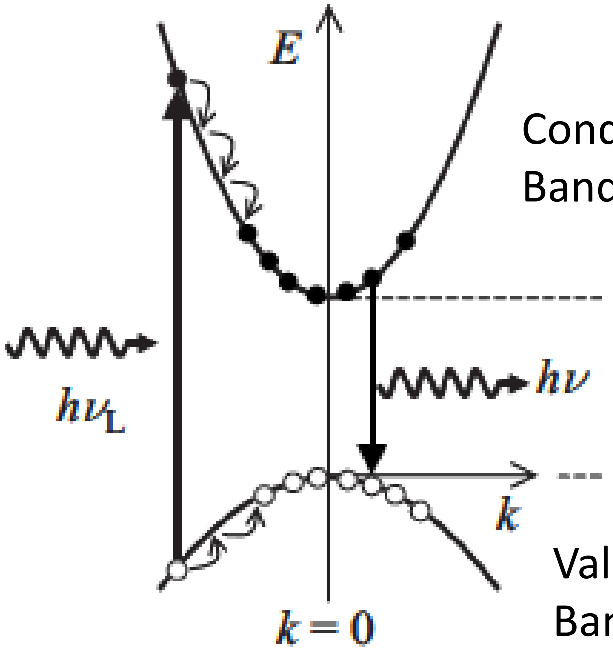

Conduction Band

Valence Band

M. Fox *Optical Properties of Solids*

Characterization: steady-state photoluminescence

- Excite material with light $(h\nu_L > h\nu_g)$
- Collect photoluminescence spectrum of excited sample $h\nu$
- Extract bandgap of spectrum by taking the first-derivative maximum of signal
- Perform as a function of temperature to determine temperature-dependent bandgap $E_g(T)$
- How long do we have photoluminescence?

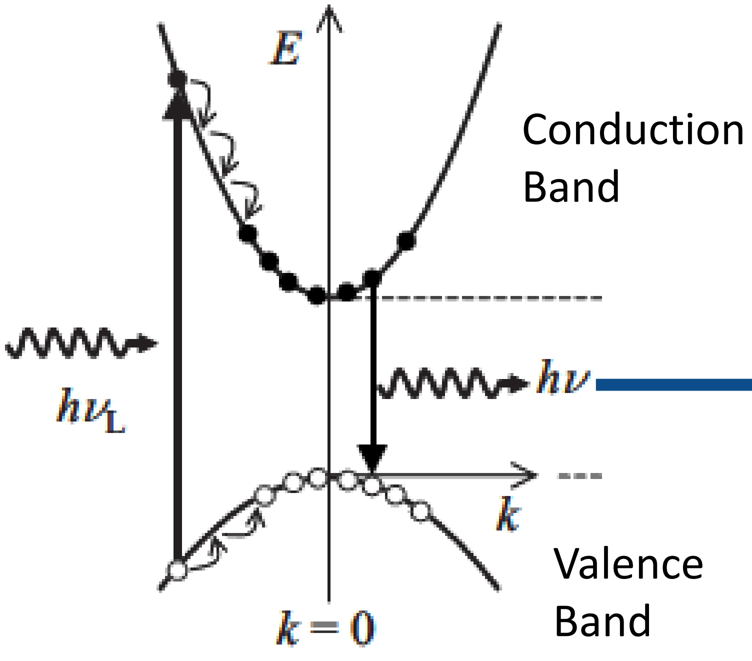

M. Fox *Optical Properties of Solids*

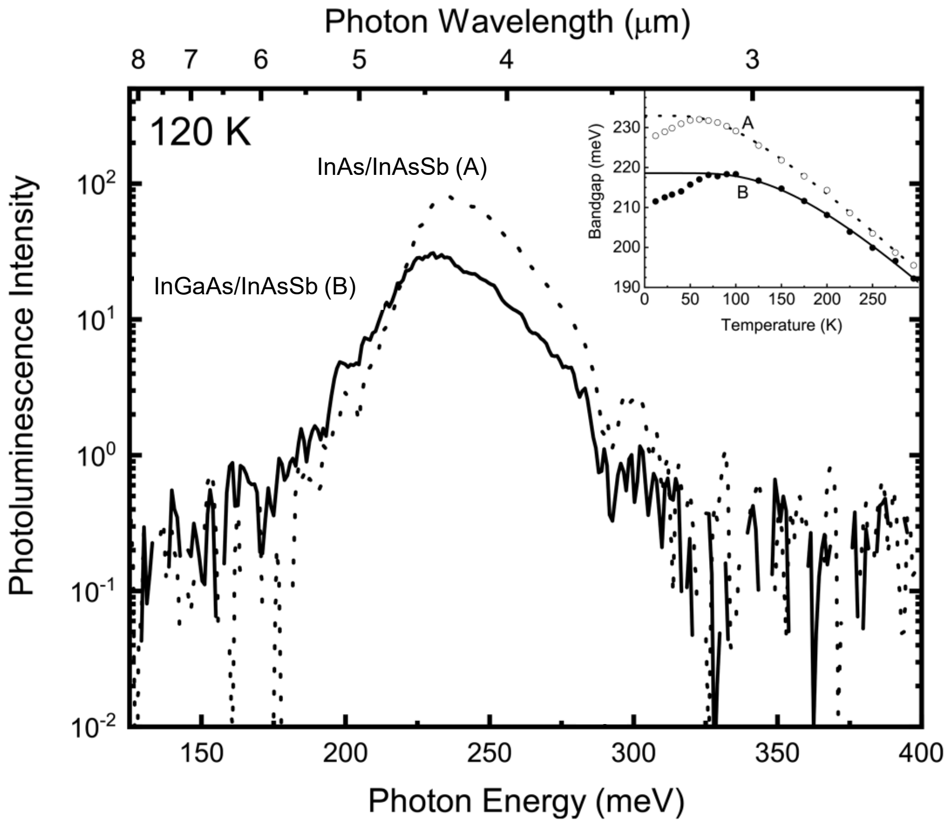

Time-resolved photoluminescence to measure lifetime

The minority carrier lifetime is a statistical measure of how long photogenerated carriers excited in a photodetector exist before returning to the ground state

The lifetime can be measured by time-resolved photoluminescence

$$\frac{1}{\tau_{\mathrm{total}}} = \frac{1}{\phi\tau_{\mathrm{rad}}} + \frac{1}{\tau_{\mathrm{SRH}}} + \frac{1}{\tau_{\mathrm{Auger}}}$$

The various recombination mechanisms have unique temperature dependences, allowing fundamental material parameters to be extracted from the recombination rate analysis

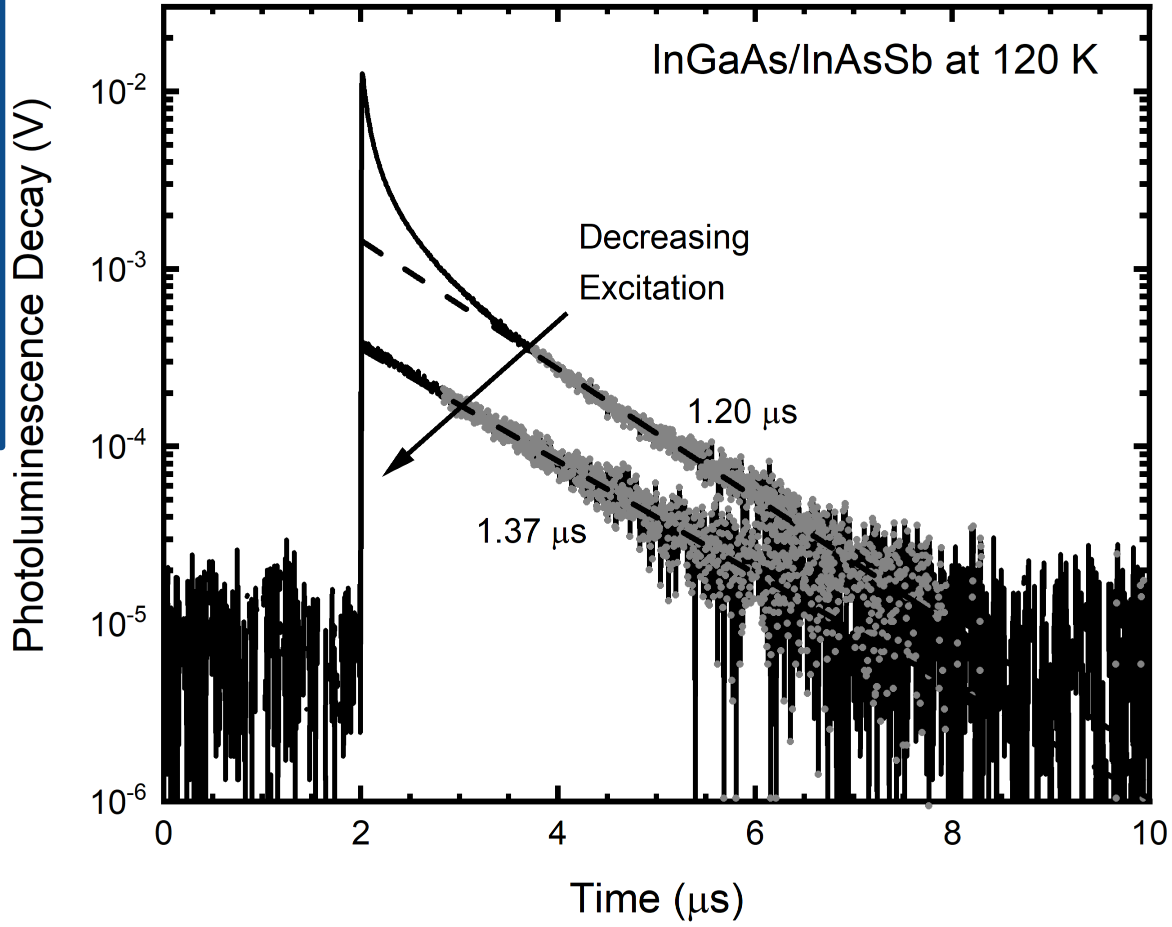

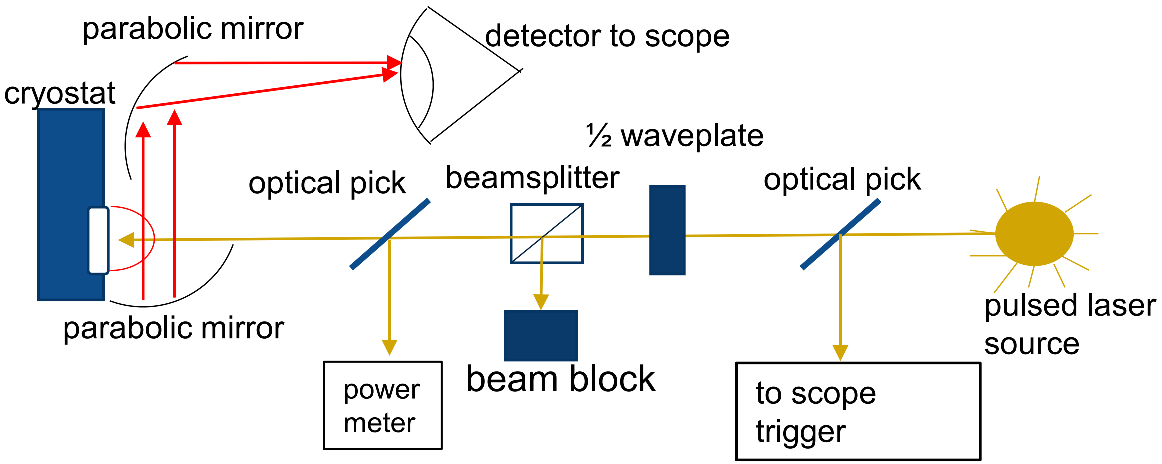

TRPL optical block diagram

Impact of adding Ga and dopants in InGaAs/InAsSb

Our InAs/InAsSb superlattice (open circles) is optimized for maximum wavefunction overlap at 5 µm wavelength

- Exhibits Shockley-Read-Hall limited lifetime of 2.3 µs
- Serves as our system's InAsSb quality benchmark

The InGaAs/InAsSb superlattice (filled circles) is similarly optimized for wavefunction overlap at 5 µm wavelength

- Lifetime is comparable at 1.4 µs, Shockley-Read-Hall limited

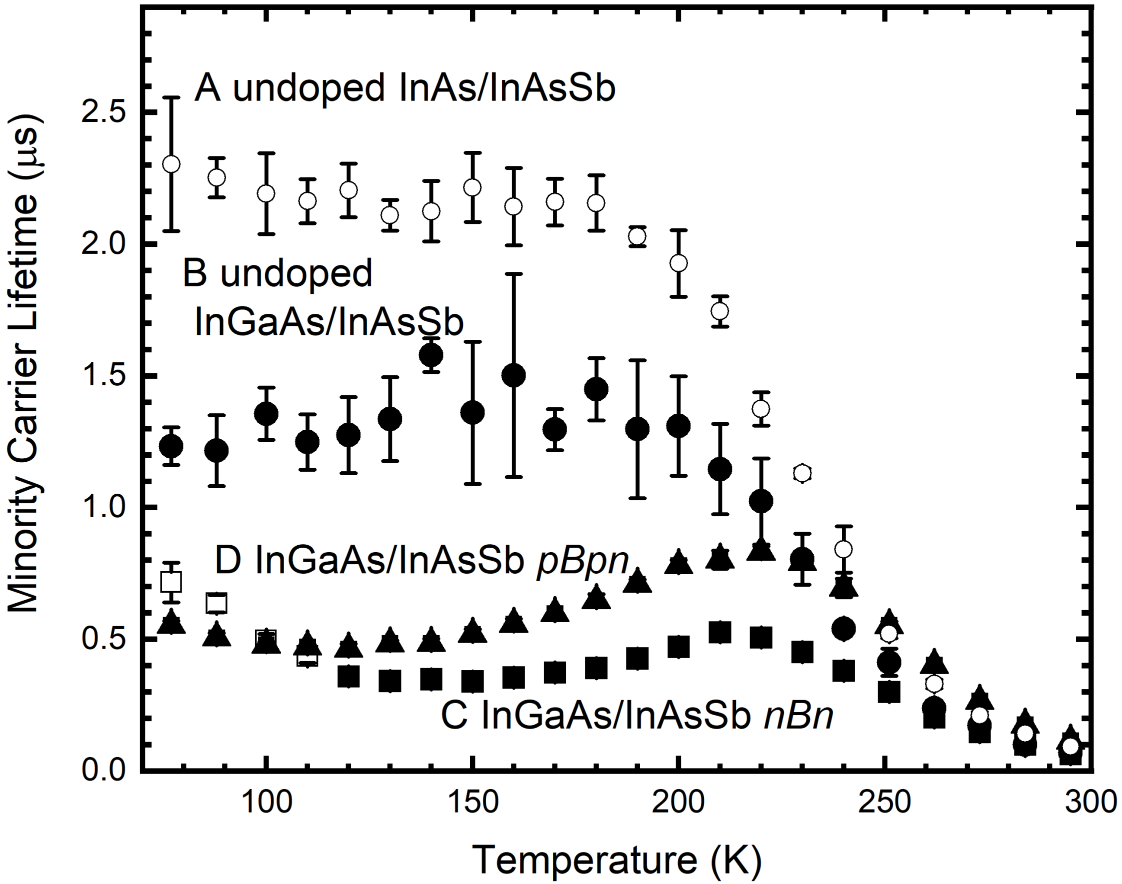

Impact of adding Ga and dopants in InGaAs/InAsSb

Our InAs/InAsSb superlattice (open circles) is optimized for maximum wavefunction overlap at 5 μm wavelength

- Exhibits Shockley-Read-Hall limited lifetime of 2.3 μs
- Serves as our system's InAsSb quality benchmark

The InGaAs/InAsSb superlattice (filled circles) is similarly optimized for wavefunction overlap at 5 μm wavelength

- Lifetime is comparable at 1.4 μs, Shockley-Read-Hall limited

A recombination rate analysis can provide information on the defects in the Shockley-Read-Hall regime and background carrier concentrations in the radiative and Auger terms

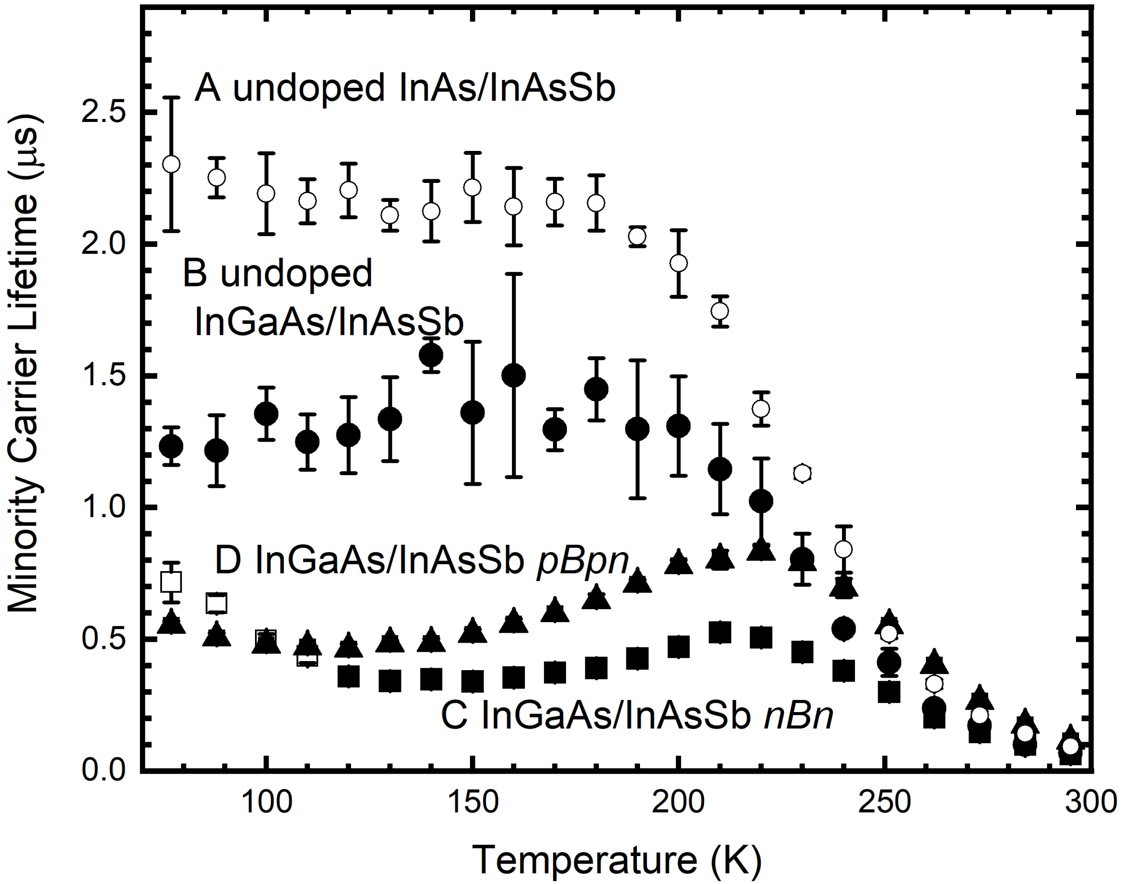

$$\frac{1}{\tau_{\text{total}}} = \frac{1}{\phi\tau_{\text{rad}}} + \frac{1}{\tau_{\text{SRH}}} + \frac{1}{\tau_{\text{Auger}}}$$

Radiative, Shockley-Read-Hall, and Auger recombination

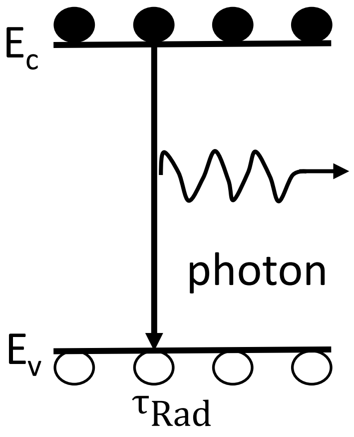

$$\tau_{rad} = \frac{n_i^2}{G_r(n_0 + p_0)}$$

$$n_i^2 = 32\pi^3 \left(\frac{kT}{h^2}\right)^3 (m_e^* m_v^*)^{3/2}\, exp\left(-E_g/kT\right)$$

$$G_r = \frac{8\pi\epsilon_\infty}{h^3c^2}\int_{E_g}^{\infty} \frac{\alpha(h\nu)(h\nu)^2 d(h\nu)}{exp(h\nu/k_BT)}$$

Image modeled after: D. K. Schroder, IEEE Trans Electron Devices **29**, 1336 (1982)

$$\frac{1}{\tau_{\text{total}}} = \frac{1}{\phi\tau_{\text{rad}}}$$

Radiative, Shockley-Read-Hall, and Auger recombination

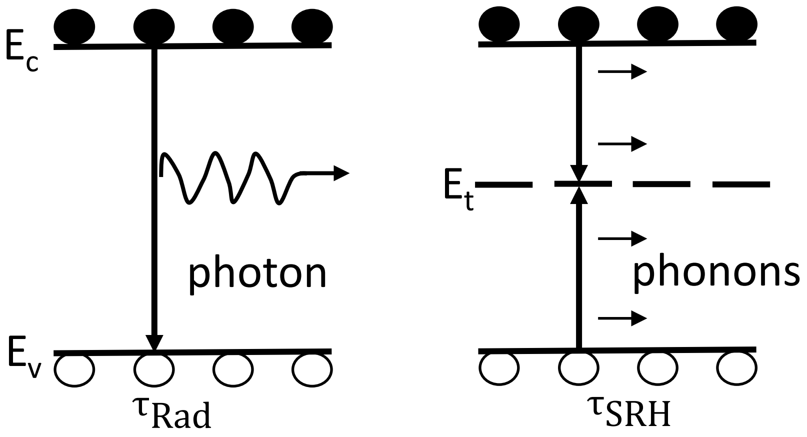

Image modeled after: D. K. Schroder, IEEE Trans Electron Devices **29**, 1336 (1982)

$$\tau_{SRH} = \frac{\tau_{p0}(n_0 + n_1) + \tau_{n0}(p_0 + p_1)}{n_0 + p_0}$$

$$\tau_{p0} = \frac{1}{\sigma_p N_t v_{th}}$$

$$\boxed{\sigma_p N_t} \;!!$$

$$\frac{1}{\tau_{\text{total}}} = \frac{1}{\phi\tau_{\text{rad}}} + \frac{1}{\tau_{\text{SRH}}}$$

Radiative, Shockley-Read-Hall, and Auger recombination

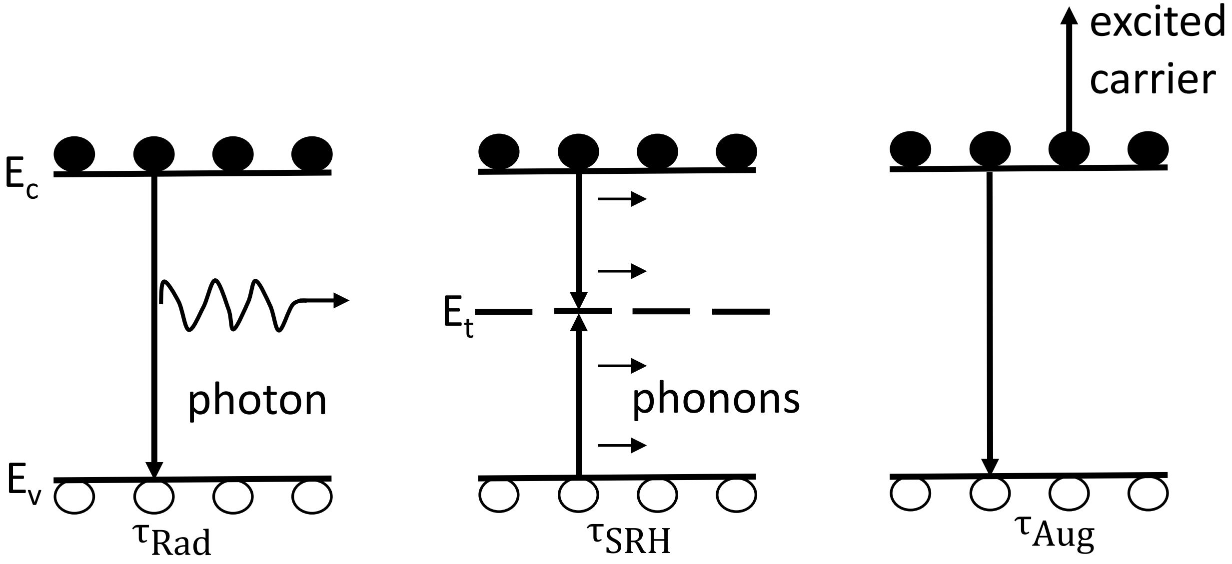

Image modeled after: D. K. Schroder, IEEE Trans Electron Devices **29**, 1336 (1982)

$$\tau_{Auger} = \frac{2n_i^2}{n_0^2 + n_0 p_0} \times \tau_{A1}$$

$$\tau_{A1} = \frac{3.8 \times 10^{-18} \epsilon_\infty^2 (1+\mu)^{1/2}(1+2\mu)}{(m_e^*/m_0)|F_1F_2|^2} \times \left(\frac{E_g}{k_BT}\right)^{3/2} \exp\left(\frac{1+2\mu}{1+\mu}\frac{E_g}{k_BT}\right)$$

$$\frac{1}{\tau_{total}} = \frac{1}{\phi\tau_{rad}} + \frac{1}{\tau_{SRH}} + \frac{1}{\tau_{Auger}}$$

Radiative, Shockley-Read-Hall, and Auger recombination

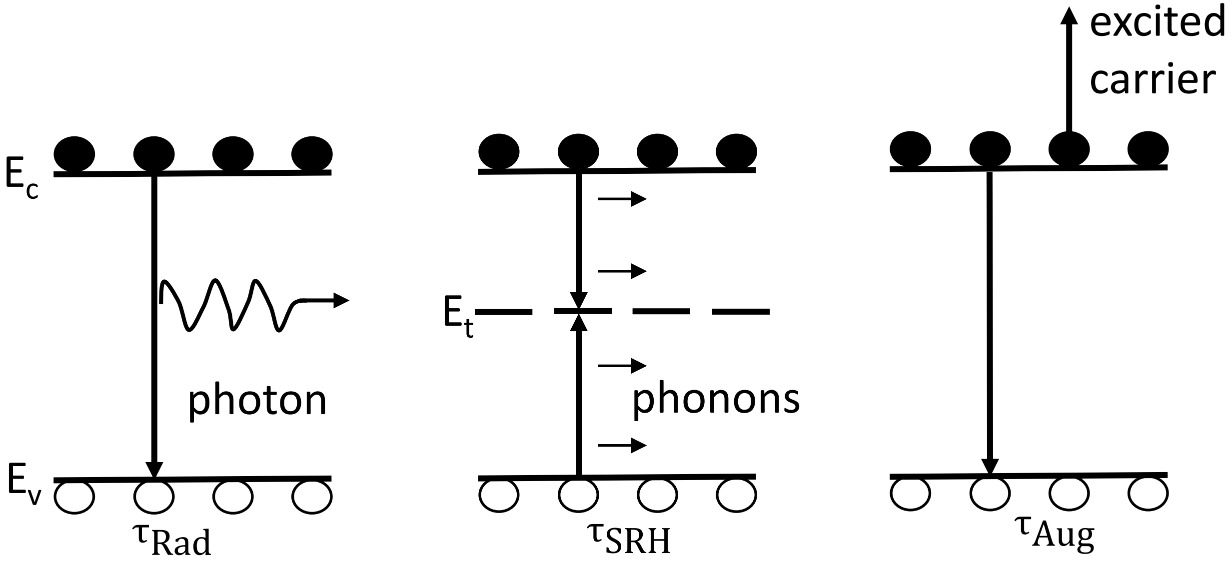

Image modeled after: D. K. Schroder, IEEE Trans Electron Devices **29**, 1336 (1982)

$$\frac{1}{\tau_{total}} = \frac{1}{\phi\tau_{rad}} + \frac{1}{\tau_{SRH}} + \frac{1}{\tau_{Auger}}$$

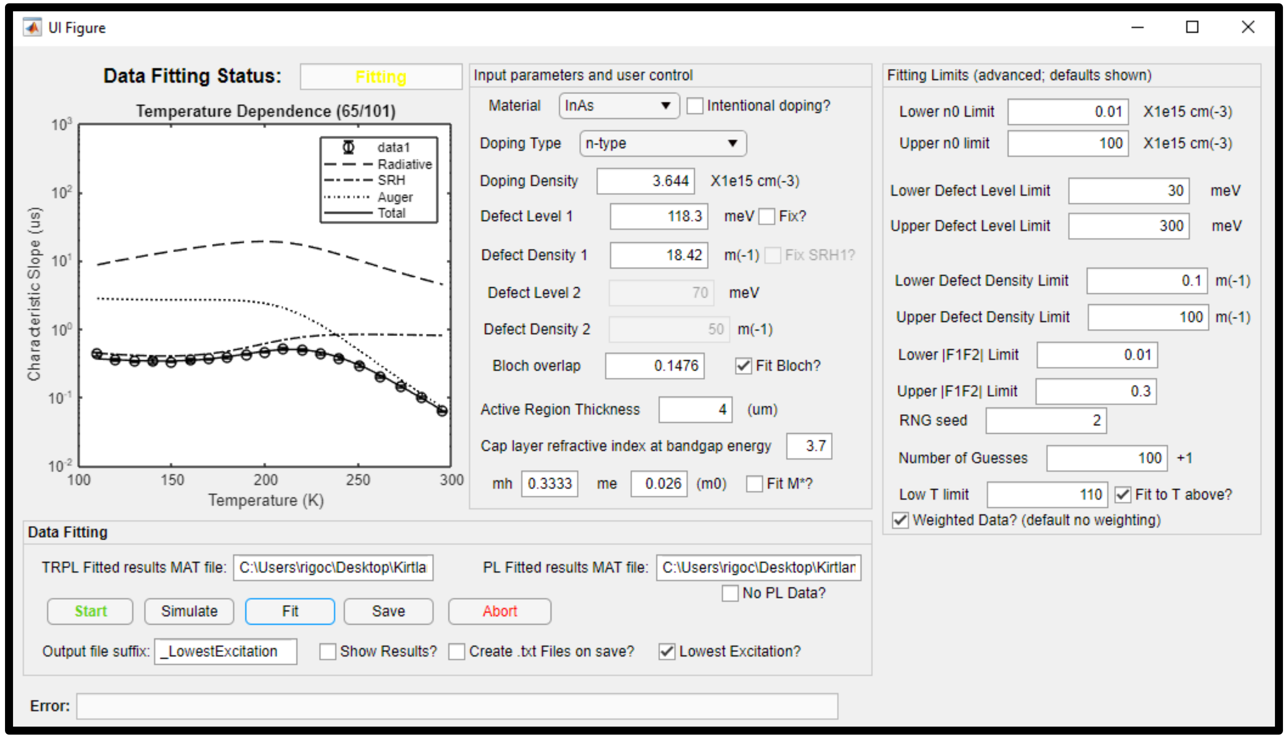

Data Fitting Status: Fitting

Input parameters and user control

Material: InAs ▼ ☐ Intentional doping?
Doping Type: n-type ▼
Doping Density: 3.644 X1e15 cm(-3)
Defect Level 1: 118.3 meV ☐ Fix?
Defect Density 1: 18.42 m(-1) ☐ Fix SRH1?
Defect Level 2: 70 meV
Defect Density 2: 50 m(-1)
Bloch overlap: 0.1476 ☑ Fit Bloch?
Active Region Thickness: 4 (um)
Cap layer refractive index at bandgap energy: 3.7
mh: 0.3333 me: 0.026 (m0) ☐ Fit M*?

Fitting Limits (advanced; defaults shown)

Lower n0 Limit: 0.01 X1e15 cm(-3)
Upper n0 limit: 100 X1e15 cm(-3)
Lower Defect Level Limit: 30 meV
Upper Defect Level Limit: 300 meV
Lower Defect Density Limit: 0.1 m(-1)
Upper Defect Density Limit: 100 m(-1)
Lower |F1F2| Limit: 0.01
Upper |F1F2| Limit: 0.3
RNG seed: 2
Number of Guesses: 100 +1
Low T limit: 110 ☑ Fit to T above?
☑ Weighted Data? (default no weighting)

Data Fitting

TRPL Fitted results MAT file: C:\Users\rigoc\Desktop\Kirtla
PL Fitted results MAT file: C:\Users\rigoc\Desktop\Kirtlan
☐ No PL Data?
Output file suffix: _LowestExcitation
☐ Show Results? ☐ Create .txt Files on save? ☑ Lowest Excitation?

Error:

Radiative, Shockley-Read-Hall, and Auger recombination

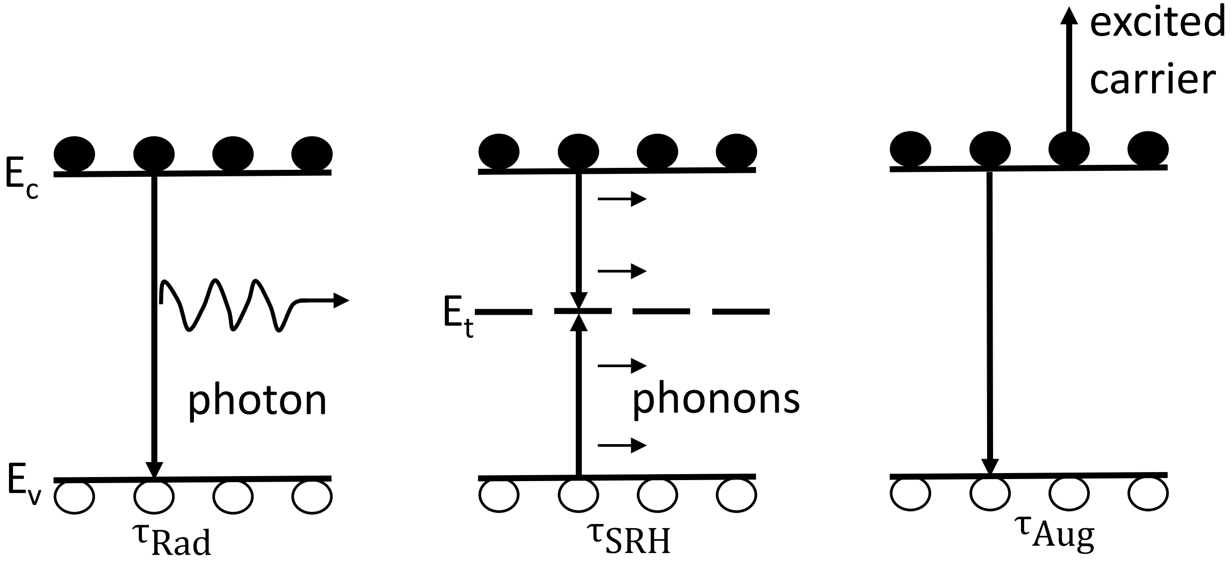

Image modeled after: D. K. Schroder, IEEE Trans Electron Devices **29**, 1336 (1982)

$$\frac{1}{\tau_{\text{total}}} = \frac{1}{\phi\tau_{\text{rad}}} + \frac{1}{\tau_{\text{SRH}}} + \frac{1}{\tau_{\text{Auger}}}$$

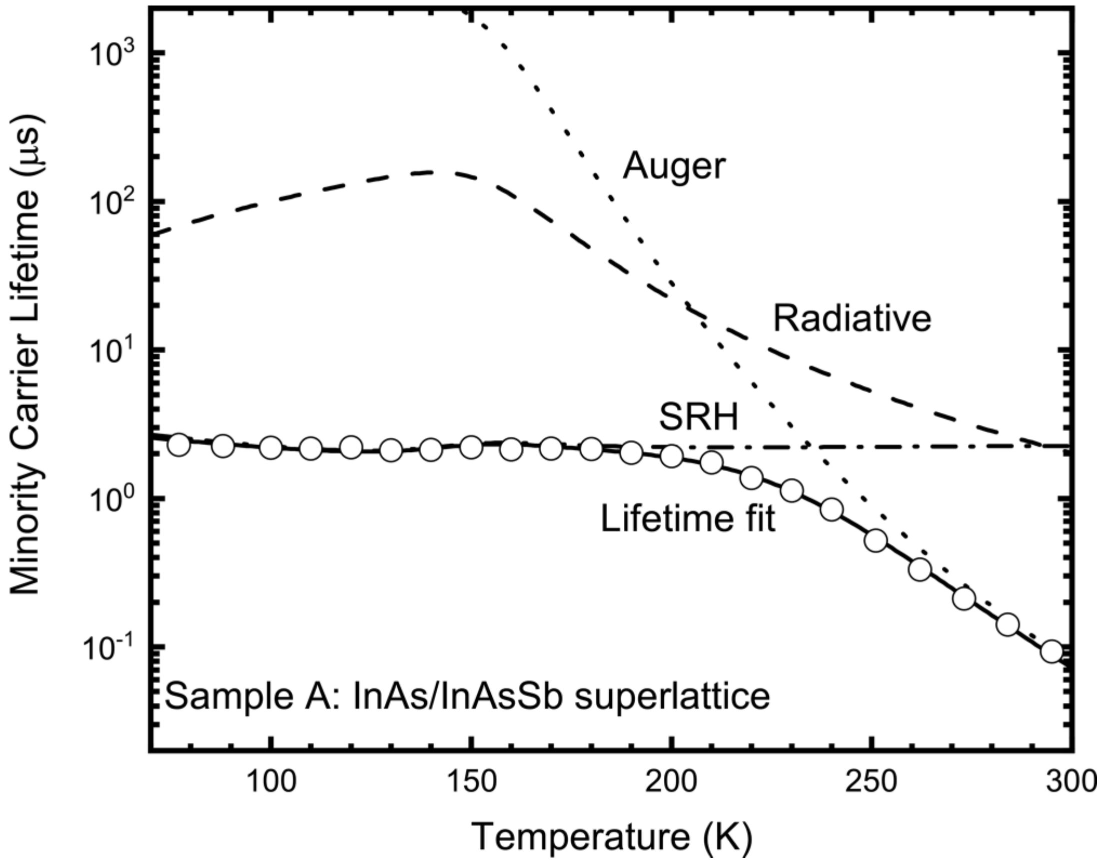

Radiative, Shockley-Read-Hall, and Auger recombination

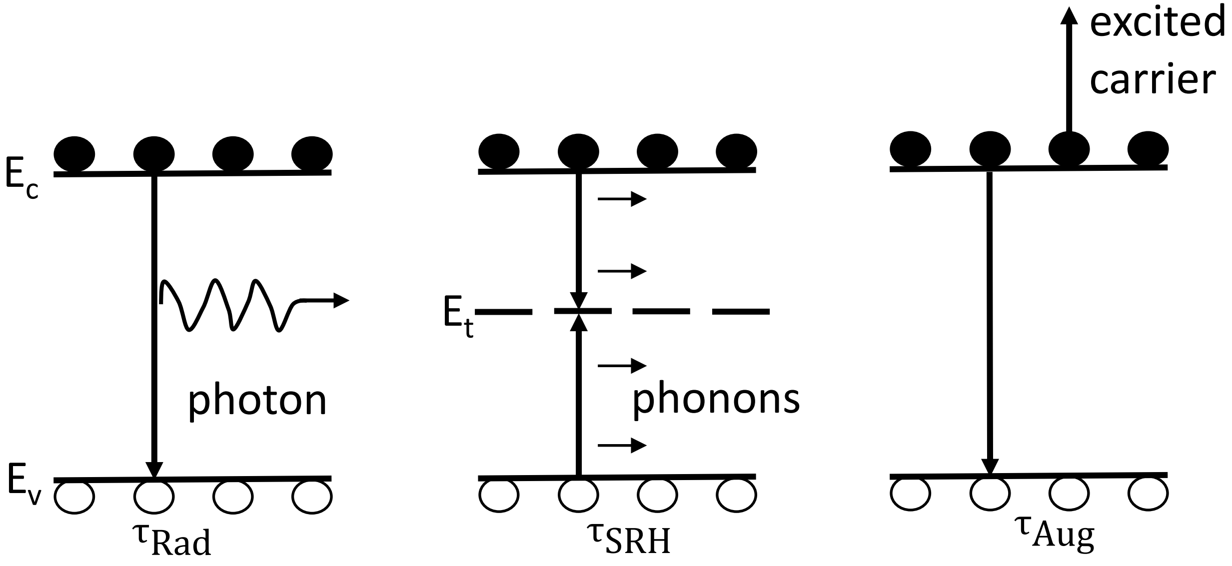

Image modeled after: D. K. Schroder, IEEE Trans Electron Devices **29**, 1336 (1982)

$$\frac{1}{\tau_{\text{total}}} = \frac{1}{\phi\tau_{\text{rad}}} + \frac{1}{\tau_{\text{SRH}}} + \frac{1}{\tau_{\text{Auger}}}$$

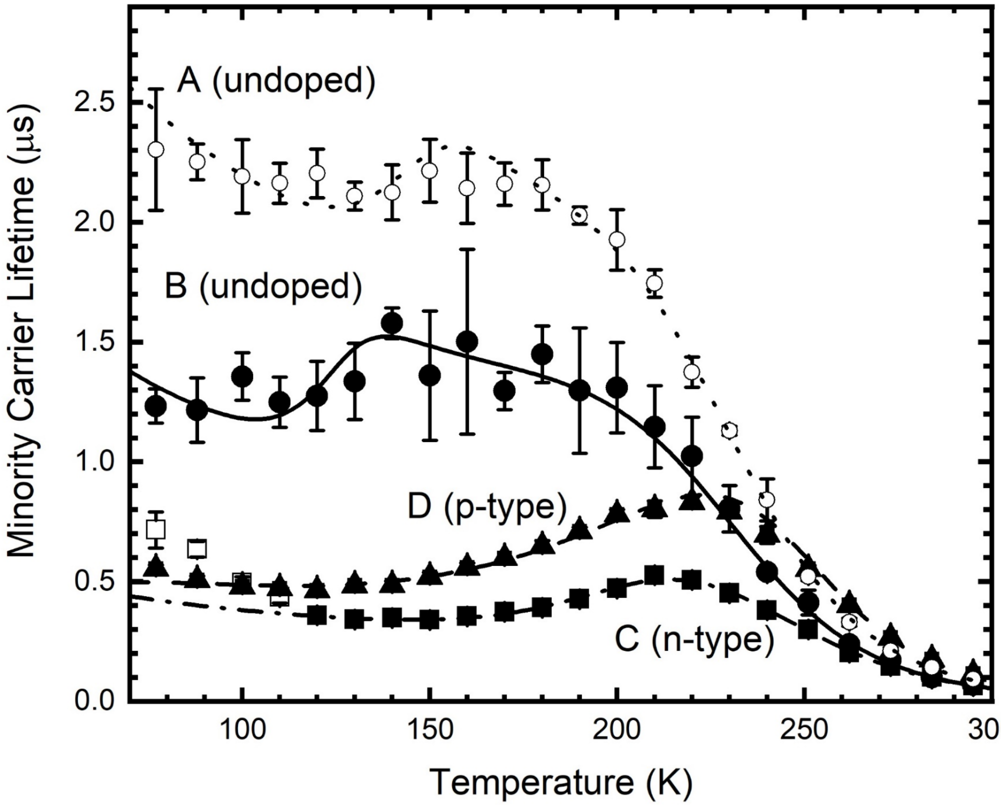

Carrier concentration & defect properties in InGaAs/InAsSb

Sample ID	Type	Majority Carrier Concentration (×10^{15} cm^{-3})	$E_c - E_t$ (meV)	σN_t (10^{-2} cm^{-1})
A	*n*-type	**0.122**	99.42	3.82
B	*n*-type	**0.029**	105.0	7.39
C	*n*-type	**3.65**	118.3	18.42
D	*p*-type	**7.79**	55.22	4.214

The background *n*-type carrier concentration is comparable for both samples, typical of high quality InAsSb alloys (>1 μs)

- Carrier concentrations in doped samples C and D consistent with the calibrated doping densities

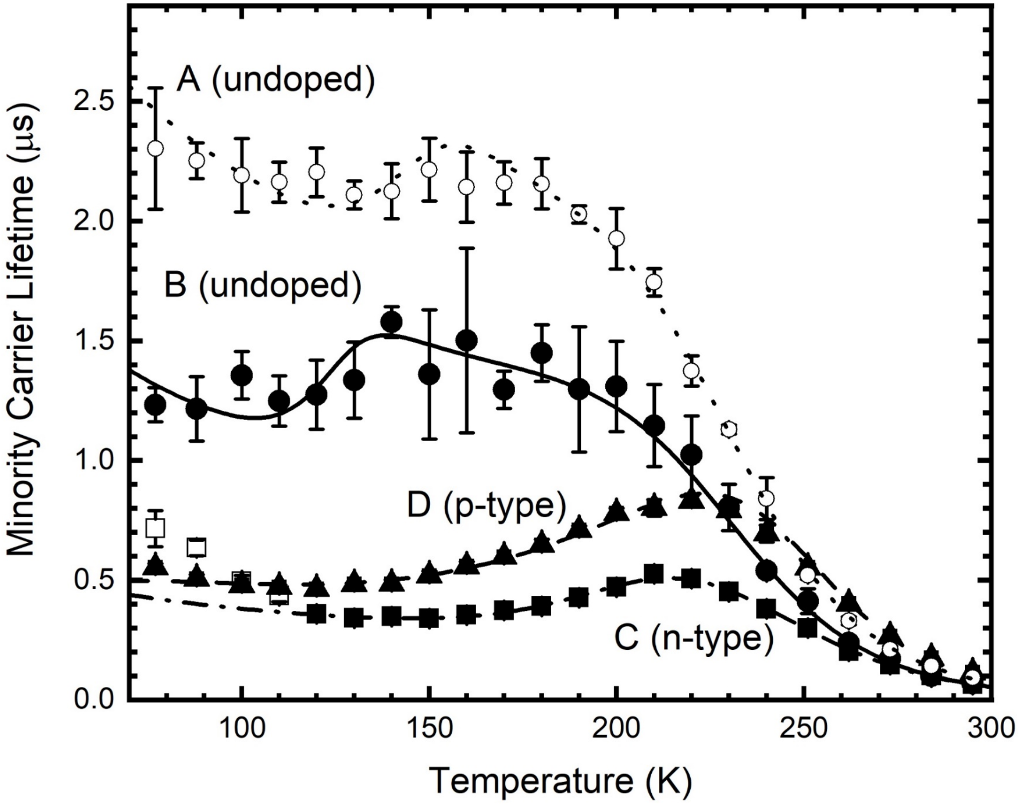

Carrasco *et al.*, J. Appl. Phys. **129**, 184501 (2021)

Carrier concentration & defect properties in InGaAs/InAsSb

Sample ID	Type	Majority Carrier Concentration (×10^{15} cm^{-3})	$E_c - E_t$ (meV)	σN_t (10^{-2} cm^{-1})
A	*n*-type	0.122	**99.42**	3.82
B	*n*-type	0.029	**105.0**	7.39
C	*n*-type	3.65	**118.3**	18.42
D	*p*-type	7.79	**55.22**	4.214

The background *n*-type carrier concentration is comparable for both samples, typical of high quality InAsSb alloys (>1 μs)

- Carrier concentrations in doped samples C and D consistent with the calibrated doping densities

Defect levels also appear to be comparable

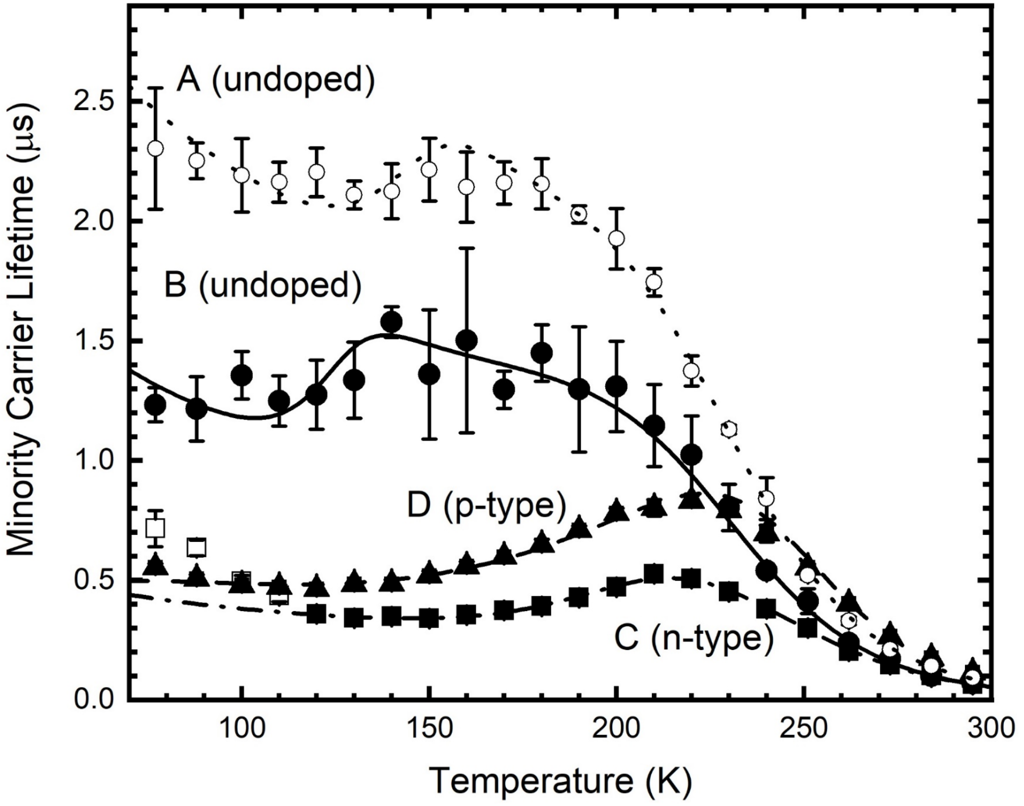

Carrasco *et al.*, J. Appl. Phys. **129**, 184501 (2021)

Carrier concentration & defect properties in InGaAs/InAsSb

Sample ID	Type	Majority Carrier Concentration (×10^{15} cm^{-3})	$E_c - E_t$ (meV)	σN_t (10^{-2} cm^{-1})
A	*n*-type	0.122	99.42	**3.82**
B	*n*-type	0.029	105.0	**7.39**
C	*n*-type	3.65	118.3	**18.42**
D	*p*-type	7.79	55.22	**4.214**

The background *n*-type carrier concentration is comparable for both samples, typical of high quality InAsSb alloys (>1 μs)

- Carrier concentrations in doped samples C and D consistent with the calibrated doping densities

Defect levels also appear to be comparable

Defect concentration ~60% higher in InGaAs/InAsSb superlattice, consistent observed decrease in lifetime of the material

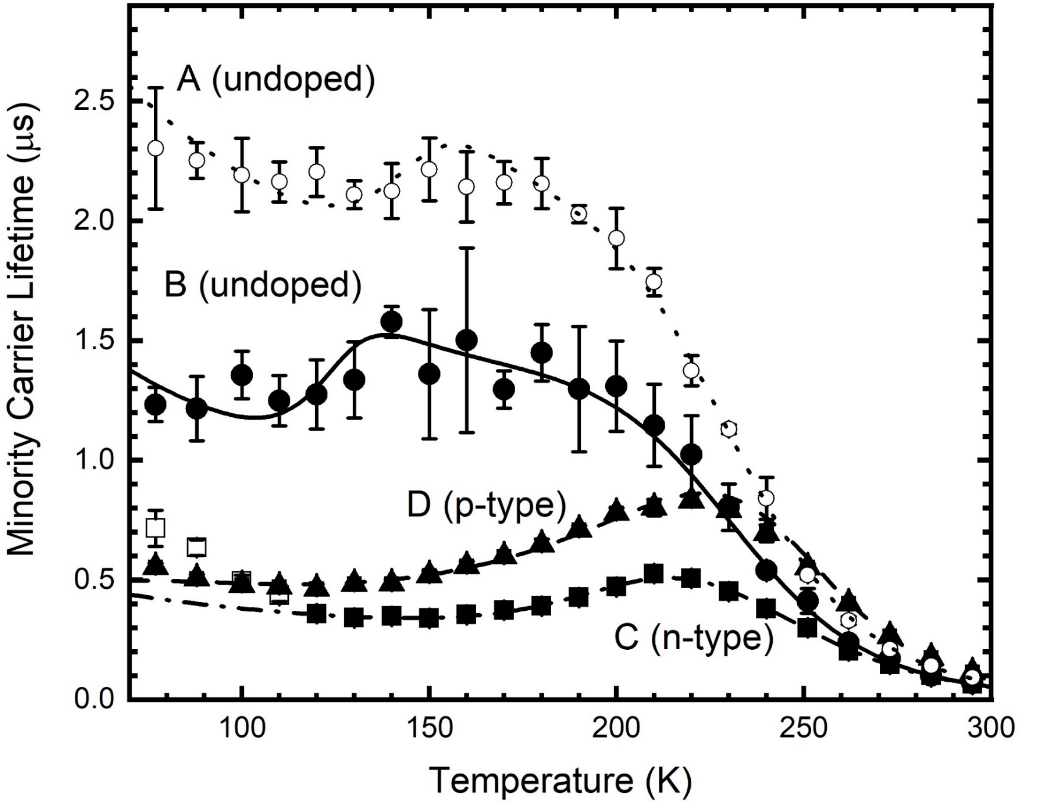

Carrasco *et al.*, J. Appl. Phys. **129**, 184501 (2021)

How would these devices fare in space?

Radiation sources in space: cosmic rays, **high energy protons in Van Allen belts**, solar flares

- Detector performance degrades in space over time

Installing test devices on a satellite to test their performance in space is expensive!

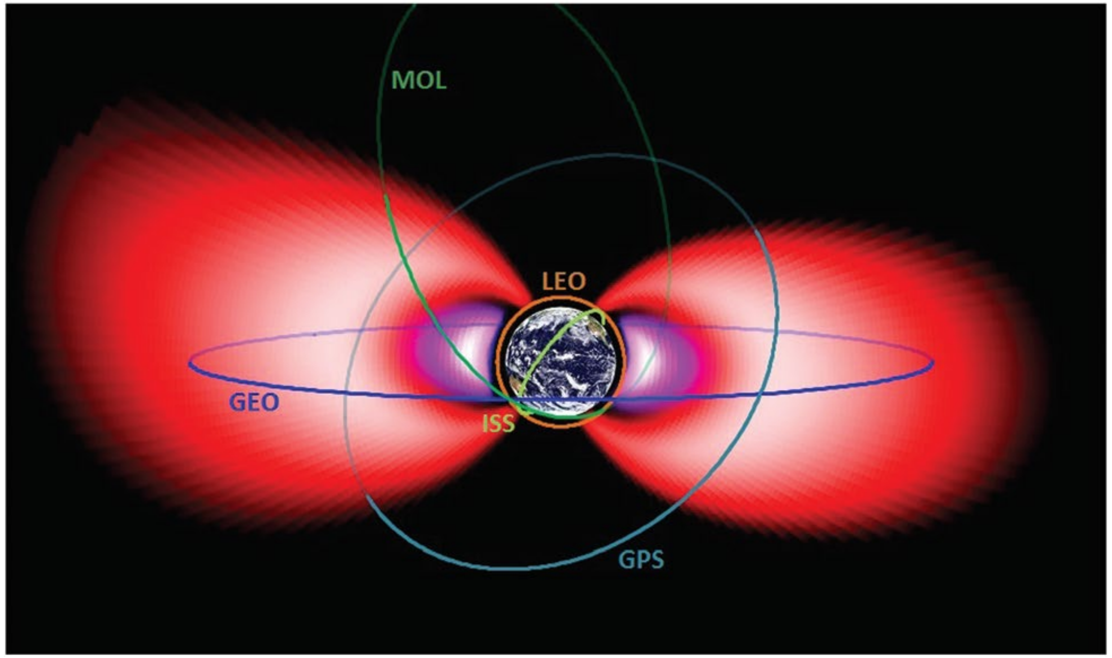

Different satellite orbits
Logan *et al.*, J. Mater. Chem. C, **7** 8905 (2019).

How would these devices fare in space?

Radiation sources in space: cosmic rays, **high energy protons in Van Allen belts**, solar flares

- Detector performance degrades in space over time

Installing test devices on a satellite to test their performance in space is expensive!

Instead take devices to proton source to simulate radiation damage over time, measure performance metrics

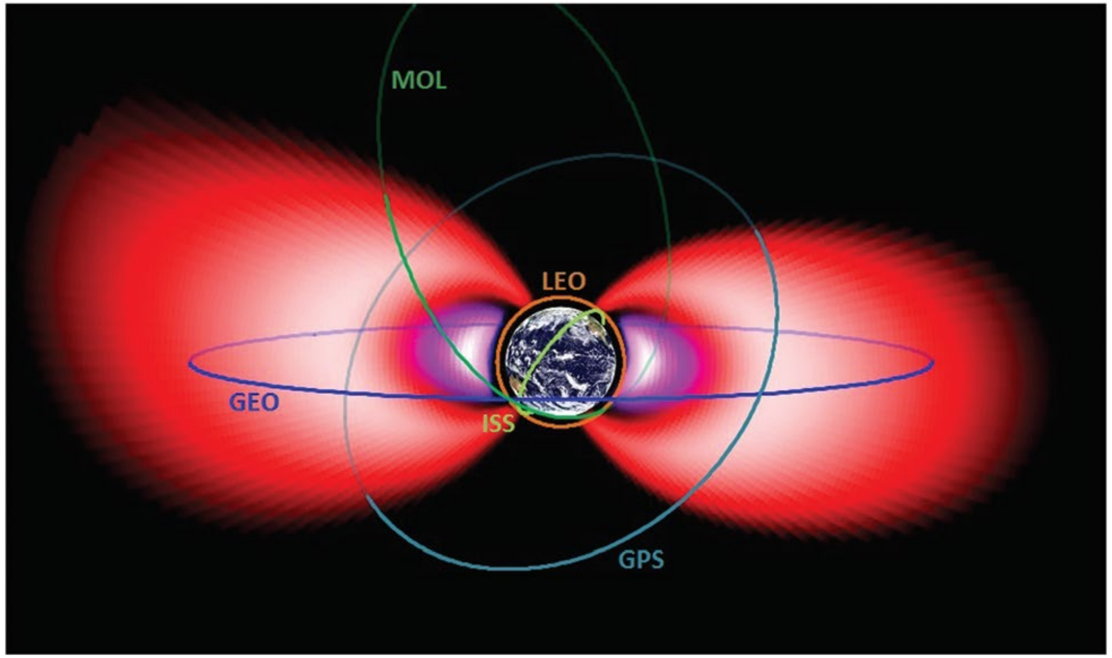

Different satellite orbits
Logan *et al.*, J. Mater. Chem. C, **7** 8905 (2019).

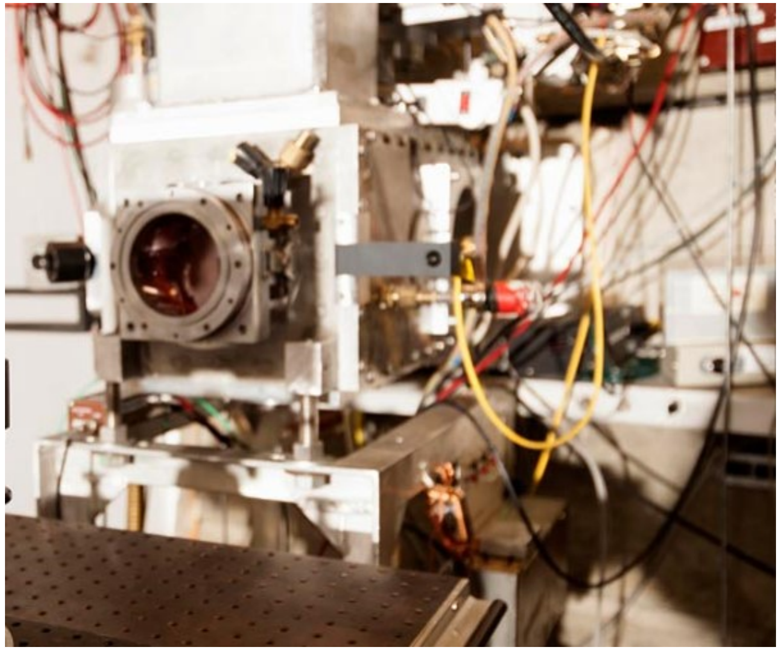

UC Davis Beamline port

InGaAs/InAsSb superlattice *pBpn* detector

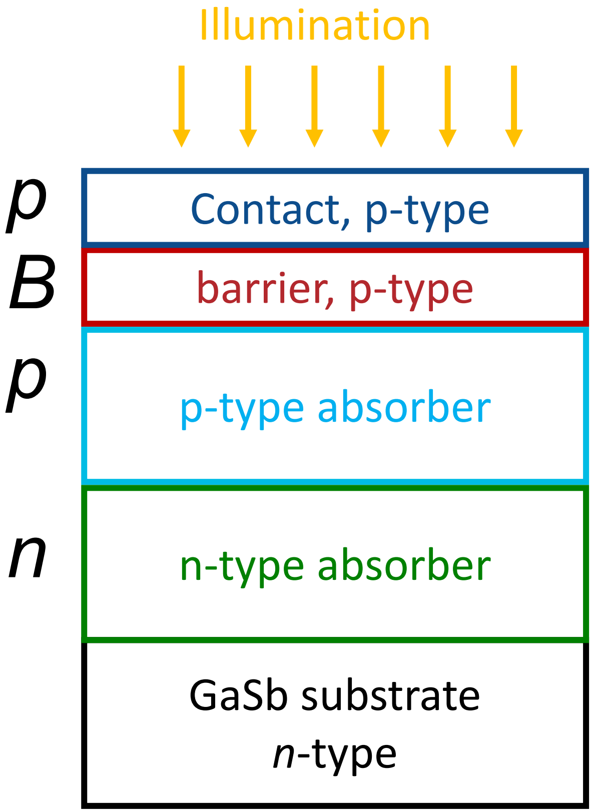

Illumination

p Contact, p-type

B barrier, p-type

p p-type absorber

n n-type absorber

GaSb substrate
n-type

InGaAs/InAsSb superlattice *pBpn* detector

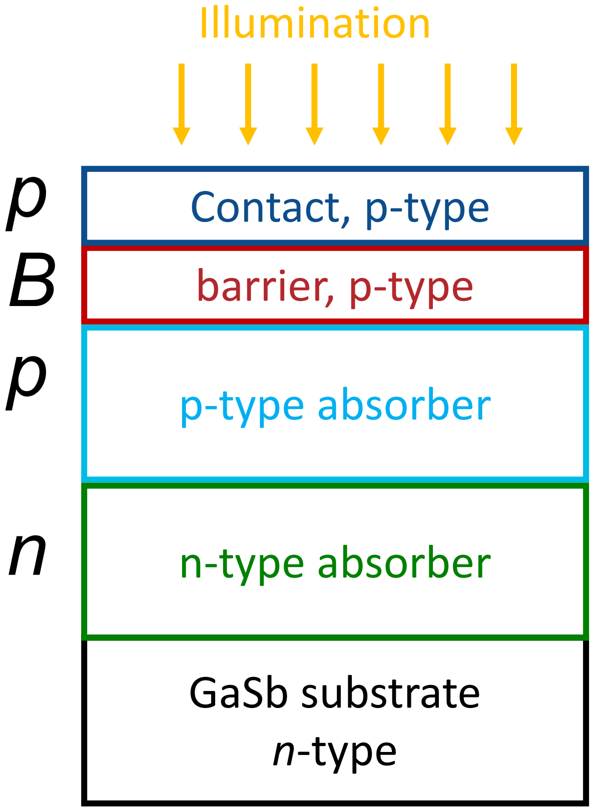

Illumination

p Contact, p-type

B barrier, p-type

p p-type absorber

n n-type absorber

GaSb substrate
n-type

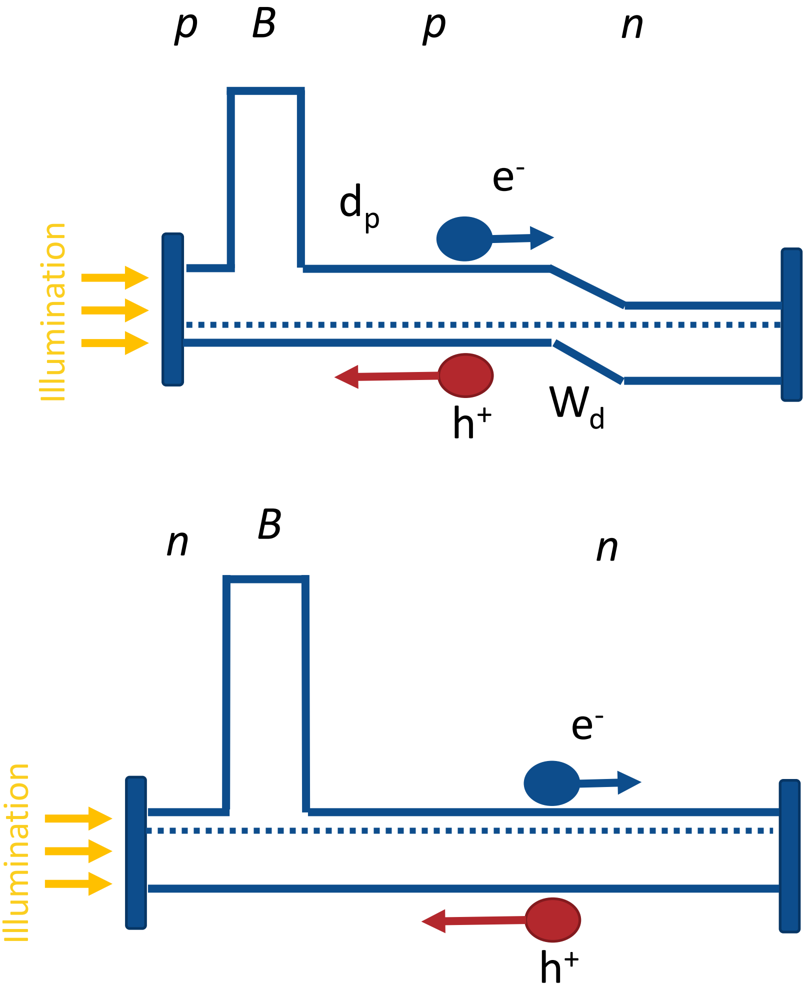

InGaAs/InAsSb superlattice *pBpn* detector

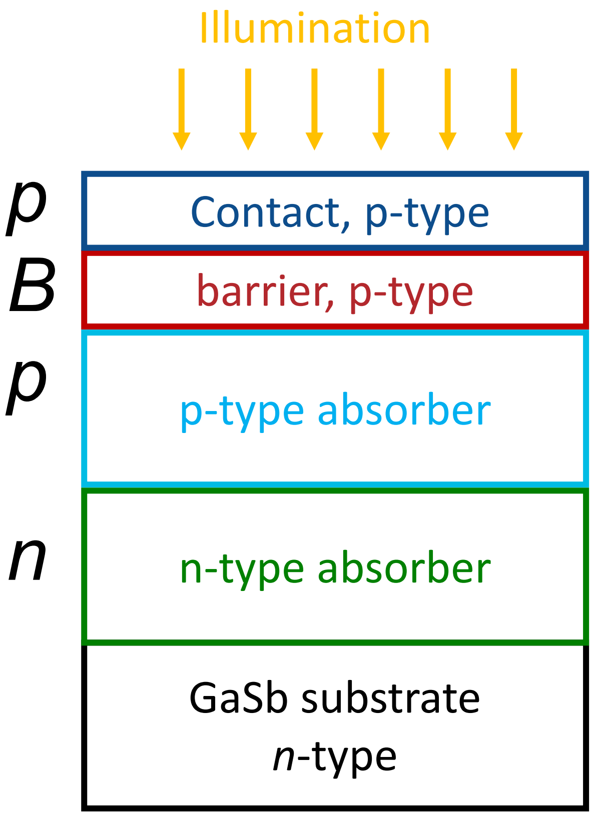

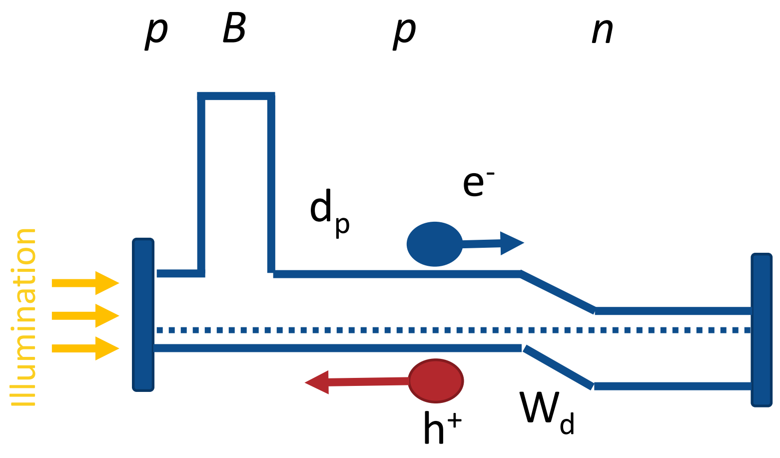

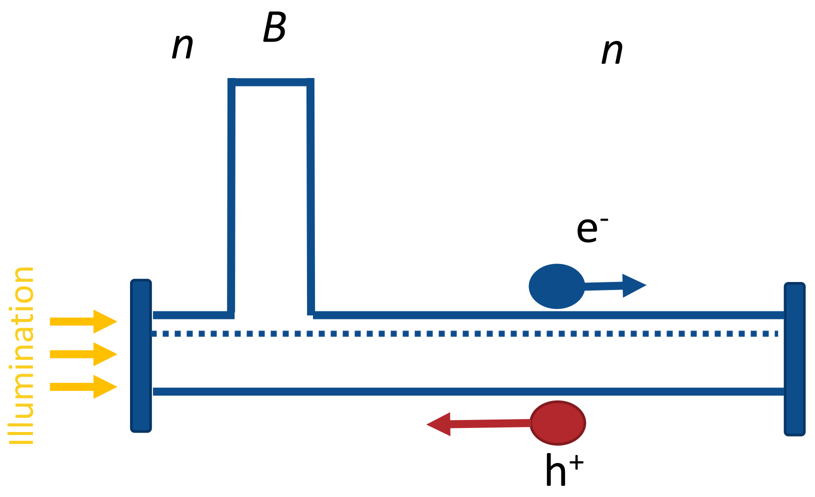

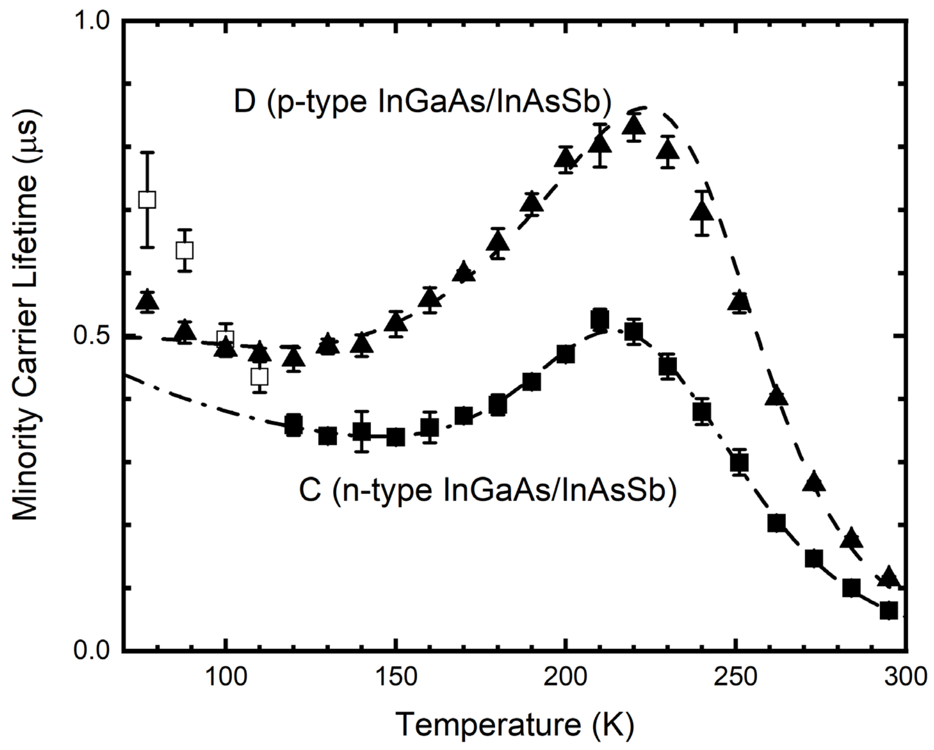

$$\tau_{MC} = \frac{1}{\tau_{SRH}} + \frac{1}{\phi\tau_{rad}} + \frac{1}{\tau_{Auger}}$$

Lifetime relationships with device performance

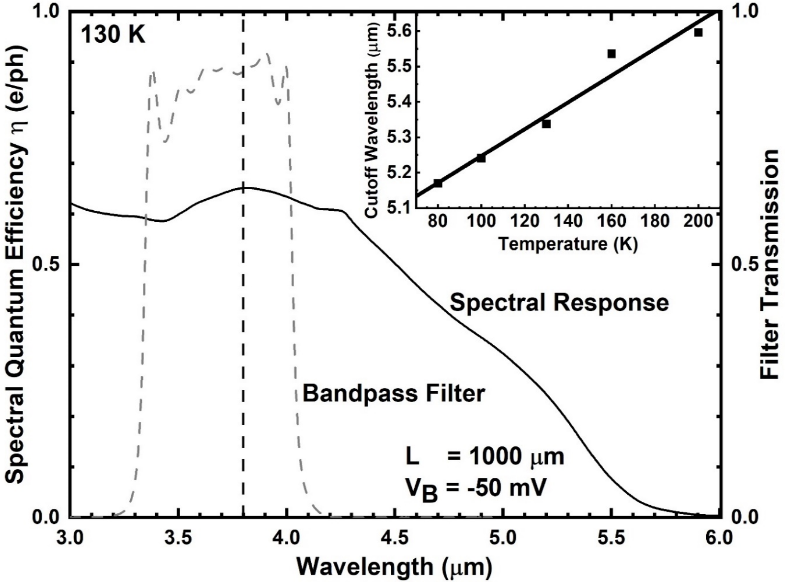

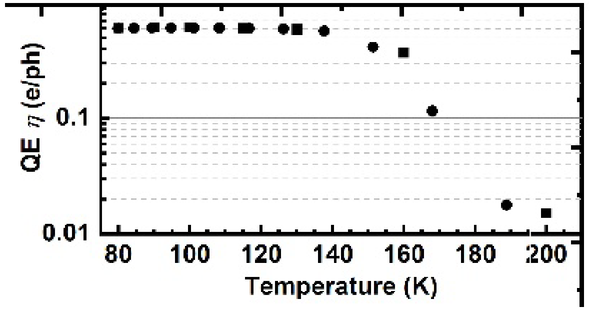

$$L_D^2 = k_B T \mu \tau_{mc}$$

$$\eta \approx \overbrace{\left(\frac{\alpha^2 L_D^2}{\alpha^2 L_D^2 - 1}\right)\left[1-\left(1+\frac{\alpha d_p}{\alpha^2 L_D^2}\right)e^{-\alpha d_p}\right]}^{\text{From } p\text{-region}} + \overbrace{\left[e^{-\alpha d_p} - e^{-\alpha(d_p+W_D)}\right]}^{\text{From depletion region}}$$

Lifetime relationships with device performance

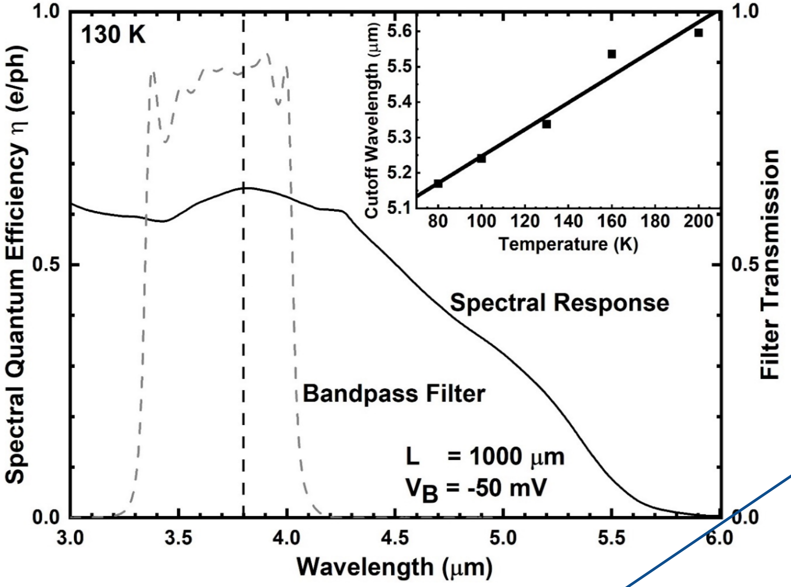

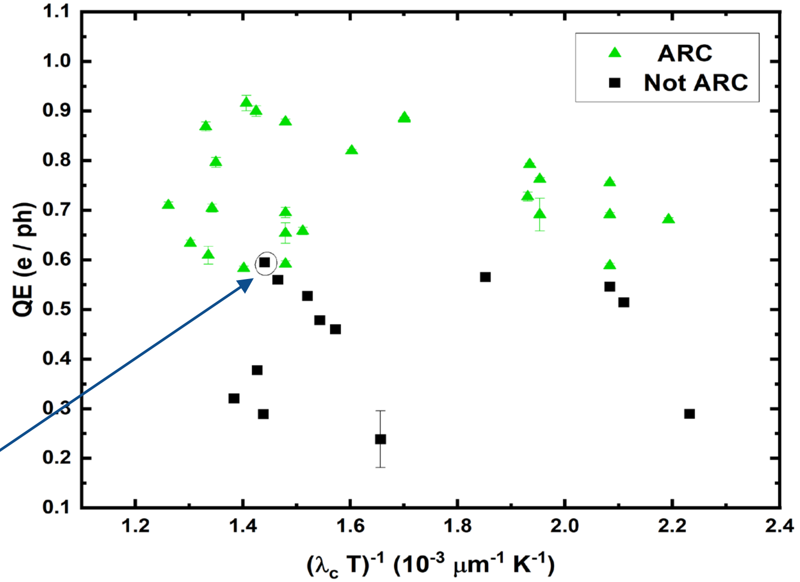

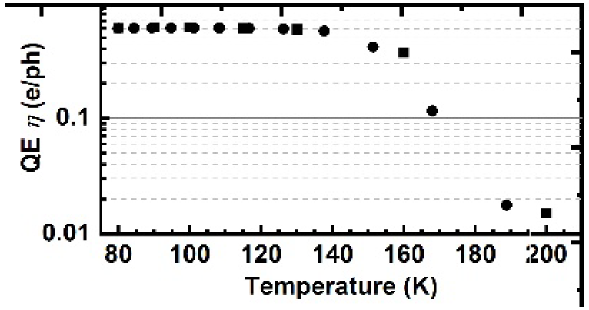

$$L_D^2 = k_B T \mu \tau_{mc}$$

$$\eta \approx \overbrace{\left(\frac{\alpha^2 L_D^2}{\alpha^2 L_D^2 - 1}\right)\left[1 - \left(1 + \frac{\alpha d_p}{\alpha^2 L_D^2}\right) e^{-\alpha d_p}\right]}^{\text{From } p\text{-region}} + \overbrace{\left[e^{-\alpha d_p} - e^{-\alpha\left(d_p + W_D\right)}\right]}^{\text{From depletion region}}$$

Lifetime relationships with device performance

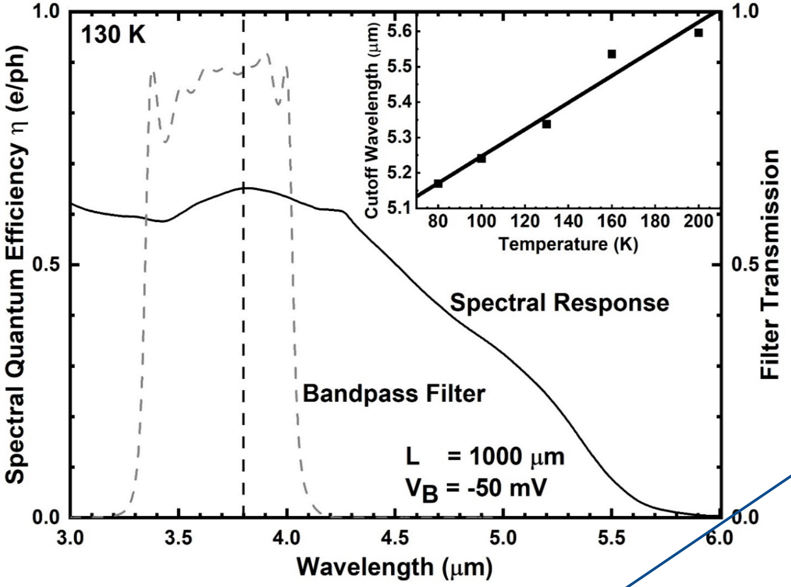

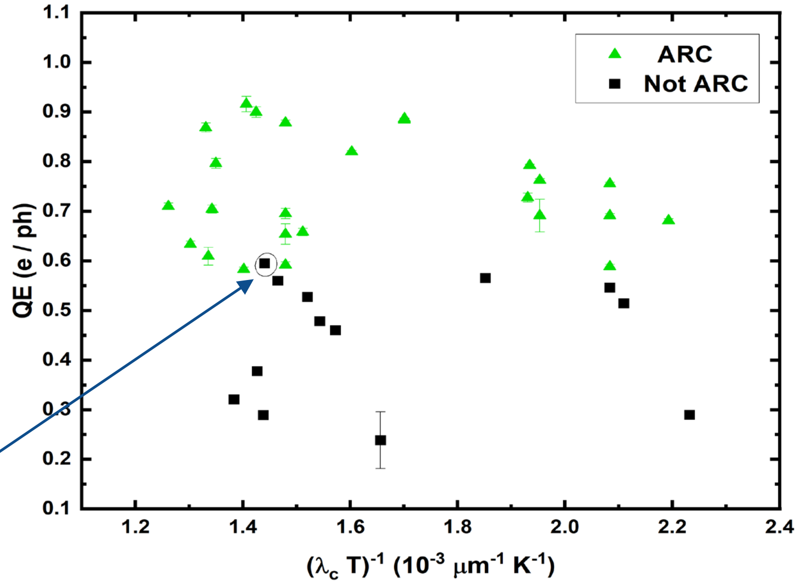

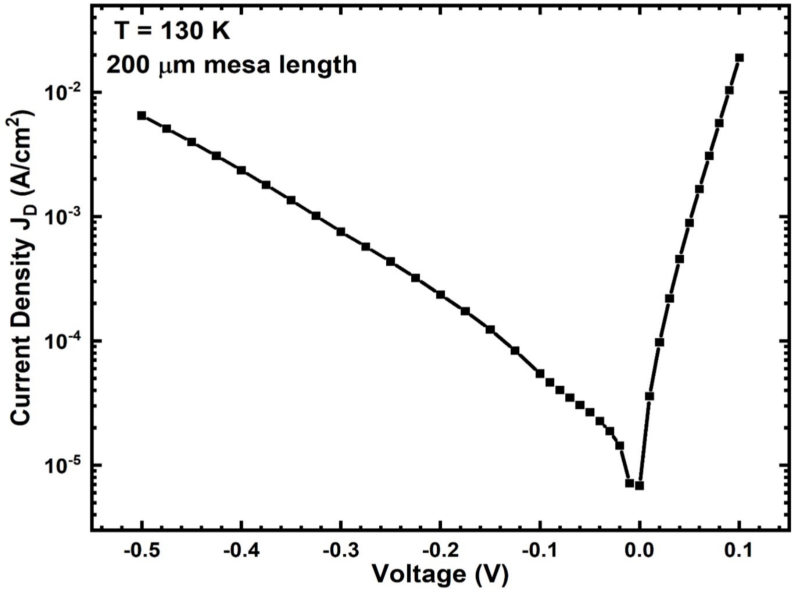

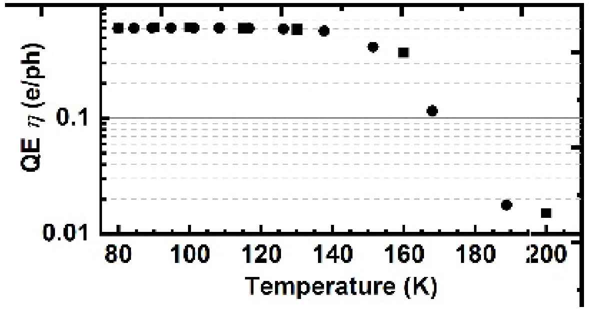

$$L_D^2 = k_B T \mu \tau_{mc}$$

$$\eta \approx \overbrace{\left(\frac{\alpha^2 L_D^2}{\alpha^2 L_D^2 - 1}\right)\left[1-\left(1+\frac{\alpha d_p}{\alpha^2 L_D^2}\right)e^{-\alpha d_p}\right]}^{\text{From } p\text{-region}} + \overbrace{\left[e^{-\alpha d_p} - e^{-\alpha(d_p+W_D)}\right]}^{\text{From depletion region}}$$

$$J_{dark} = J_{depletion} + J_{diffusion} + J_{tunneling}$$

$$J_{diffusion} = \frac{q n_i^2 d_p}{p_0 \tau_{MC}}$$

$$J_{depletion} = \frac{q n_i W_D}{\tau_g} \propto \frac{q n_i W_D}{\tau_{MC}}$$

Proton irradiation effects on quantum efficiency

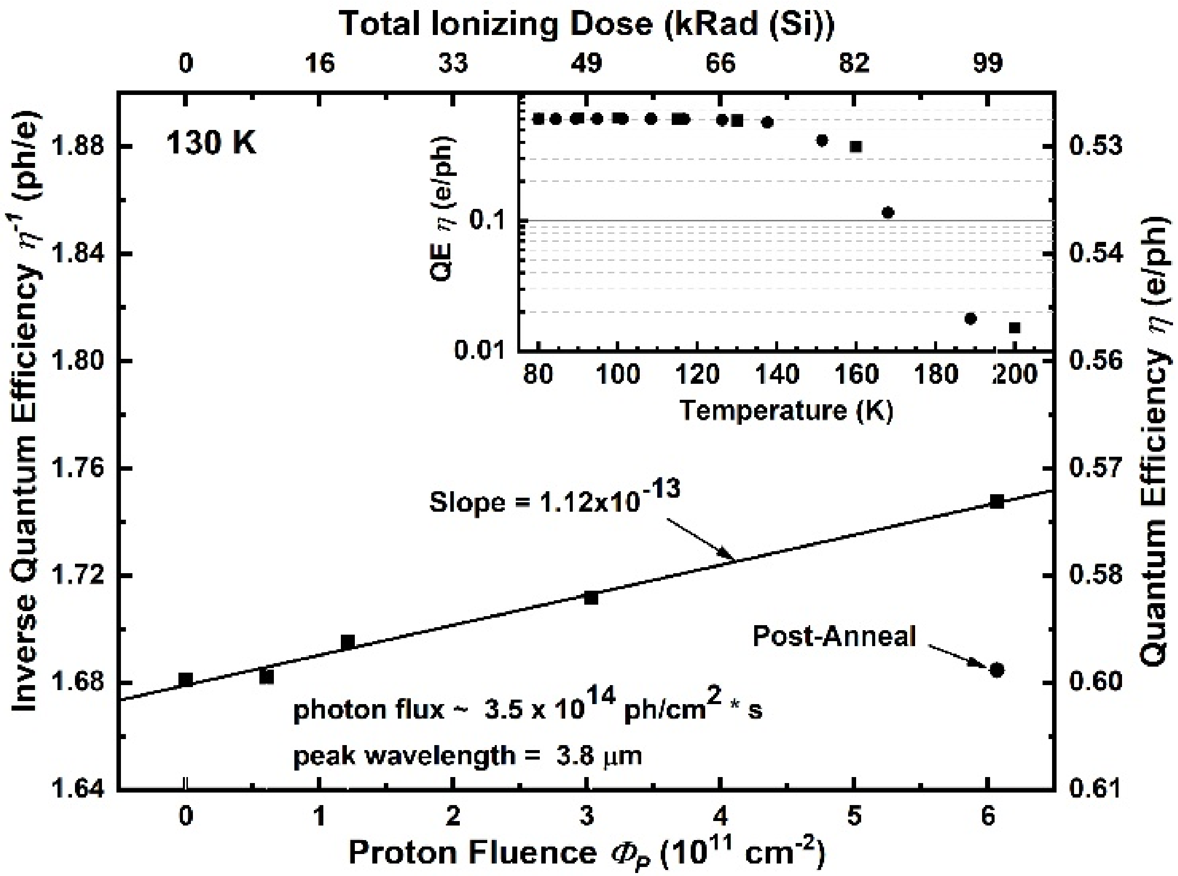

Linear decrease from ~59.7% to ~57.3% quantum efficiency

- Damage factor of 1.12×10^{-13} ph cm^2/e

Proton irradiation effects on quantum efficiency

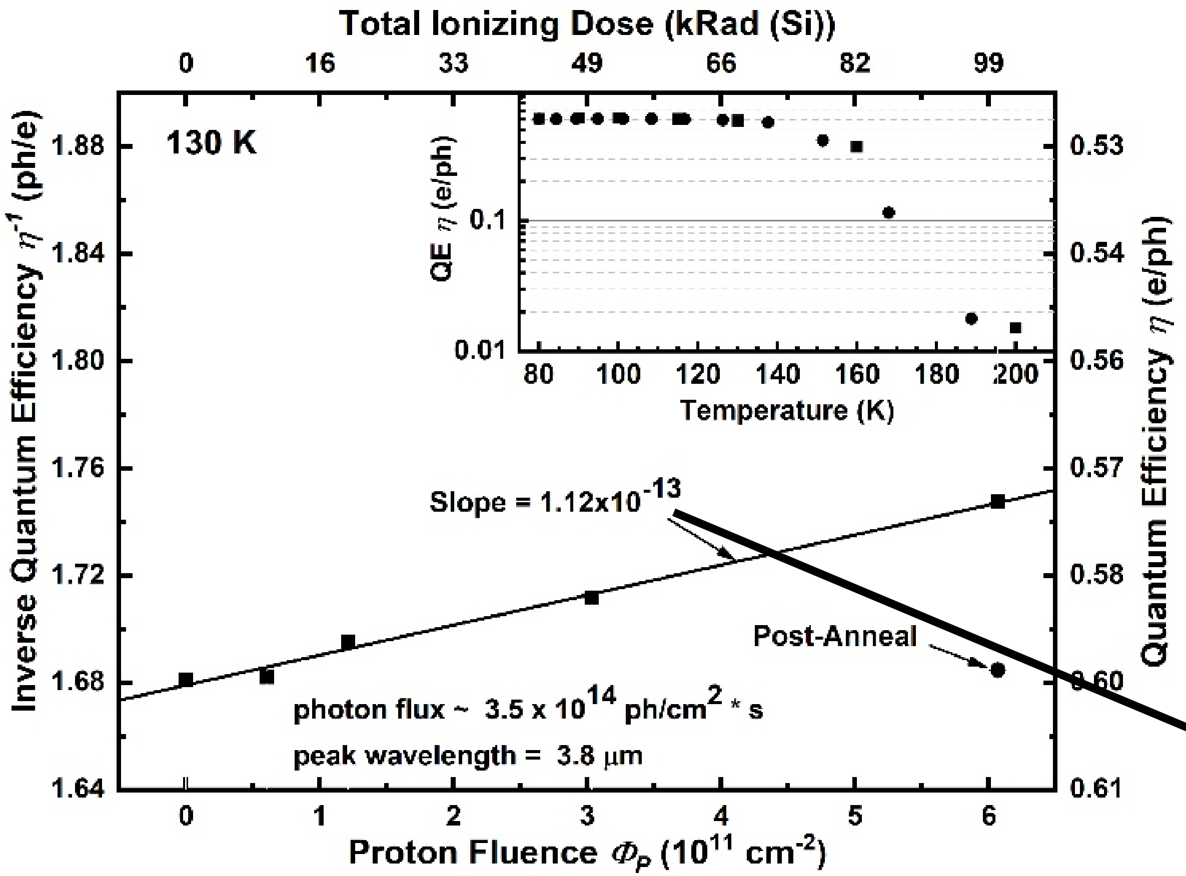

Linear decrease from ~59.7% to ~57.3% quantum efficiency

- Damage factor of 1.12×10^{-13} ph cm^2/e
- Among the lowest III-V device *nBn*'s measured

Full recovery post-anneal

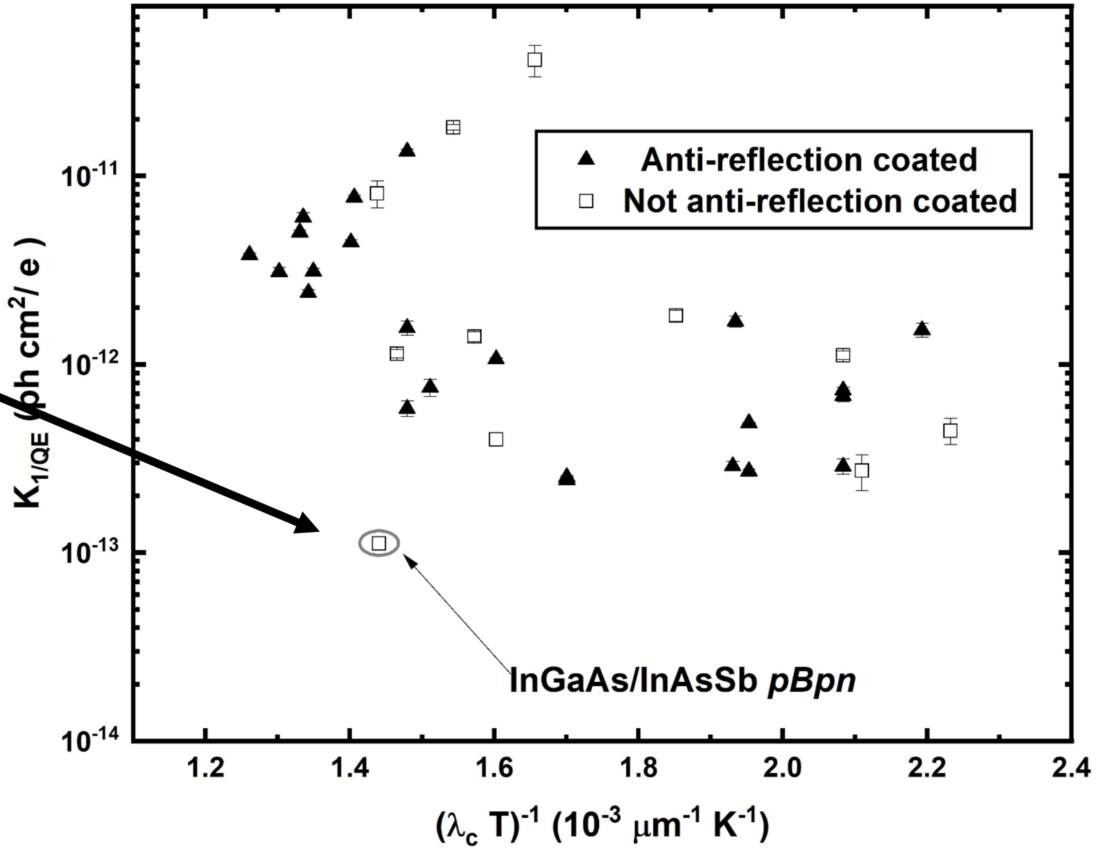

Proton irradiation effects on dark current

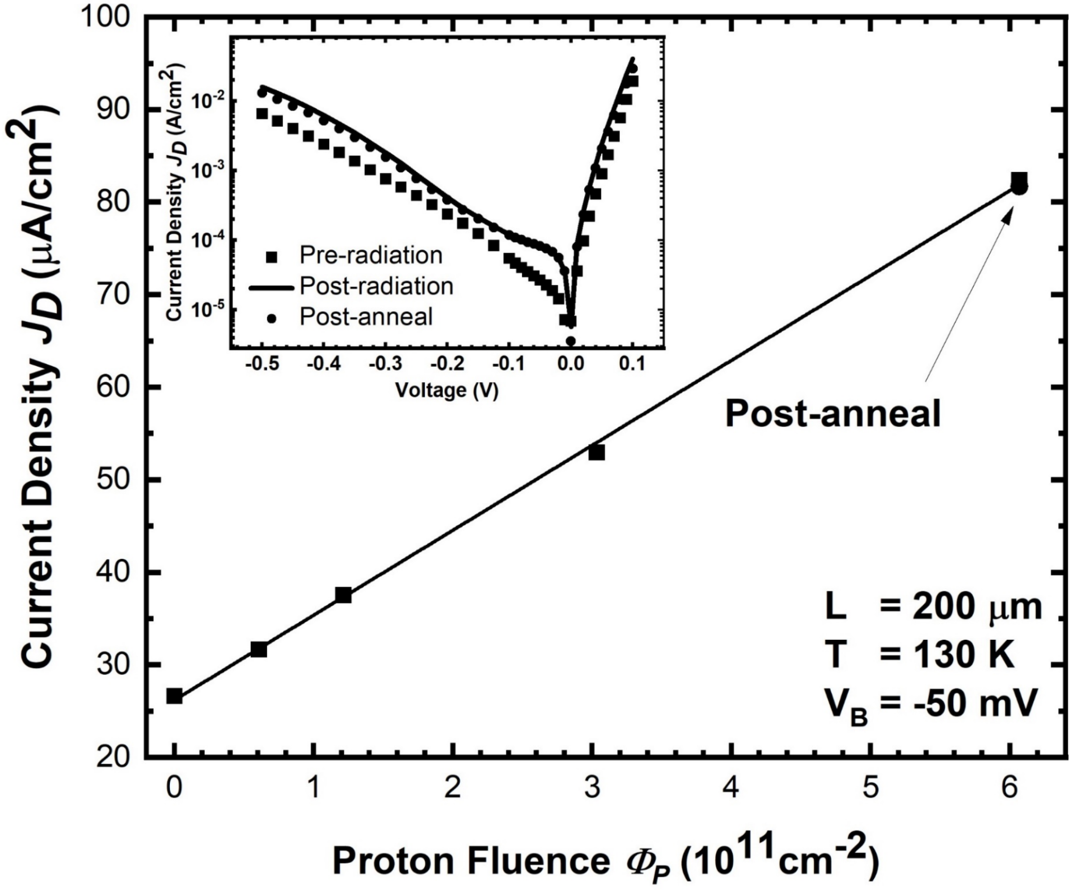

Negligible dark current recovery post-anneal

- This kind of result is **atypical**, Dark-current usually recovers to ~1/3 of its original value

Proton irradiation effects on dark current

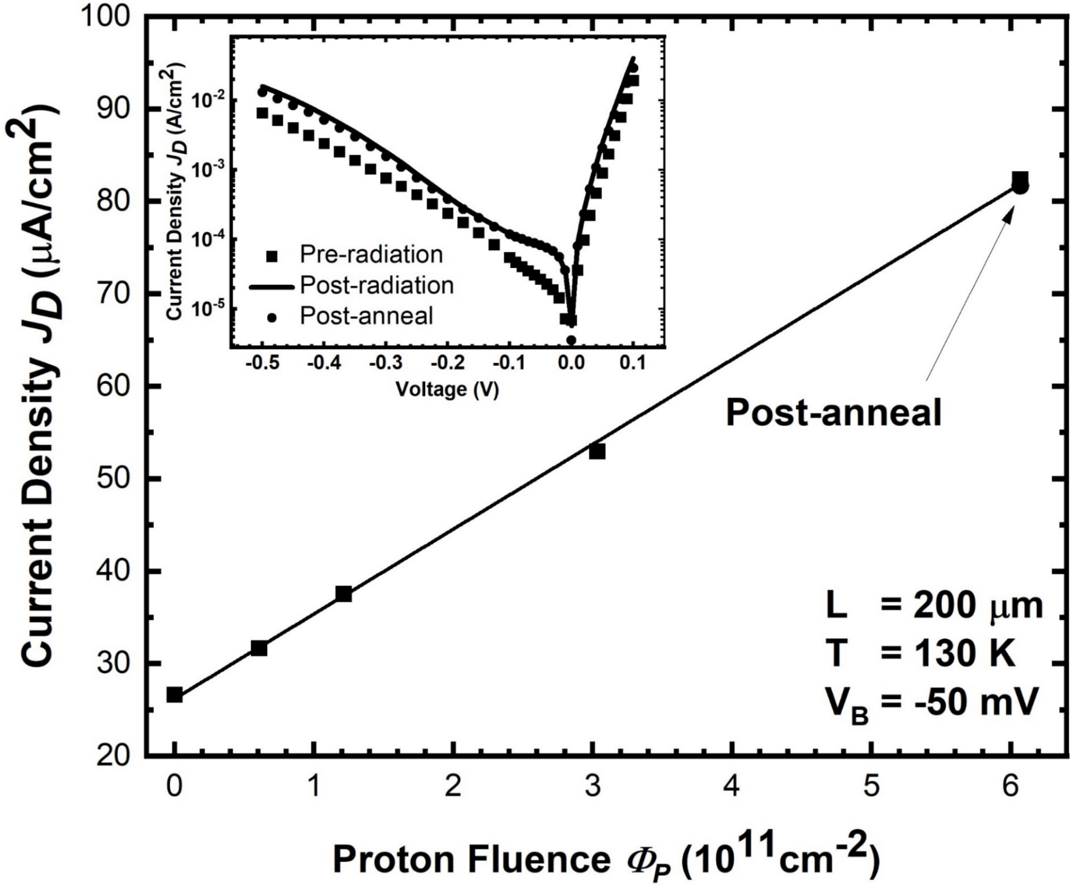

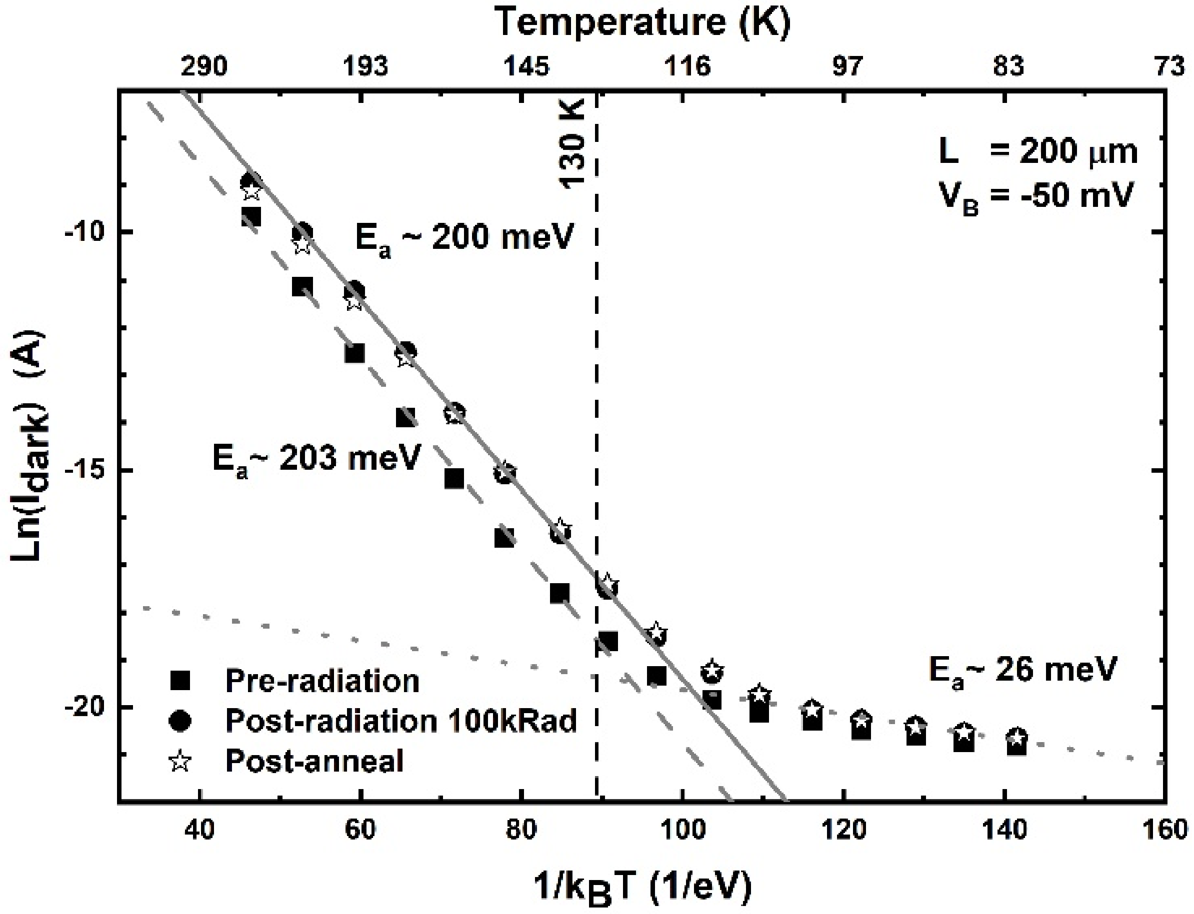

Negligible dark current recovery post-anneal

- This kind of result is **atypical**, Dark-current usually recovers to ~1/3 of its original value

$$J_{diffusion} = \frac{q n_i^2 L_n}{N_A \tau_{MC}}$$

Minority carrier lifetime damage factor

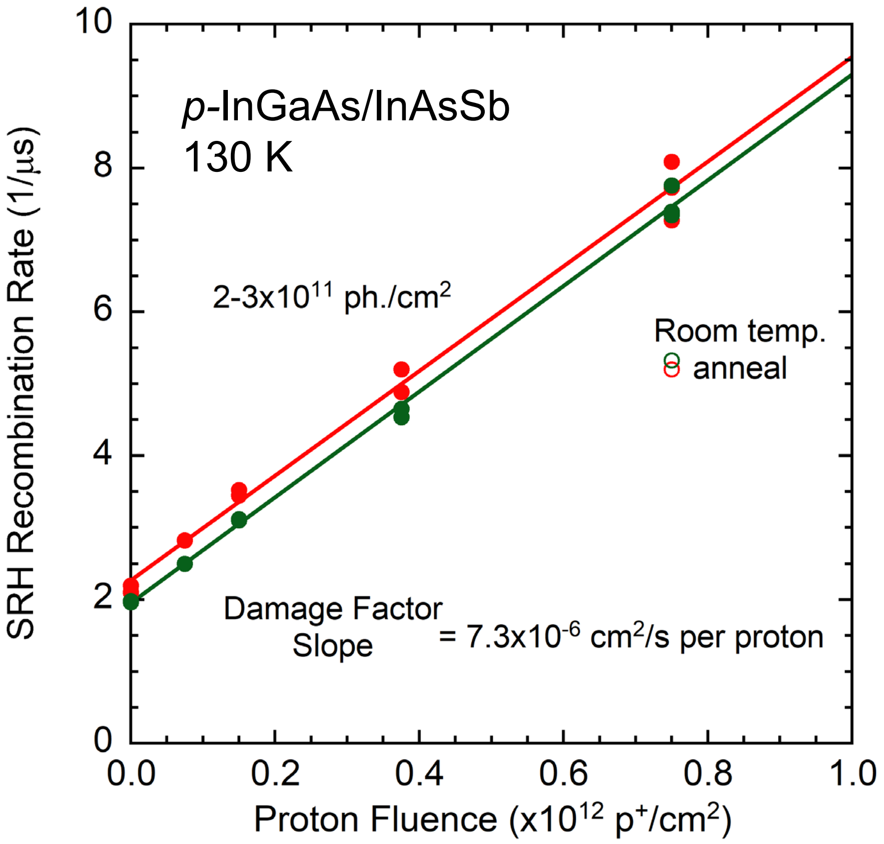

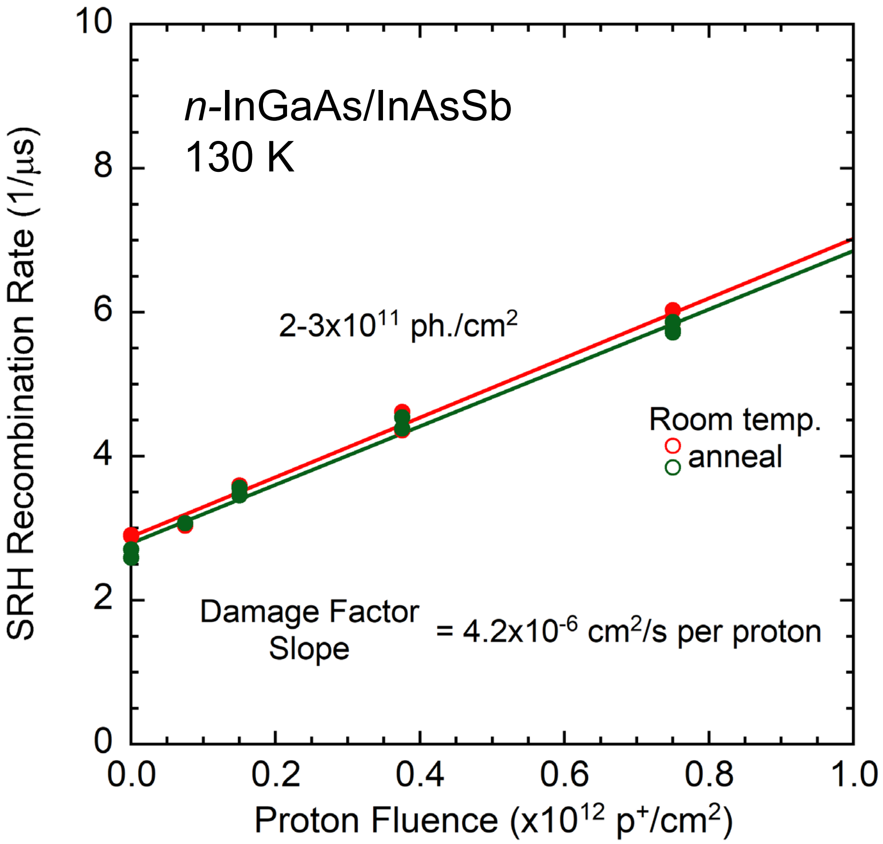

$$\boxed{R_{SRH}(\Phi_p) = \frac{1}{\tau_{SRH}(\Phi_p)} = \sigma v_{th}\left(N_{T0} + \frac{dN_T}{d\Phi_P}\Phi_p\right) = \frac{1}{\tau_{SRH}(\Phi_p = 0)} + K_{1/\tau}\Phi_p}$$

Irradiation-induced incorporation of donors

	Irradiation Condition	σN_t (10^{-2} cm^{-1})	Doping ($\times 10^{15}$ cm^{-3})
p-InGaAs/InAsSb	Pre-Rad	4.21	7.8
	Post-Rad	15.9	3.2
	Post-Anneal	10.4	3.9

Inf. Phys. Technol. **97**, 448 (2019)
Appl. Phys. Lett. **108**, 263504 (2016)

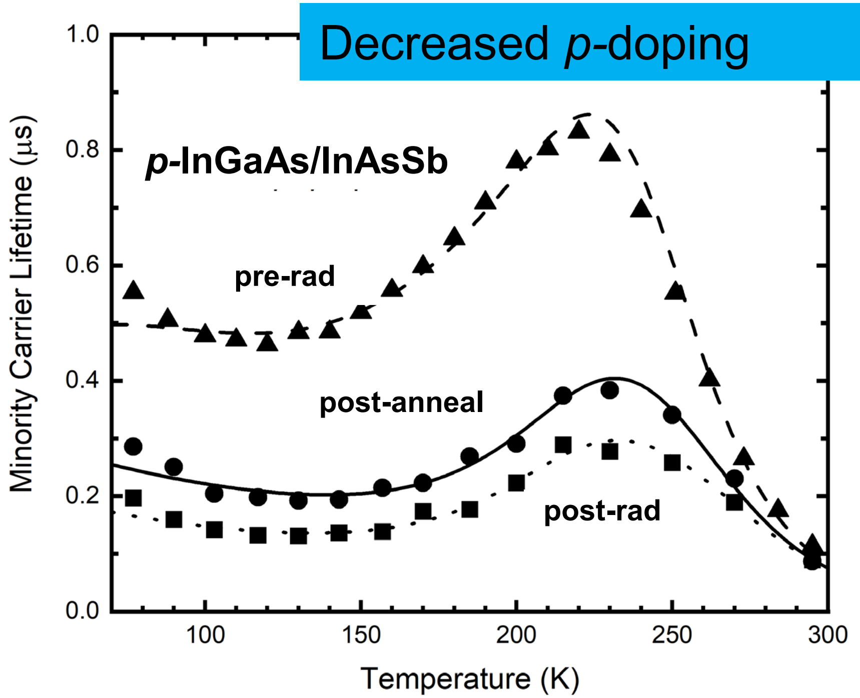

Decreased *p*-doping

Irradiation-induced incorporation of donors

	Irradiation Condition	σN_t (10^{-2} cm^{-1})	Doping ($\times 10^{15}$ cm^{-3})
p-InGaAs/InAsSb	Pre-Rad	4.21	7.8
	Post-Rad	15.9	3.2
	Post-Anneal	10.4	3.9
n-InGaAs/InAsSb	Pre-Rad	18.4	3.6
	Post-Rad	34.4	7.1
	Post-Anneal	27.7	3.9

Inf. Phys. Technol. **97**, 448 (2019)
Appl. Phys. Lett. **108**, 263504 (2016)

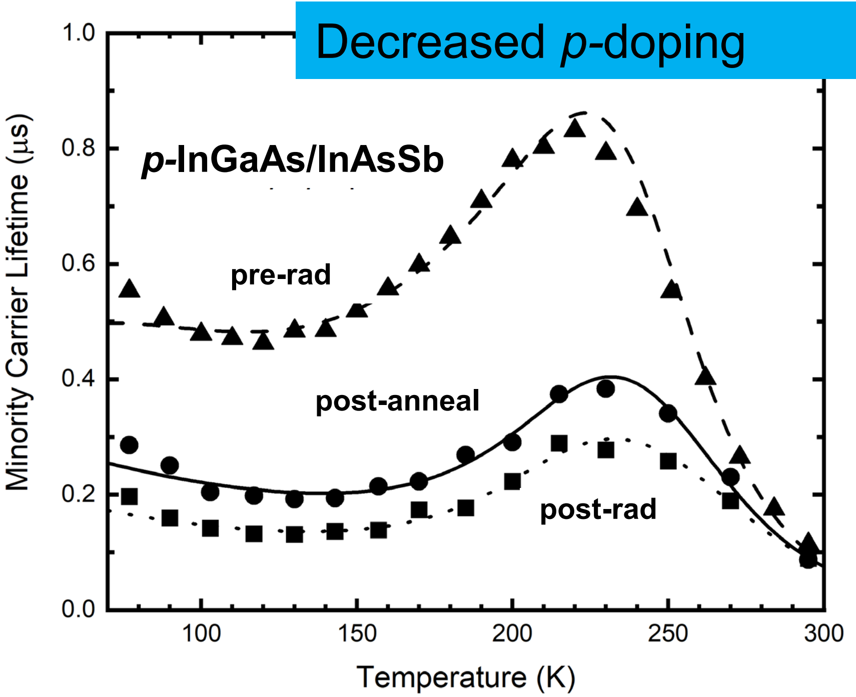

Decreased *p*-doping

Asymmetry in doping concentration recovery

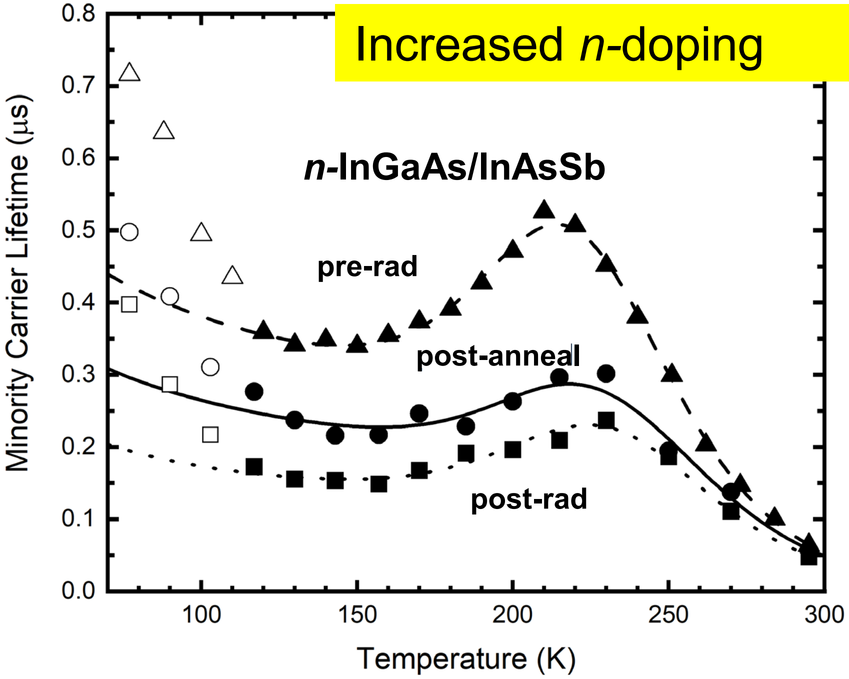

Increased *n*-doping

Overall impact of proton irradiation damage

Irradiation Condition	Doping ($\times 10^{15}$ cm^{-3})
p-InGaAs/InAsSb (PreRad)	7.8
p-InGaAs/InAsSb (Post-Anneal)	3.9
n-InGaAs/InAsSb (PreRad)	3.6
n-InGaAs/InAsSb (Post-Anneal)	3.9

Permanent decrease in p-side acceptor concentration N_A leads to larger depletion in *p*-side absorber ($W_p' > W_p$)

- Full recovery in quantum efficiency post-anneal due to reduction in thickness of the quasi-neutral p-region ($d_p' < d_p$)
- Negligible recovery in dark current post-anneal due to increase in acceptor concentration N_A

Pre-rad *pn*-junction

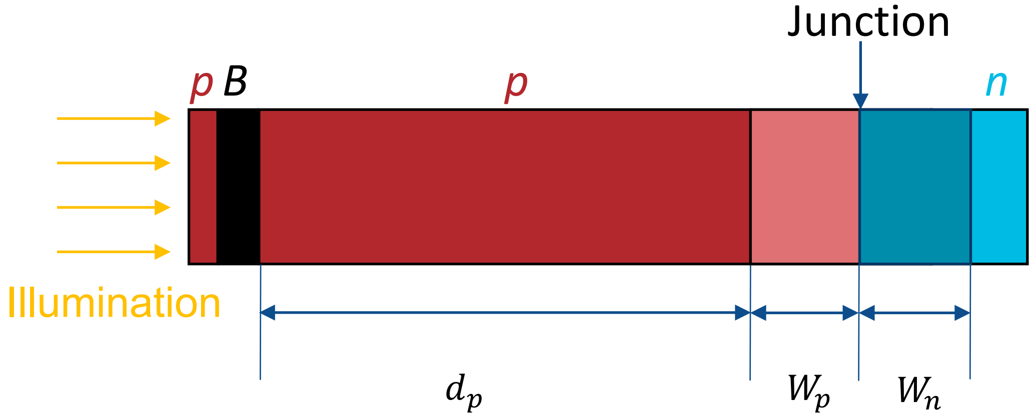

Post-anneal *pn*-junction

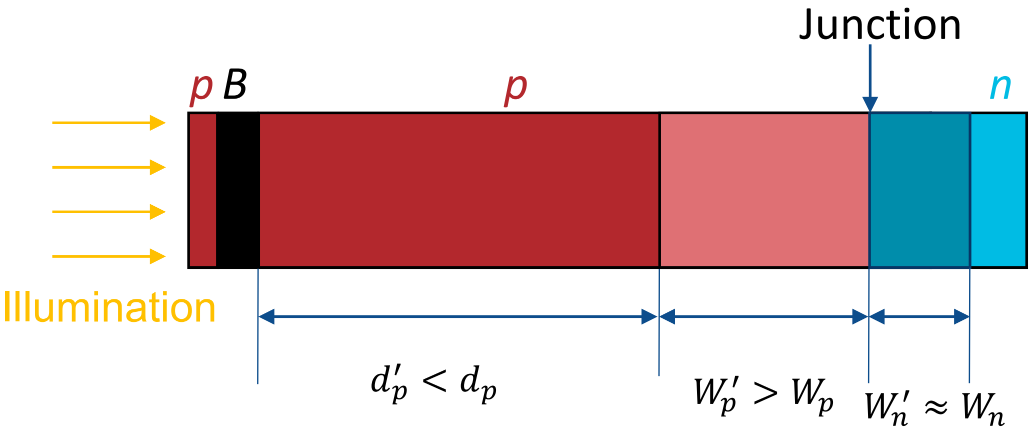

$$\eta \approx \overbrace{\left(\frac{\alpha^2 L_D^2}{\alpha^2 L_D^2 - 1}\right)\left[1-\left(1+\frac{\alpha d_p}{\alpha^2 L_D^2}\right)e^{-\alpha d_p}\right]}^{\text{From } p\text{-region}} + \overbrace{\left[e^{-\alpha d_p} - e^{-\alpha(d_p + W_D)}\right]}^{\text{From depletion region}}$$

$$J_{diffusion} = \frac{q n_i^2 d_p}{N_A \tau_{MC}}$$

Carrasco *et al.*, J. Appl. Phys. **130**, 114501 (2021)

Conclusions: part I

- Complete recovery of irradiation-induced QE degradation after anneal (~50% typical in *nBn*)
- Dark current and dark current damage factor typical of *nBn*'s; but negligible recovery in dark-current
- Materials-level characterization and application of fundamental physics led to the discovery of irradiation-induced doping and asymmetric recovery with anneal, explaining the anomalously high device performance

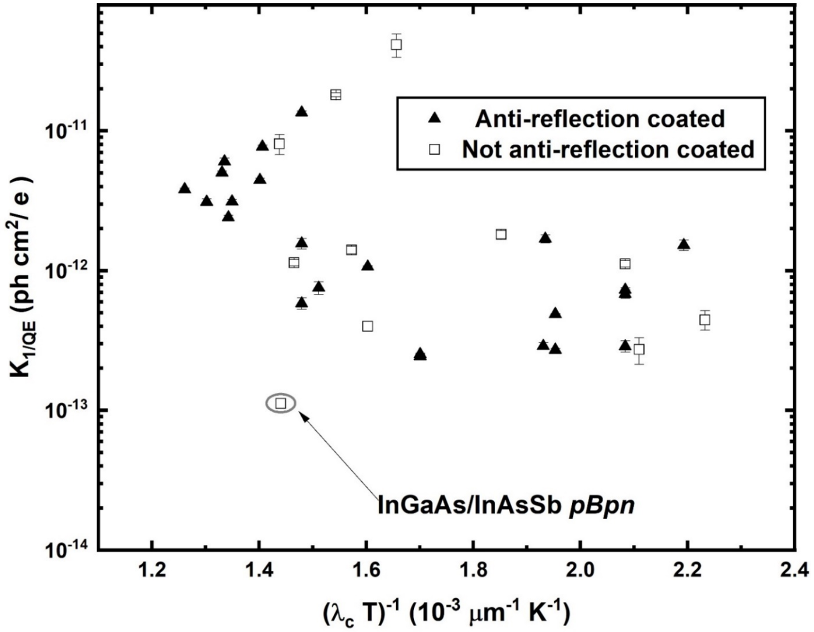

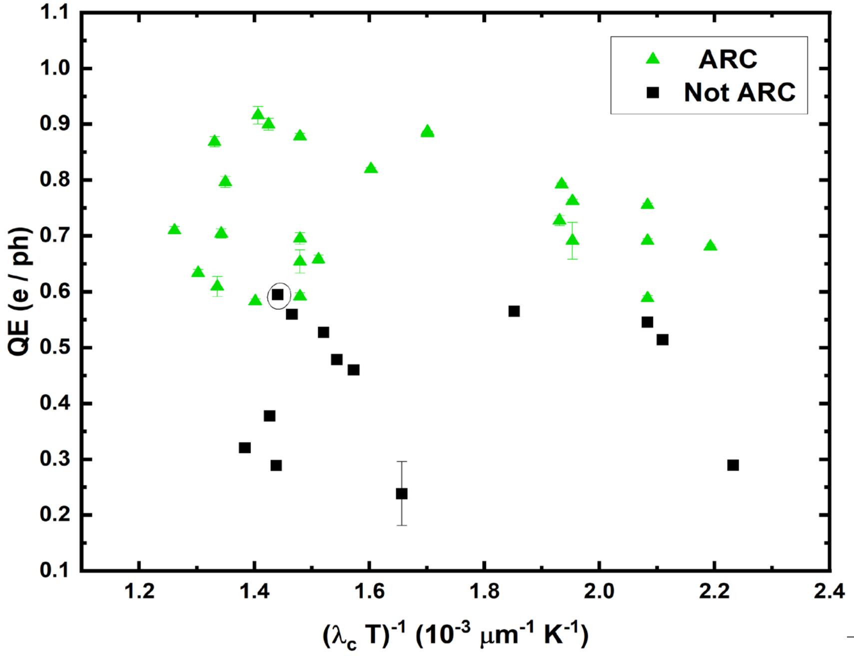

Low-cost, high yield material solutions needed to satisfy satellite-based sensing

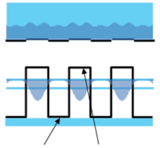

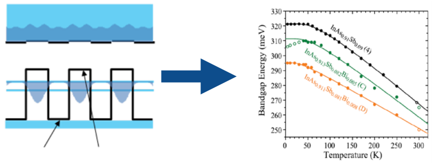

- A III-V superlattice solution to mid-wave infrared sensing

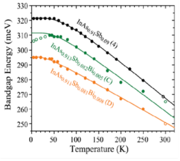

- **A bulk III-V solution to mid-wave infrared sensing**
  - ➢ Quinary GaInAsSbBi alloys
- **Results**
  - ➢ Photoluminescence and minority carrier lifetime of quinary GaInAsSbBi

- **A group IV solution to mid-wave infrared sensing**

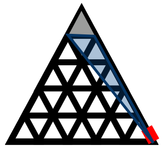

- **Beyond mid-wave materials and toward topological quantum materials**

A bulk III-V alloy solution to mid-wave sensing

- 5 µm cutoff photodetectors → heat tracking and space detection

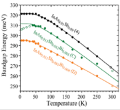

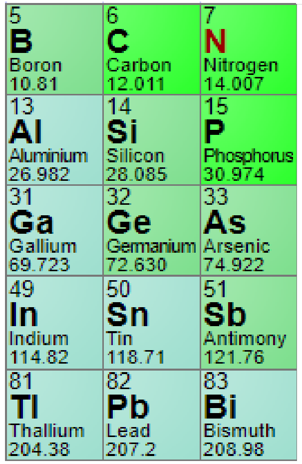

III	IV	V
5 **B** Boron 10.81	6 **C** Carbon 12.011	7 **N** Nitrogen 14.007
13 **Al** Aluminium 26.982	14 **Si** Silicon 28.085	15 **P** Phosphorus 30.974
31 **Ga** Gallium 69.723	32 **Ge** Germanium 72.630	33 **As** Arsenic 74.922
49 **In** Indium 114.82	50 **Sn** Tin 118.71	51 **Sb** Antimony 121.76
81 **Tl** Thallium 204.38	82 **Pb** Lead 207.2	83 **Bi** Bismuth 208.98

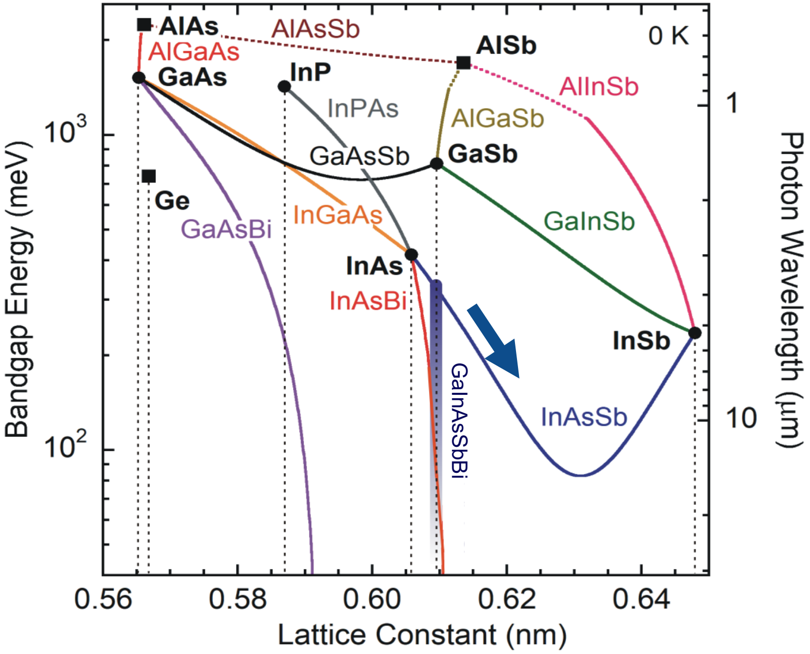

A bulk III-V alloy solution to mid-wave sensing

- 5 µm cutoff photodetectors → heat tracking and space detection
- Quaternary InAsSbBi lowers bandgap of ternary InAsSb considerably[1]
  - ➢ 0.8% Bi extends cutoff by 0.5 μm

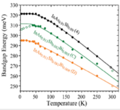

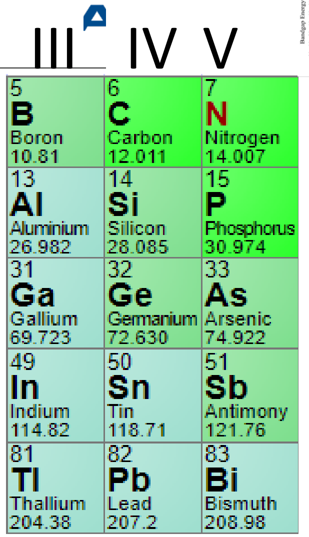

III	IV	V
5 **B** Boron 10.81	6 **C** Carbon 12.011	7 **N** Nitrogen 14.007
13 **Al** Aluminium 26.982	14 **Si** Silicon 28.085	15 **P** Phosphorus 30.974
31 **Ga** Gallium 69.723	32 **Ge** Germanium 72.630	33 **As** Arsenic 74.922
49 **In** Indium 114.82	50 **Sn** Tin 118.71	51 **Sb** Antimony 121.76
81 **Tl** Thallium 204.38	82 **Pb** Lead 207.2	83 **Bi** Bismuth 208.98

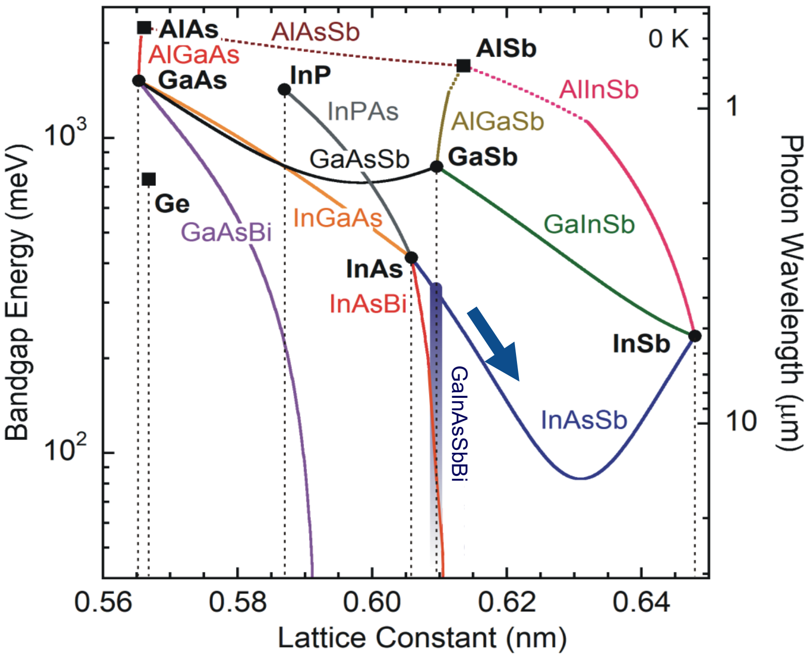

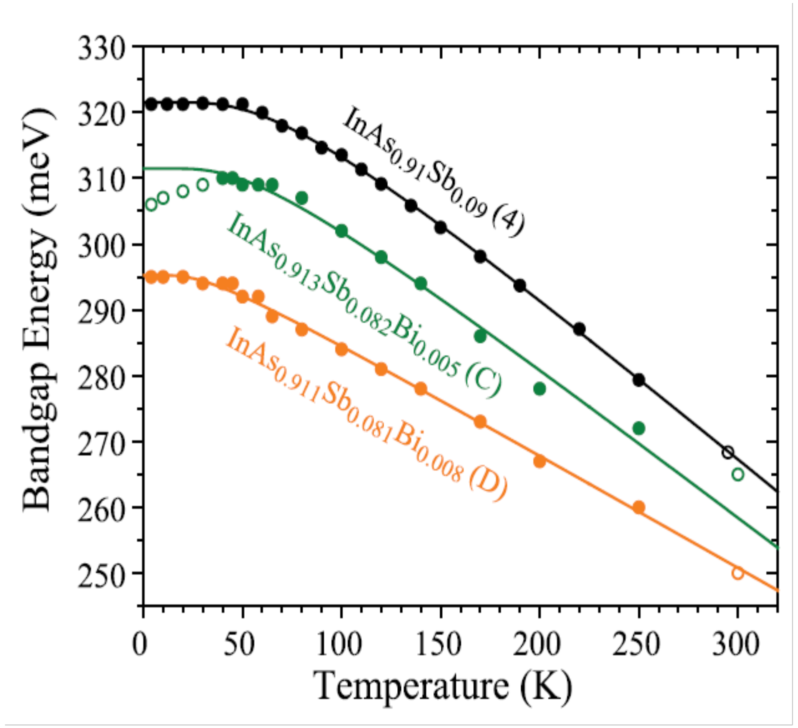

[1] P. Petluru, *et al.*, Appl. Phys. Lett. **117**, 061103 (2020).

A bulk III-V alloy solution to mid-wave sensing

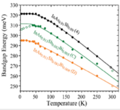

- 5 µm cutoff photodetectors → heat tracking and space detection
- Quaternary InAsSbBi lowers bandgap of ternary InAsSb considerably[1]
    - ➢ 0.8% Bi extends cutoff by 0.5 μm
- Low growth temperatures necessary to incorporate enough Bi
    - ➢ Low growth temperatures decrease minority carrier lifetime
- GaAsBi is typically grown at higher temperatures with easier Bi incorporation[2]

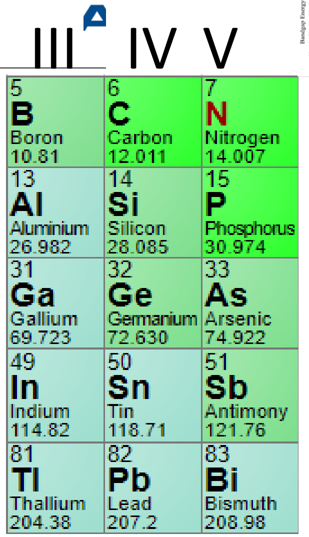

III	IV	V
5 **B** Boron 10.81	6 **C** Carbon 12.011	7 **N** Nitrogen 14.007
13 **Al** Aluminium 26.982	14 **Si** Silicon 28.085	15 **P** Phosphorus 30.974
31 **Ga** Gallium 69.723	32 **Ge** Germanium 72.630	33 **As** Arsenic 74.922
49 **In** Indium 114.82	50 **Sn** Tin 118.71	51 **Sb** Antimony 121.76
81 **Tl** Thallium 204.38	82 **Pb** Lead 207.2	83 **Bi** Bismuth 208.98

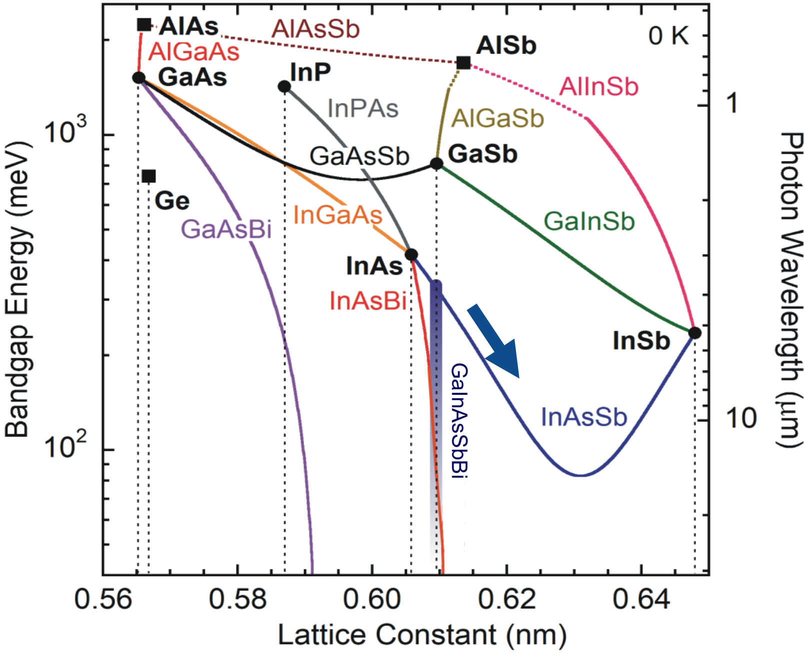

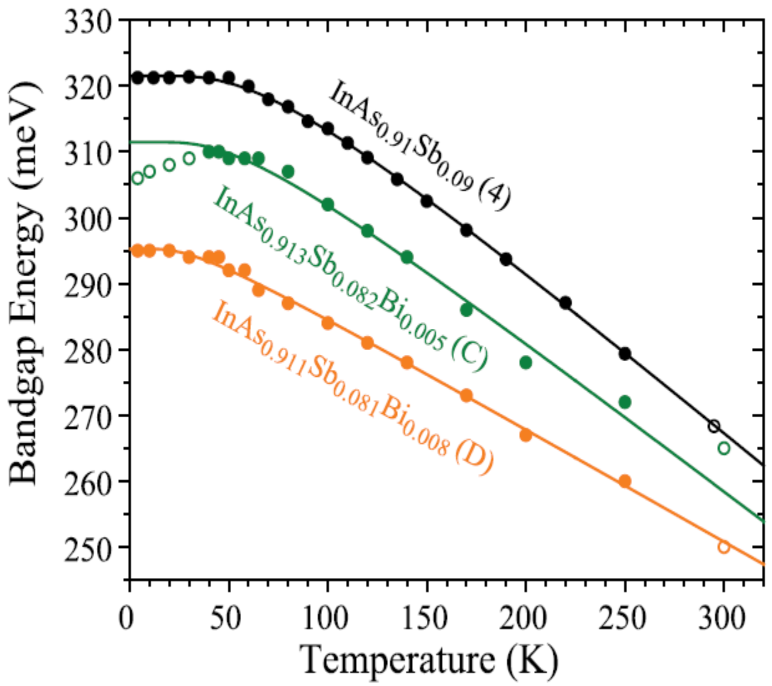

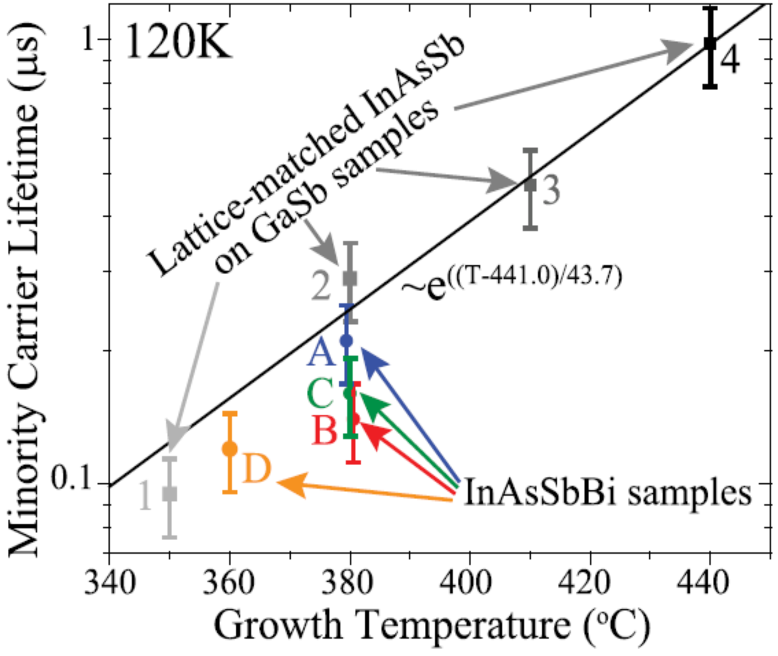

[1] P. Petluru, *et al.*, Appl. Phys. Lett. **117**, 061103 (2020).
[2] V. B.-Yekta, *et al.*, Semicond. Sci. Technol. **30**, 094007 (2015).

Surface and crystal quality of GaInAsSbBi

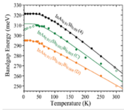

- Droplet free quinary evidenced by smooth Normarski
- Increased strain state tunability of alloy with inclusion of Ga
- Rutherford backscattering data shows successful inclusion of 0.13% Bi

10x

50x

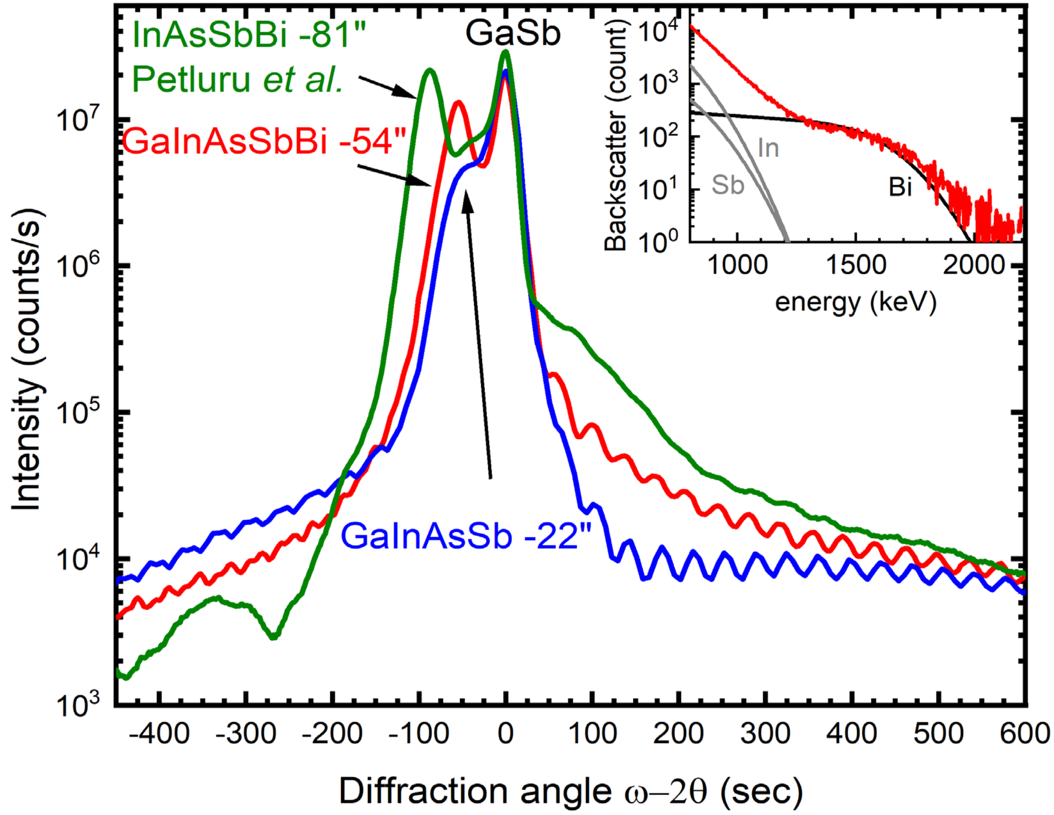

Redshift due to Bi incorporation

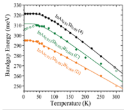

- Incorporating Bi redshifts the band gap of the quaternary
  - ➢ Incorporation at higher growth temperatures shows benefit of adding Ga
  - ➢ Increase in photoluminescence width due to Bi alloy disorder

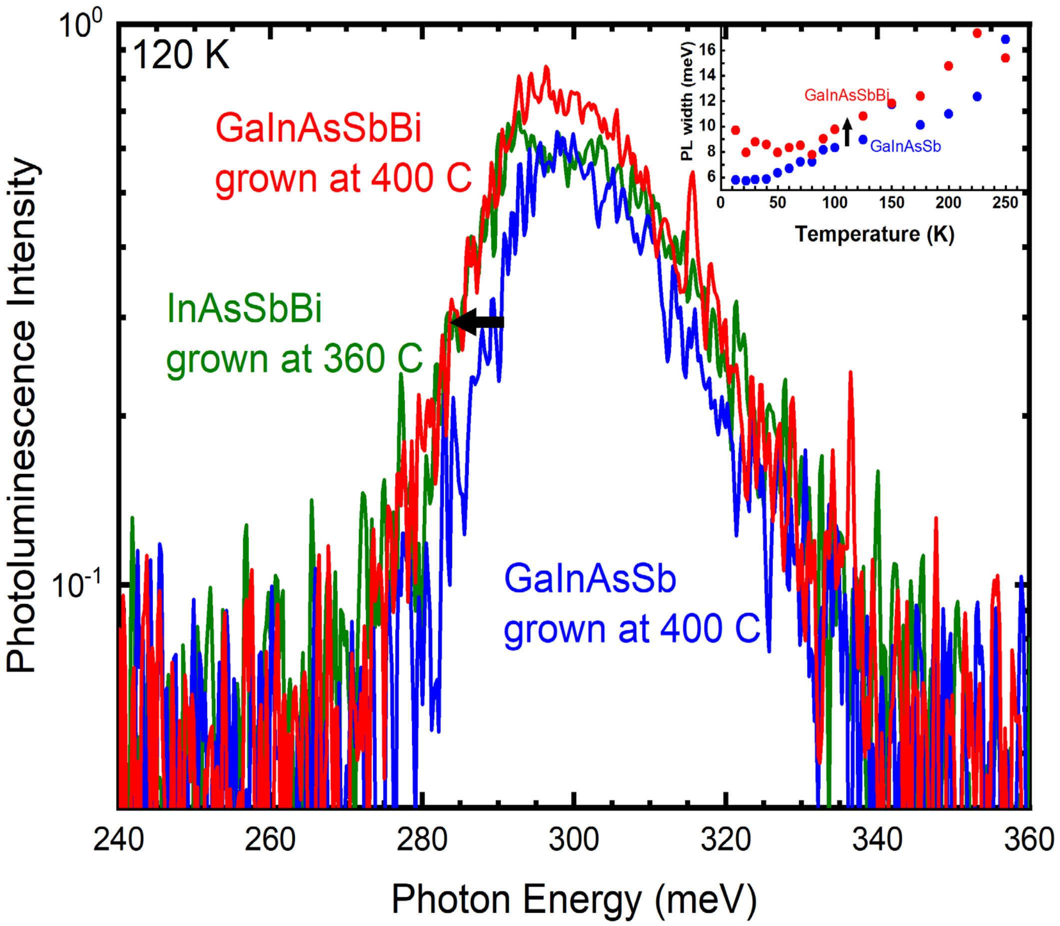

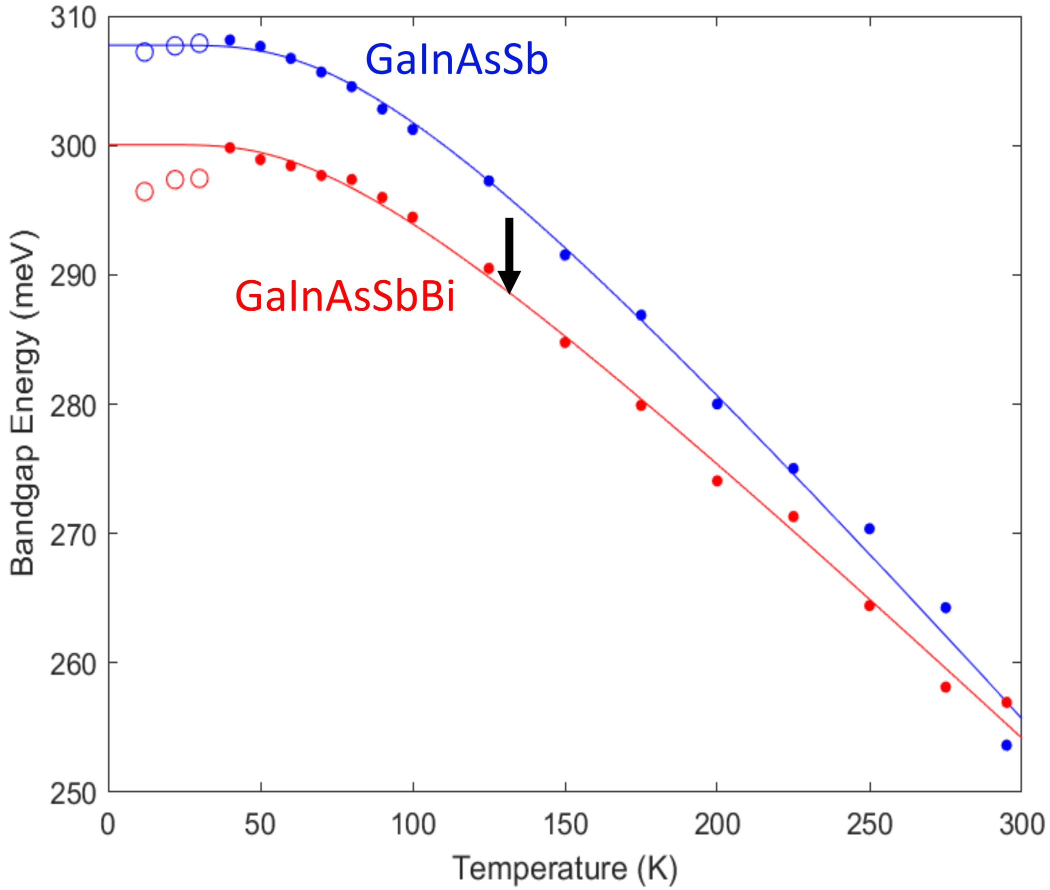

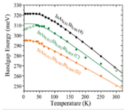

Lifetime improvement due to Bi incorporation

- Incorporating Bi introduces alloy disorder that could cause n-doping
- Bi as a surfactant may have caused improvement in minority carrier lifetime

Sample	Type	Majority Carrier Concentration (cm^{-3})	$E_c - E_t$ (meV)	σN_t (10^{-2} cm^{-1})
GaInAsSb	*n*-type	6.08×10^{14}	73.9	86.3
GaInAsSbBi	*n*-type	8.60×10^{14}	96.6	24.3

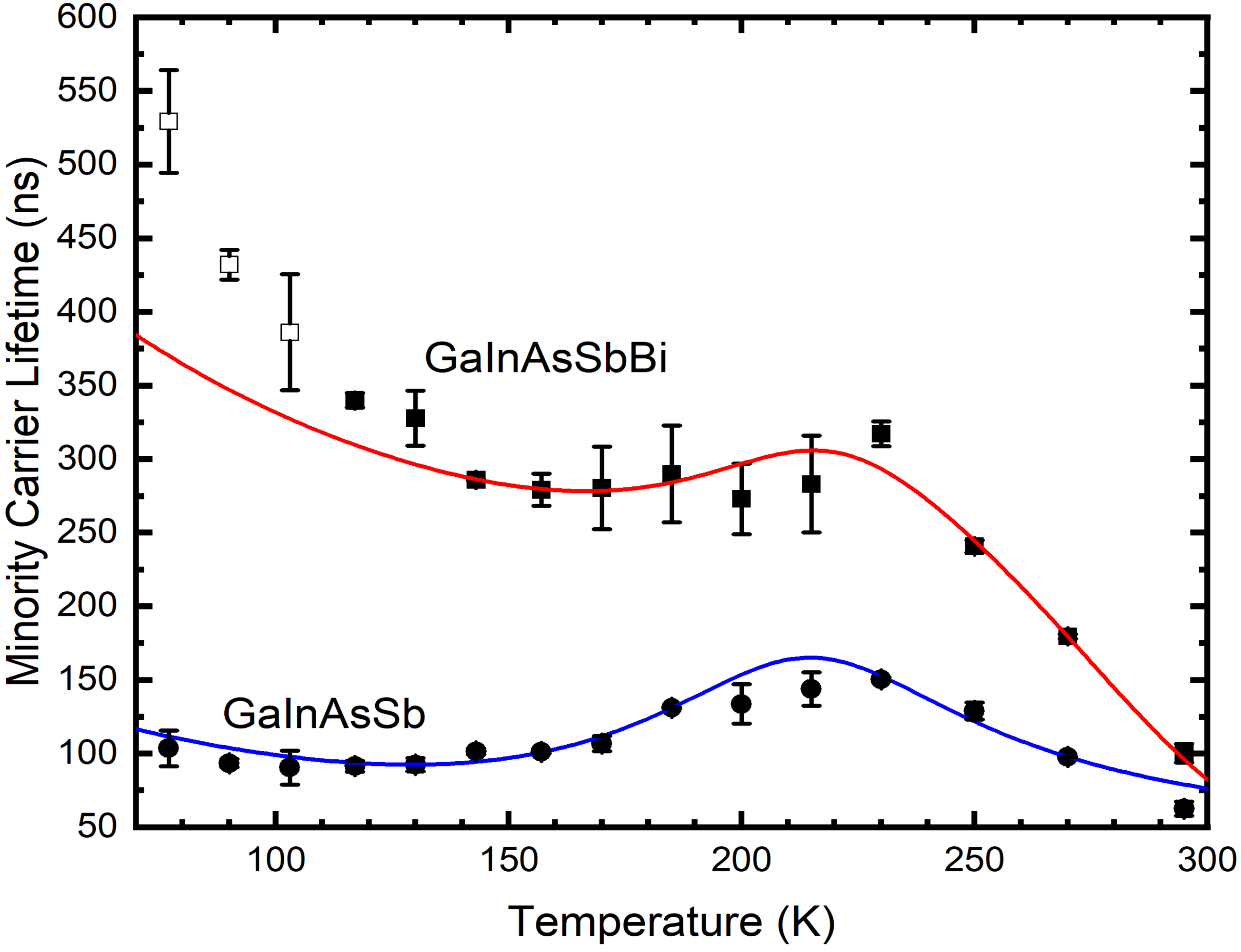

Carrasco *et al.*, J. Appl. Phys. **129**, 184501 (2021); Carrasco *et al.*, Appl. Phys. Lett. (in progress)

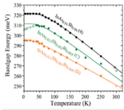

Conclusions: part II

- **Quinary GaInAsSbBi was grown at 400 C by MBE for the first time**
- Higher growth temperature allows for better optical quality of III-V bismide
- Incorporating Ga allows for easier Bi incorporation

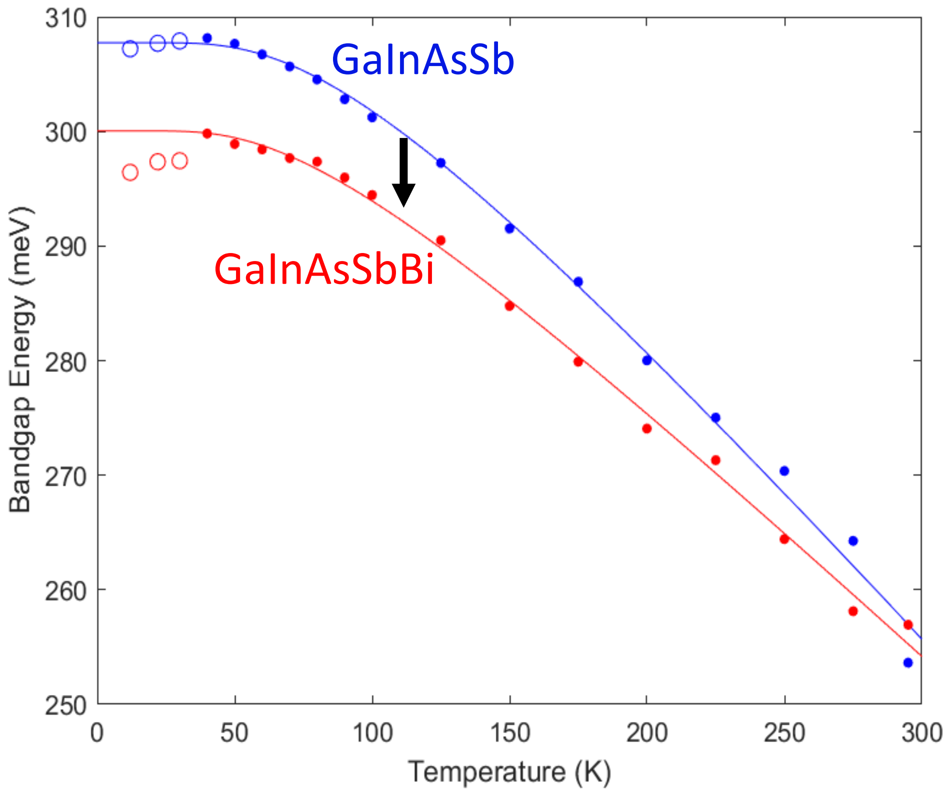

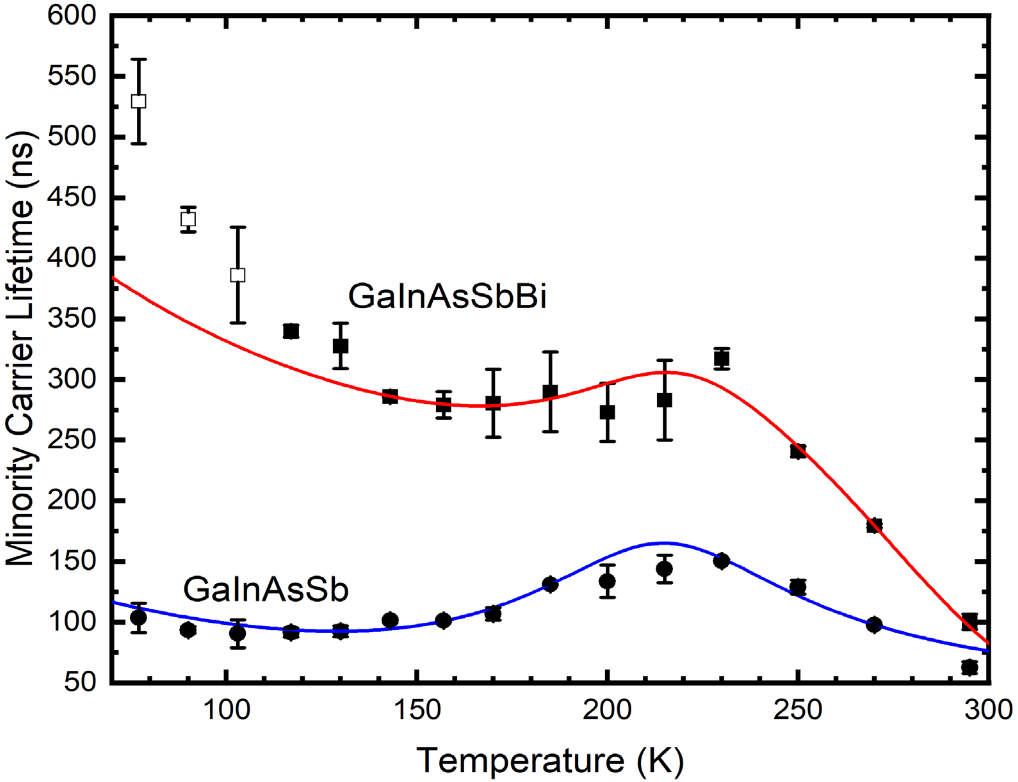

Low-cost, high yield material solutions needed to satisfy satellite-based sensing

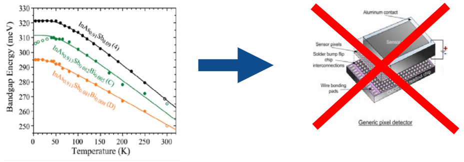

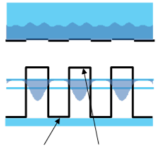

- A III-V superlattice solution to mid-wave infrared sensing

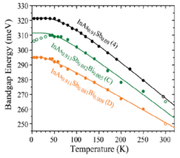

- A bulk III-V solution to mid-wave infrared sensing

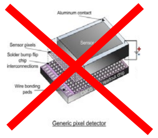

- **A group IV solution to mid-wave infrared sensing**
  - GeSn alloys with Sn contents $\leq 27\%$
- **Methods**
  - Spectroscopic ellipsometry
- **Results**
  - Dielectric function and critical points of GeSn alloys

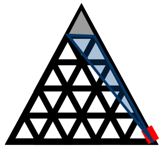

- **Beyond mid-wave materials and toward topological quantum materials**

A group IV solution to mid-wave sensing

- Group IV material can monolithically integrate to Si integrated circuits
  - No antiphase domains (growing group III-V on Si)
  - Potential for not using In bump bonds during device processing (avoid antiphase domains of group III-V growth)

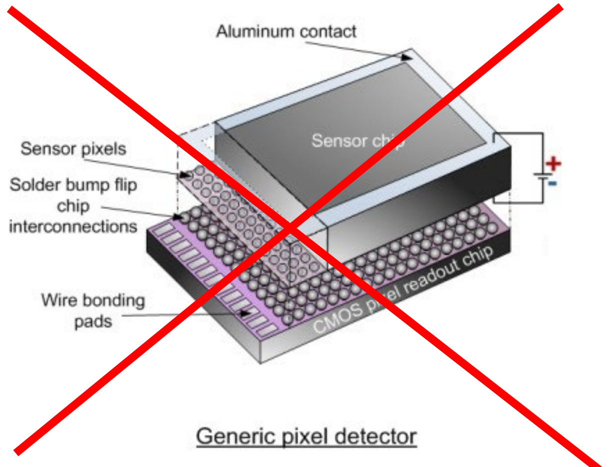

Generic pixel detector

http://x-ray.camera/technology/flip-chip-bonding/

III = IV V

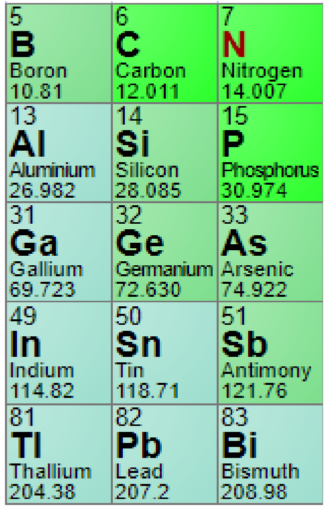

5 **B** Boron 10.81	6 **C** Carbon 12.011	7 **N** Nitrogen 14.007
13 **Al** Aluminium 26.982	14 **Si** Silicon 28.085	15 **P** Phosphorus 30.974
31 **Ga** Gallium 69.723	32 **Ge** Germanium 72.630	33 **As** Arsenic 74.922
49 **In** Indium 114.82	50 **Sn** Tin 118.71	51 **Sb** Antimony 121.76
81 **Tl** Thallium 204.38	82 **Pb** Lead 207.2	83 **Bi** Bismuth 208.98

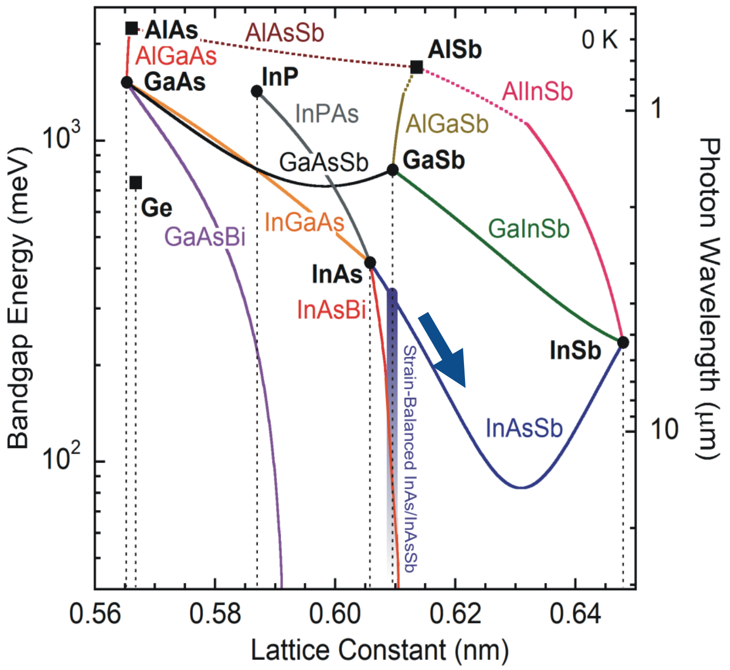

switch to linear scale →

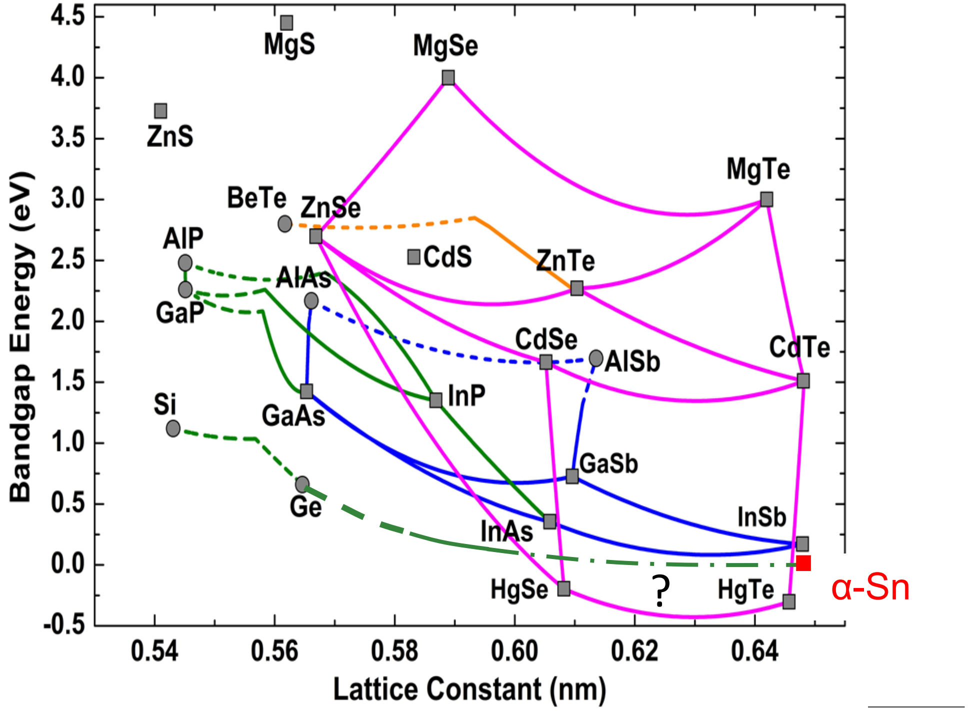

Spectroscopic ellipsometry

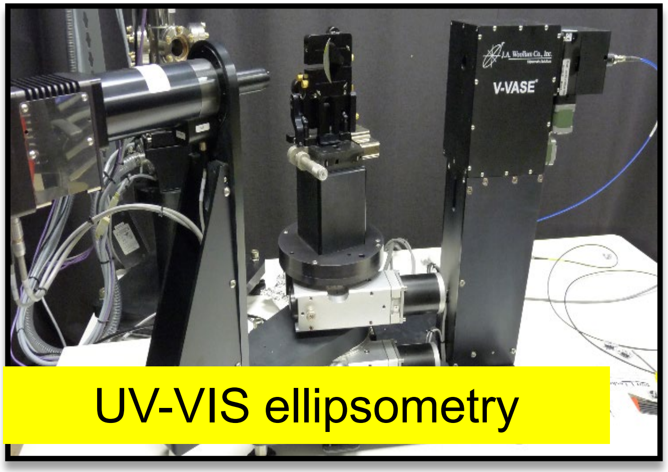

UV-VIS ellipsometry

- Measures:
  - 0.50 – 6.5 eV in 0.01 eV steps (2.4 µm - 191 nm)
- Results:
  - $\tilde{\epsilon}(\omega)=\epsilon_1(\omega)+i\epsilon_2(\omega)$
  - Band gaps
  - Interband transitions

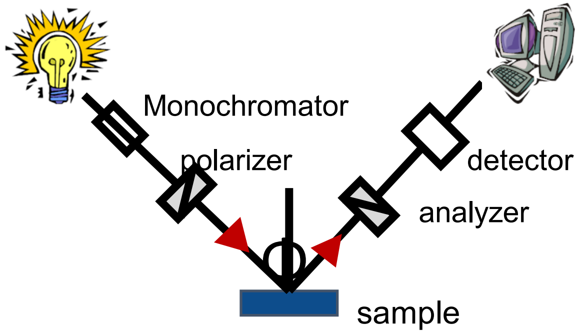

Spectroscopic ellipsometry

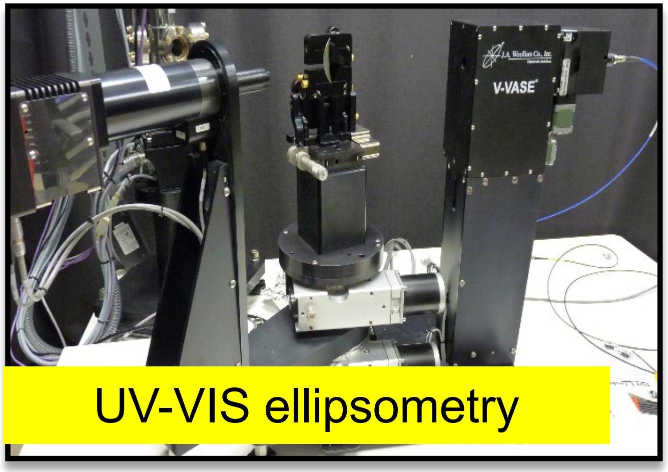

UV-VIS ellipsometry

- Measures:
  - 0.50 – 6.5 eV in 0.01 eV steps (2.4 µm - 191 nm)
- Results:
  - $\tilde{\epsilon}(\omega)=\epsilon_1(\omega)+i\epsilon_2(\omega)$
  - Band gaps
  - Interband transitions

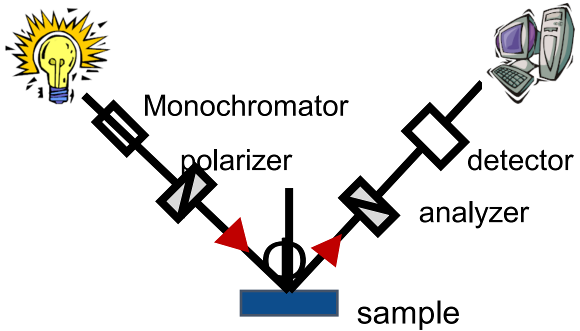

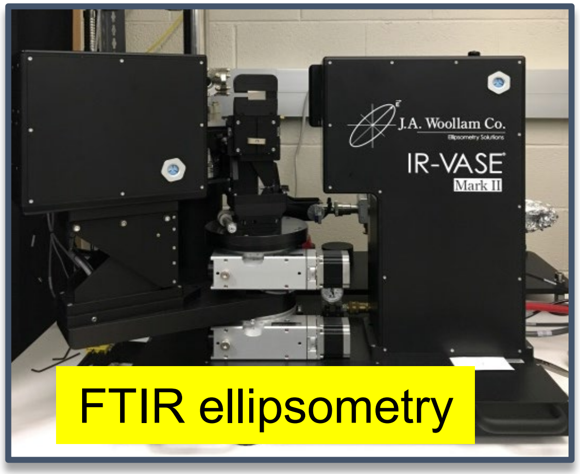

FTIR ellipsometry

- Measures:
  - 0.03 – 0.70 eV (40 - 1.8 µm)
- Results:
  - $\tilde{\epsilon}(\omega)=\epsilon_1(\omega)+i\epsilon_2(\omega)$
  - ~~IR phonon vibrations~~
  - Narrow band gaps
  - Free-carrier absorption

Spectroscopic ellipsometry

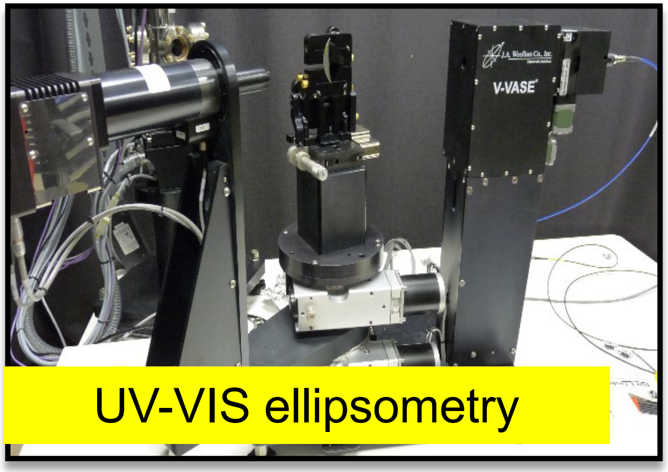

- Measures:
  - 0.50 – 6.5 eV in 0.01 eV steps (2.4 µm - 191 nm)
- Results:
  - $\tilde{\epsilon}(\omega)=\epsilon_1(\omega)+i\epsilon_2(\omega)$
  - Band gaps
  - Interband transitions

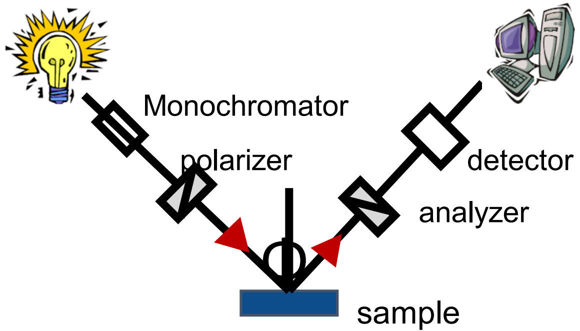

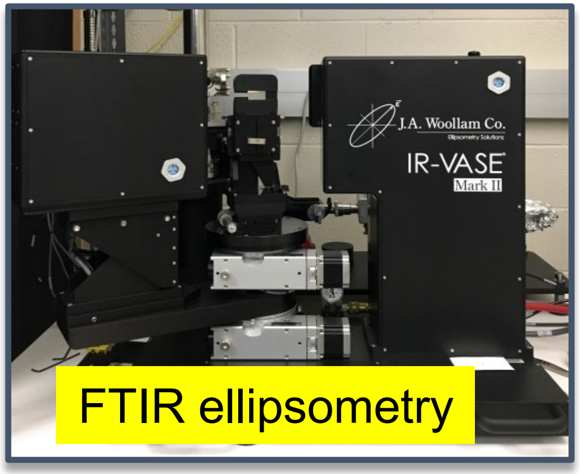

- Measures:
  - 0.03 – 0.70 eV (40 - 1.8 µm)
- Results:
  - $\tilde{\epsilon}(\omega)=\epsilon_1(\omega)+i\epsilon_2(\omega)$
  - ~~IR phonon vibrations~~
  - Narrow band gaps
  - Free-carrier absorption

- Measure $\rho = \tan(\psi)\exp(i\Delta) = r_p/r_s$
- Data modeling required to extract dielectric function $\tilde{\epsilon} = \epsilon_1 + i\epsilon_2$
- With the extracted dielectric function, absorption coefficient α and refractive index *n* can be calculated
  - Absorption is important for determining quantum efficiency η
  - $\eta = \left(\frac{\alpha^2 L_D^2}{1-\alpha^2 L_D^2}\right)\left\{e^{-\alpha L_A} - \frac{1}{\cosh(L_A/L_D)} + \frac{e^{-\alpha L_A}\tanh(L_A/L_D)}{\alpha L_D}\right\}$

Spectroscopic ellipsometry of relaxed films

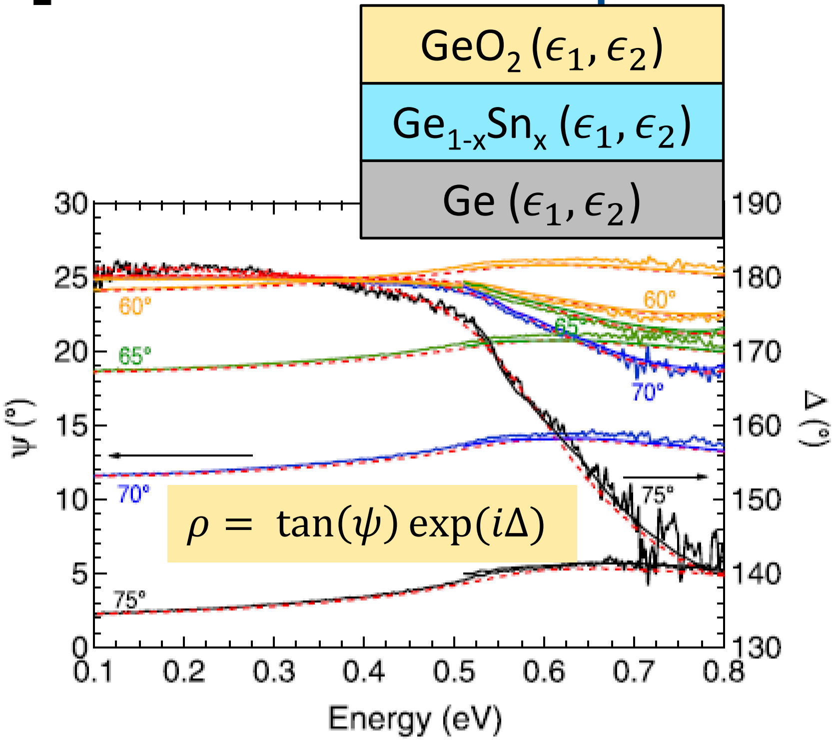

$GeO_2\ (\epsilon_1, \epsilon_2)$

$Ge_{1-x}Sn_x\ (\epsilon_1, \epsilon_2)$

$Ge\ (\epsilon_1, \epsilon_2)$

$$\rho = \tan(\psi)\exp(i\Delta)$$

Example of ellipsometric angles in IR

Fernando *et al.*, J. Vac. Sci. Technol. B. **36**, 021202 (2018)

Spectroscopic ellipsometry of relaxed films

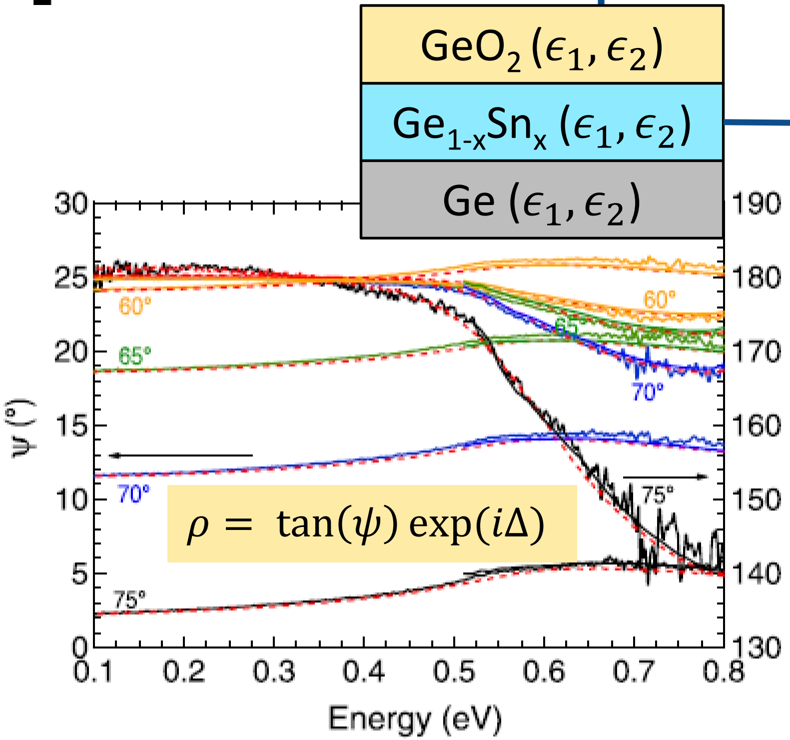

GeO$_2$ (ϵ_1, ϵ_2)

Ge$_{1-x}$Sn$_x$ (ϵ_1, ϵ_2)

Ge (ϵ_1, ϵ_2)

$$\rho = \tan(\psi)\exp(i\Delta)$$

Example of ellipsometric angles in IR

Fernando *et al.*, J. Vac. Sci. Technol. B. **36**, 021202 (2018)

Analyze over full spectral range and as a function of Sn content

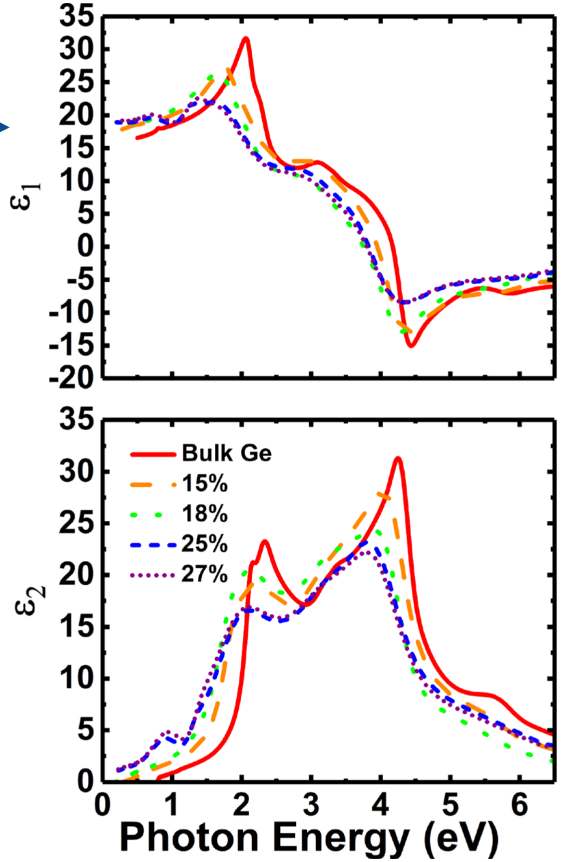

Imbrenda *et al.*, Appl. Phys. Lett. **113**, 122104 (2018)

Spectroscopic ellipsometry of relaxed films

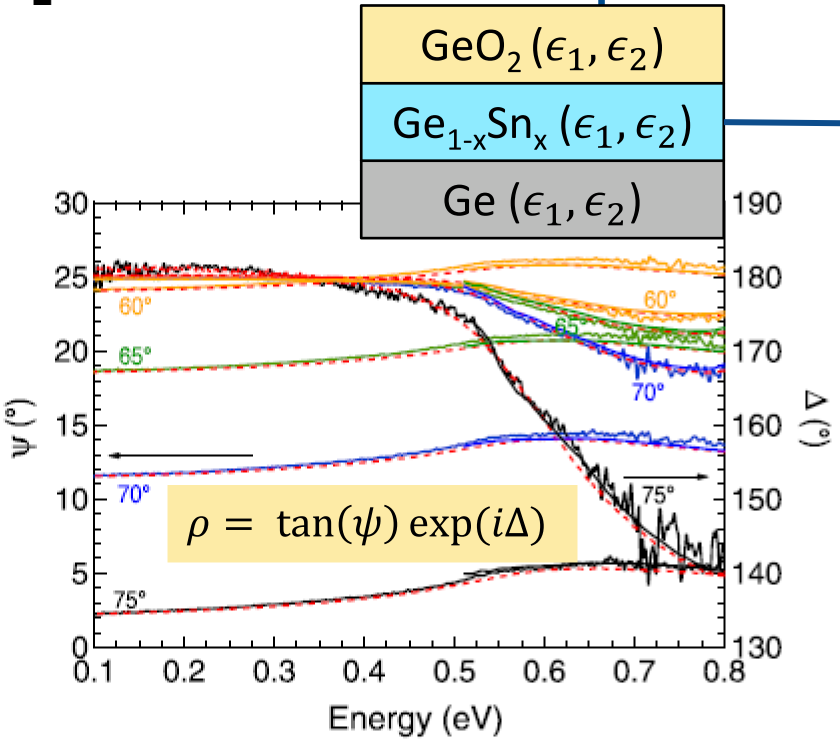

$$\rho = \tan(\psi)\exp(i\Delta)$$

Example of ellipsometric angles in IR

Fernando *et al.*, J. Vac. Sci. Technol. B. **36**, 021202 (2018)

Analyze over full spectral range and as a function of Sn content

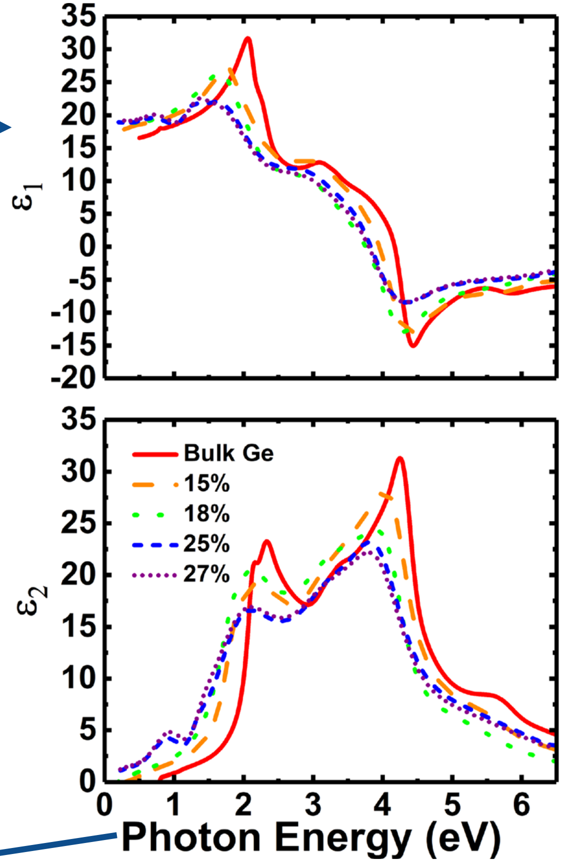

Extract absorption coefficient α

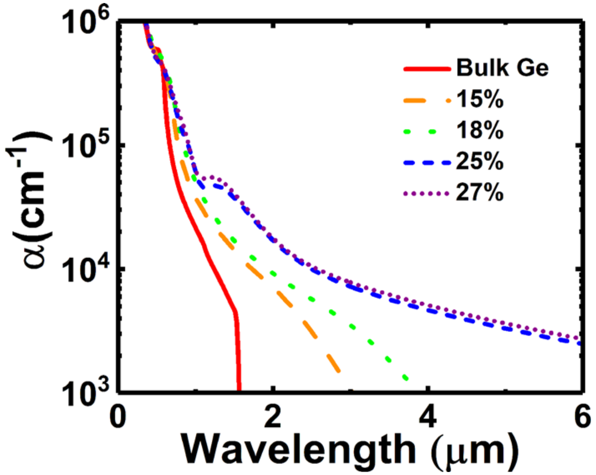

Absorption beyond 6 μm observed

Imbrenda *et al.*, Appl. Phys. Lett. **113**, 122104 (2018)

Direct interband transitions

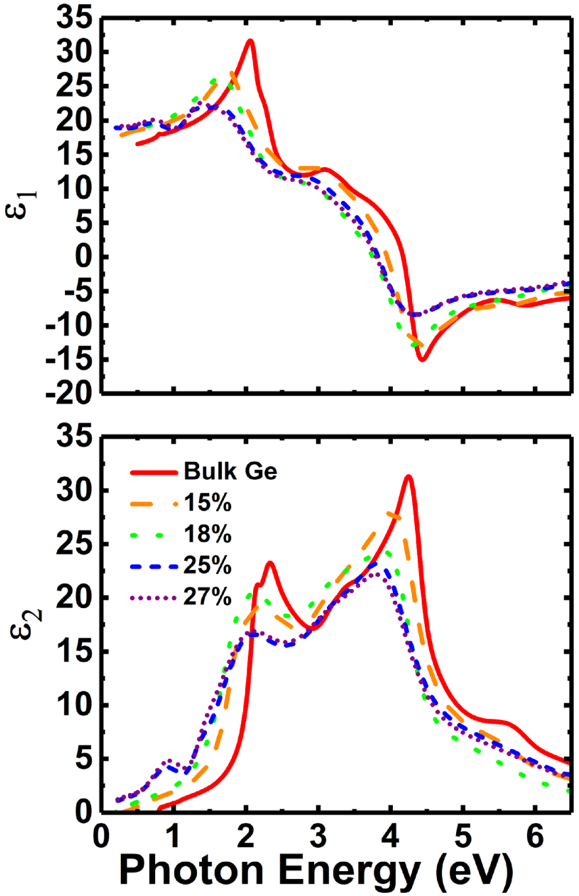

$$\xrightarrow{\dfrac{d^2\epsilon}{dE^2}}$$

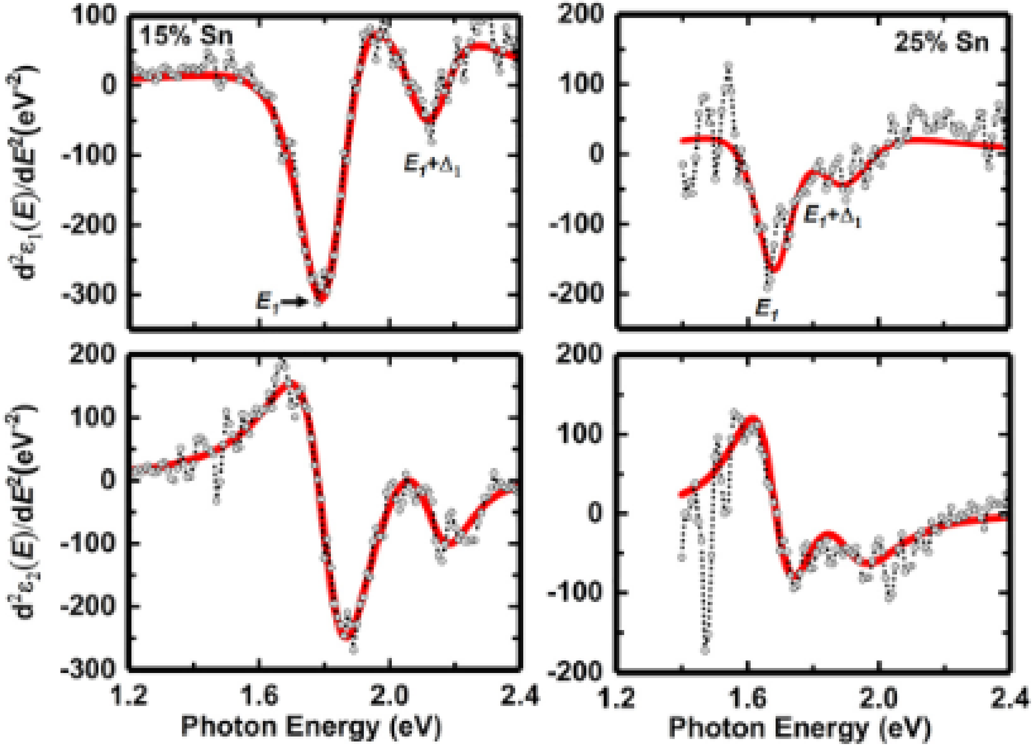

Imbrenda *et al*., Appl. Phys. Lett. **113**, 122104 (2018); Imbrenda *et al*., Appl. Phys. Lett. **119**, 162102 (2021)

Direct interband transitions

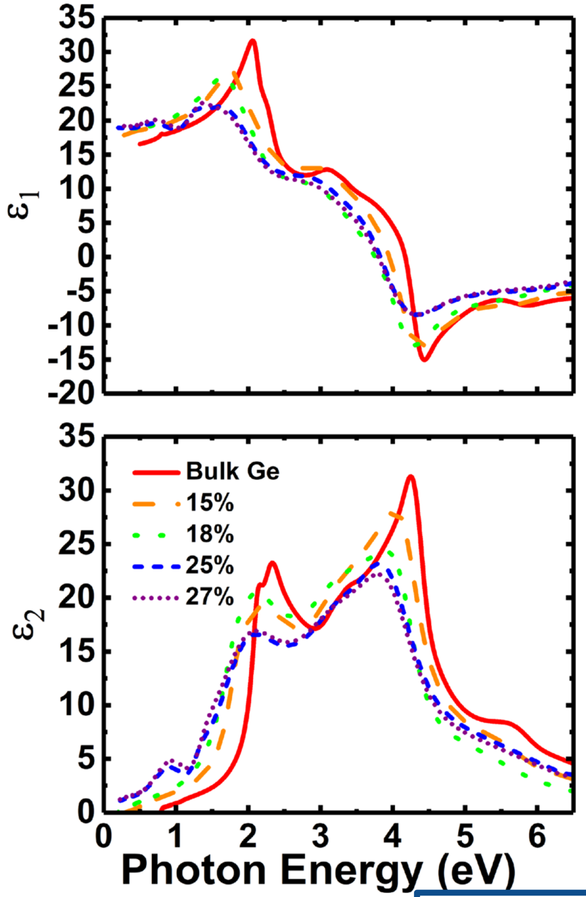

$$\frac{d^2\epsilon}{dE^2}$$

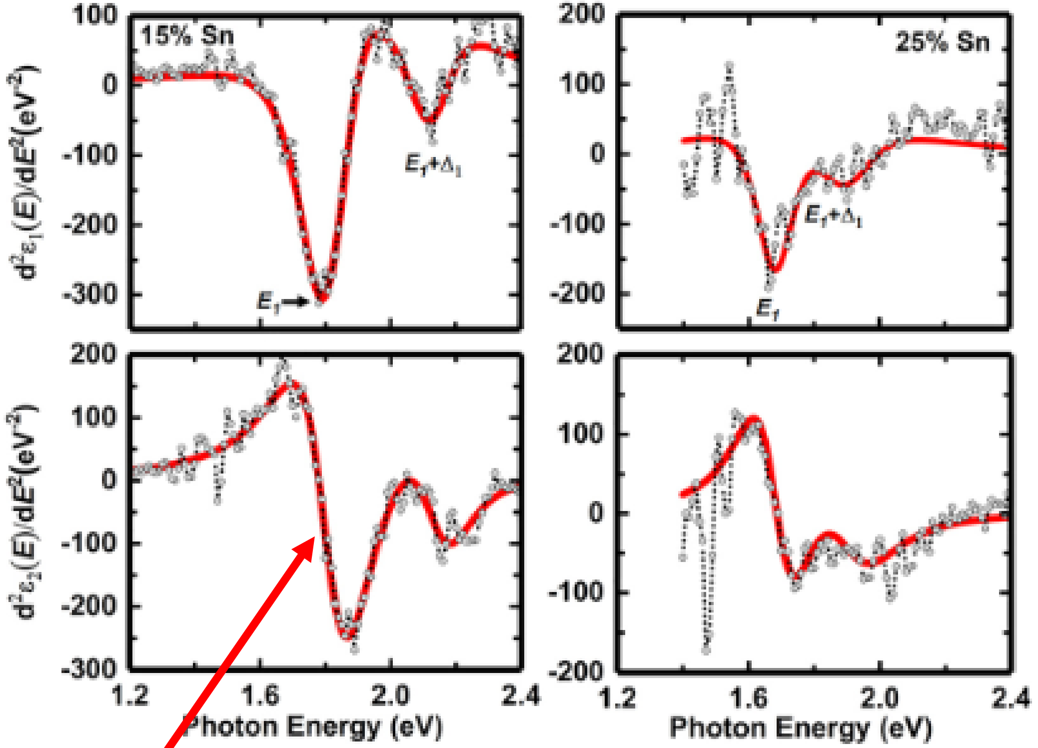

A … amplitude
E … CP energy
Γ … broadening
φ … phase angle
μ ... ”dimension”

μ = 1	0D
μ = 1/2	1D
μ = 0	2D
μ = -1/2	3D

$$\epsilon(\omega) = B - A(\omega - E - i\Gamma)^{-\mu} e^{i\varphi}$$

- Numerical second derivative of complex dielectric function performed.
  - Allows determination of critical point parameters

Imbrenda *et al*., Appl. Phys. Lett. **113**, 122104 (2018); Imbrenda *et al*., Appl. Phys. Lett. **119**, 162102 (2021)

Critical point trends

- Accounting for strain, E_1 and $E_1 + \Delta_1$ critical points red shift toward longer wavelengths, consistent with predictions

$$E_1^s = E_1^r + \frac{\Delta_1}{2} + \Delta E_H - \sqrt{\frac{(\Delta_1)^2}{4} + (\Delta E_S)^2}$$

$$(E_1 + \Delta_1)^s = (E_1 + \Delta_1)^r - \frac{\Delta_1}{2} + \Delta E_H + \sqrt{\frac{(\Delta_1)^2}{4} + (\Delta E_S)^2}$$

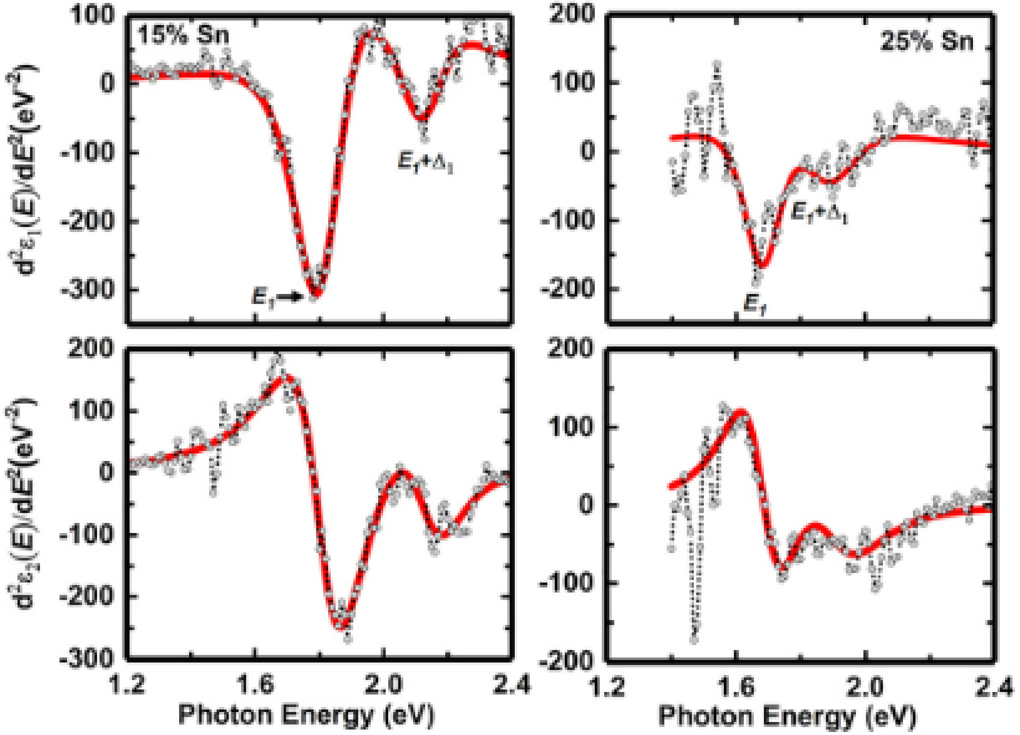

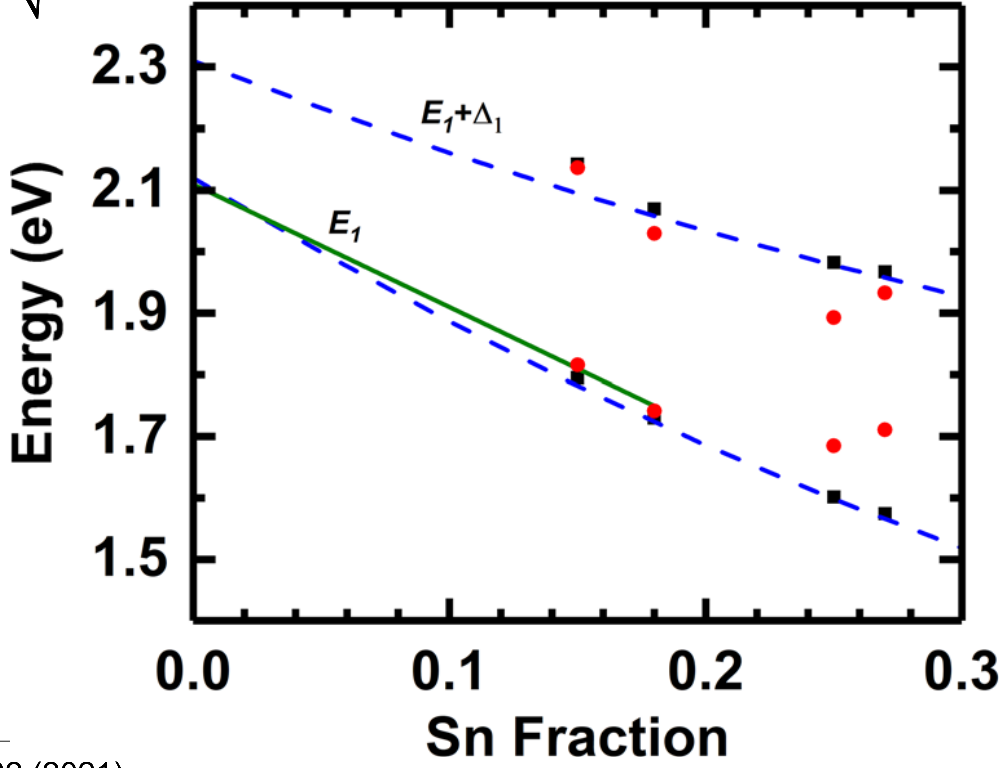

Imbrenda *et al*., Appl. Phys. Lett. **113**, 122104 (2018); Imbrenda *et al*., Appl. Phys. Lett. **119**, 162102 (2021)

Conclusions: part III

- MBE grown GeSn alloys at ~100 ^{o}C
- Absorption observed beyond 6 μm
- E_1 and $E_1 + \Delta_1$ critical points red shift toward longer wavelengths, consistent with predictions

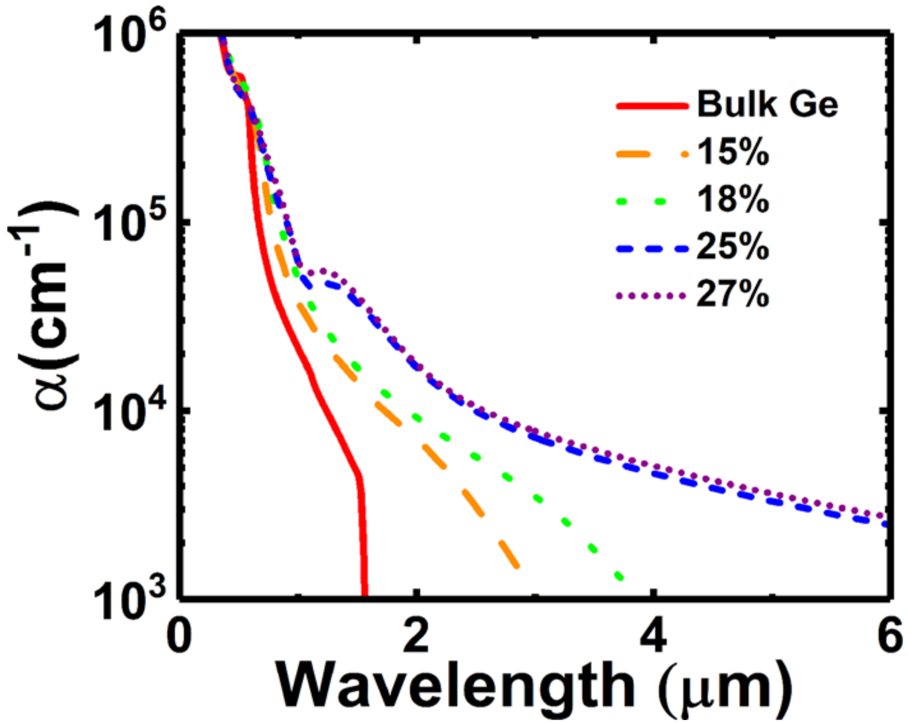

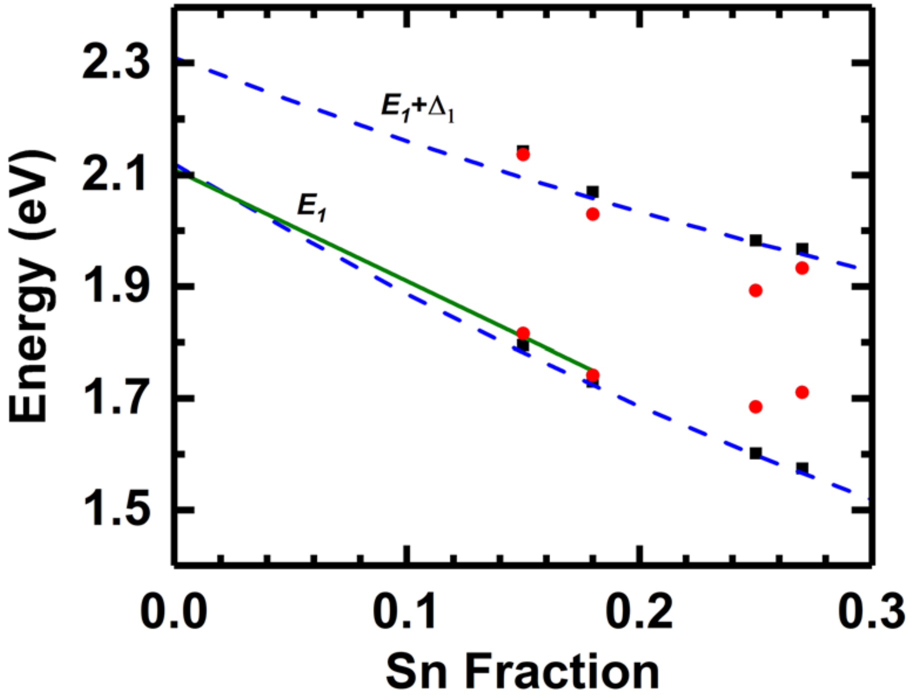

Imbrenda *et al*., Appl. Phys. Lett. **113**, 122104 (2018); Imbrenda *et al*., Appl. Phys. Lett. **119**, 162102 (2021);

Low-cost, high yield material solutions needed to satisfy satellite-based sensing

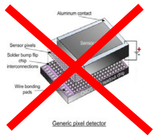

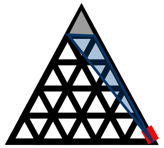

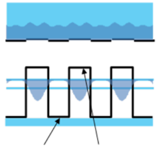

- A III-V superlattice solution to mid-wave infrared sensing

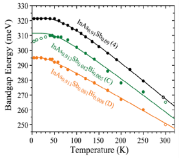

- A bulk III-V solution to mid-wave infrared sensing

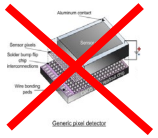

- A group IV solution to mid-wave infrared sensing

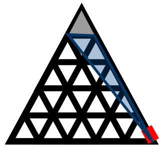

- **Beyond mid-wave materials and toward topological quantum materials**
  - ➢ α-Sn and Sn-rich GeSn alloys with Ge contents $\leq 6\%$
- **Results**
  - ➢ Dielectric function and band structure critical points of α-Sn and Sn-rich GeSn alloys
- **Conclusions and Future work**

Beyond mid-wave sensing

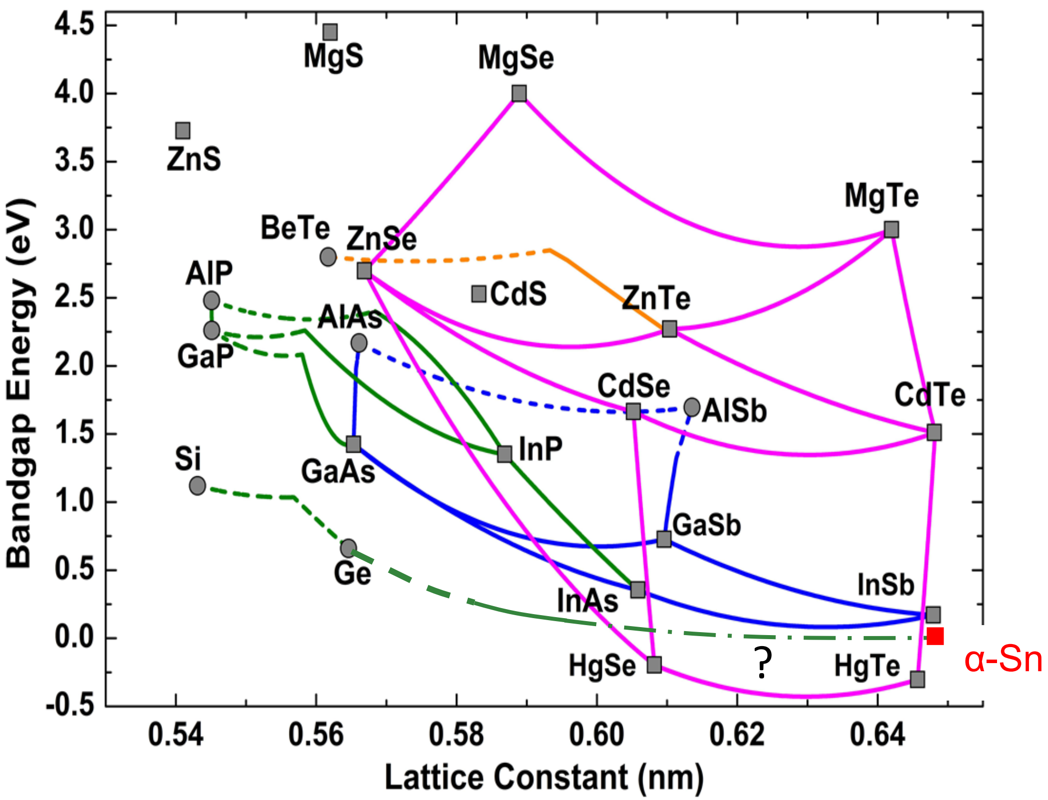

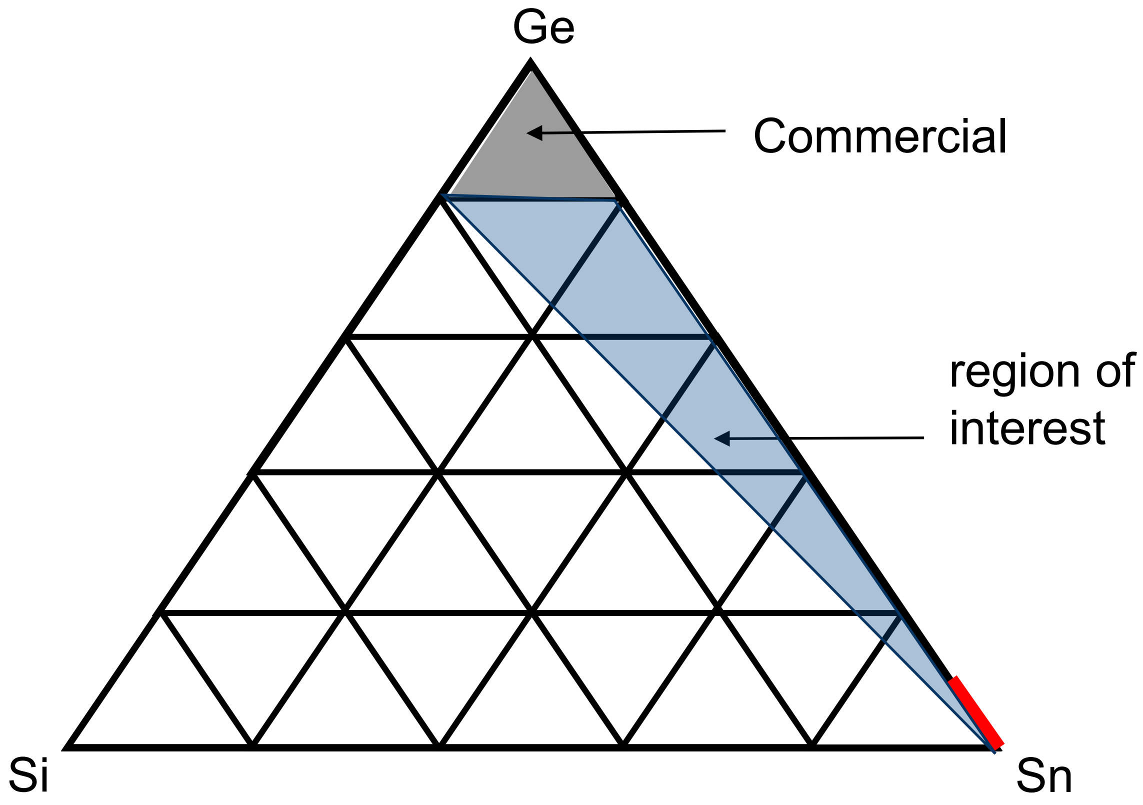

- SiGeSn alloys are of great interest for IR detector applications.
  - Group IV alloys are compatible with Si-CMOS processing.
- Studying the endpoint constituent, α-Sn allows for exploration of the full range of the alloys.
- What's different in a topological insulator?

Band structure of Ge versus α-Sn

Küfner, Nanotechnology **24**, 405702 (2013)

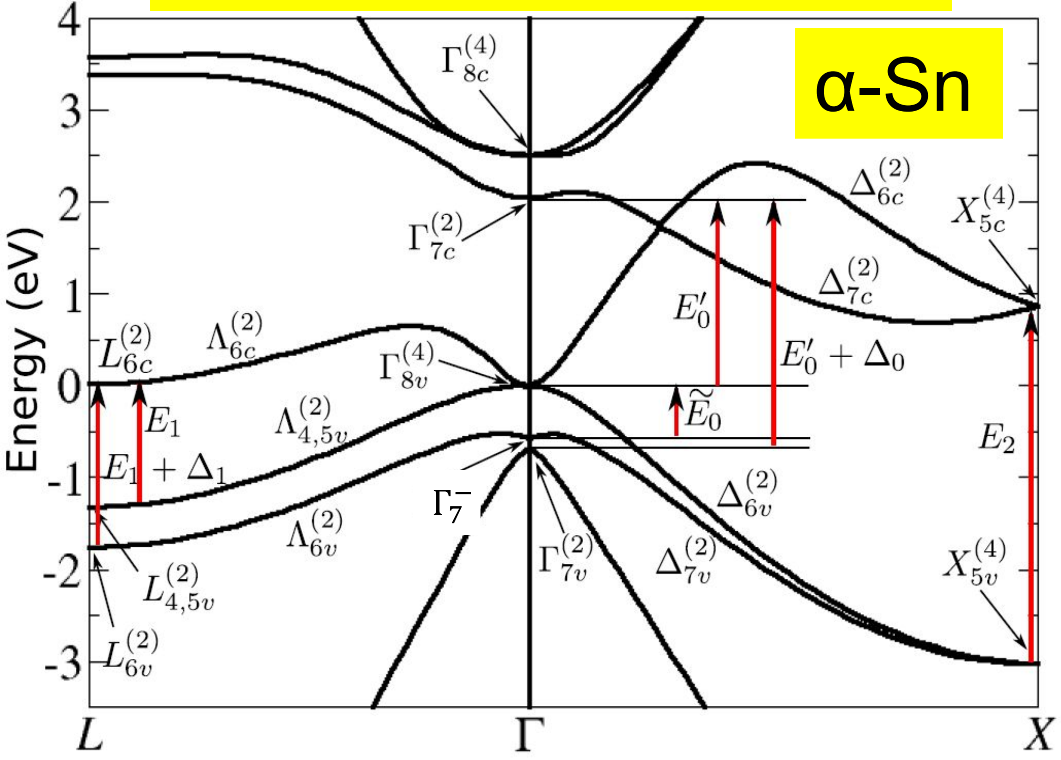

P. Y. Yu, M. Cardona: Fundamentals of Semiconductors. Springer (2010)

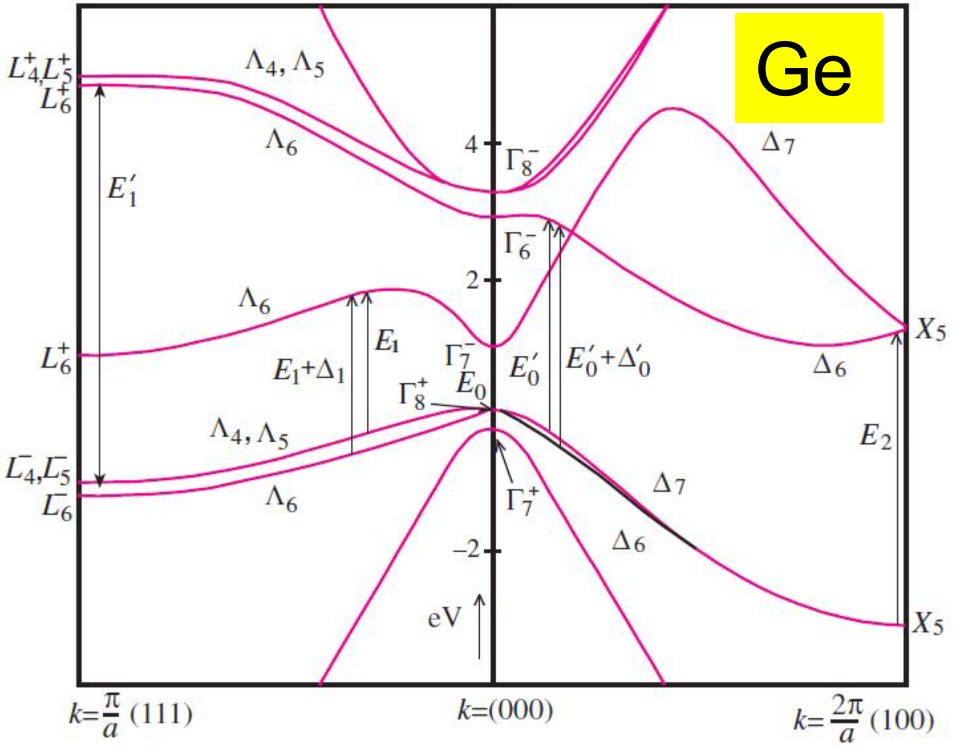

Band structure of Ge versus α-Sn

Küfner, Nanotechnology **24**, 405702 (2013)

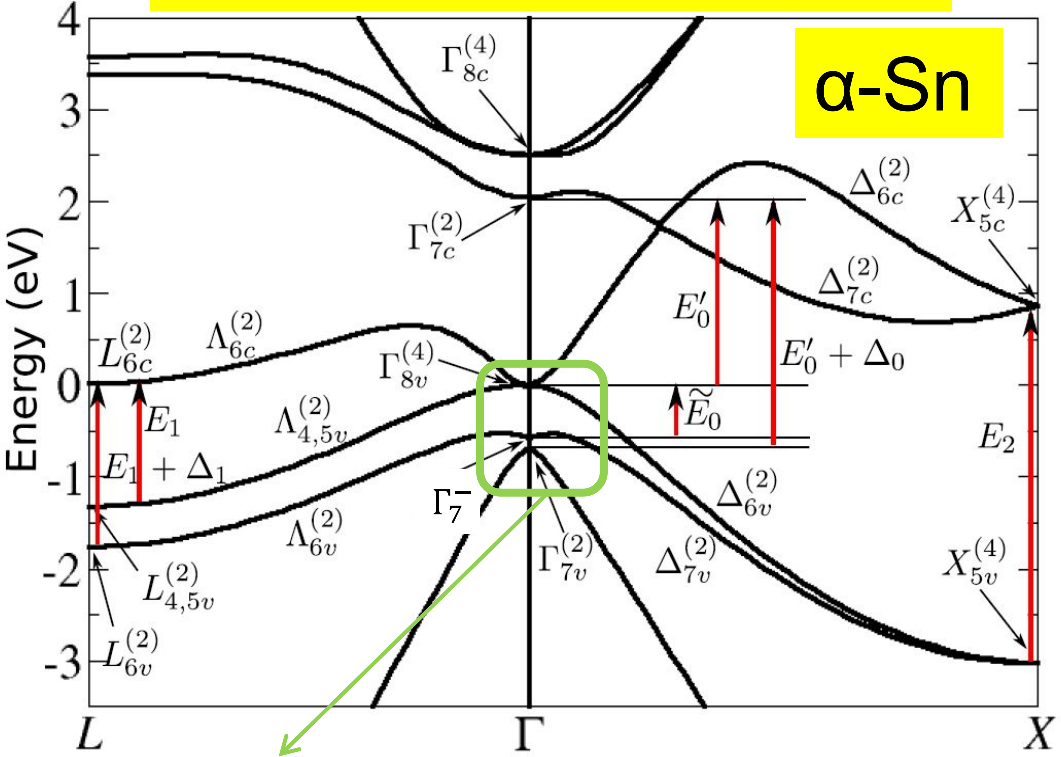

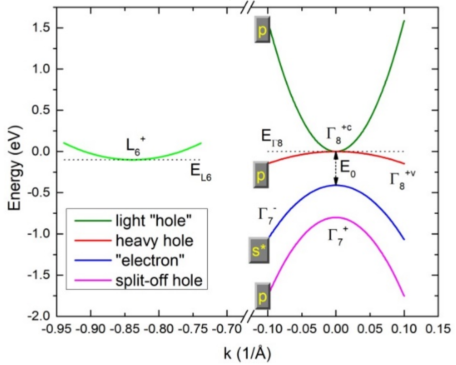

P. Y. Yu, M. Cardona: Fundamentals of Semiconductors. Springer (2010)

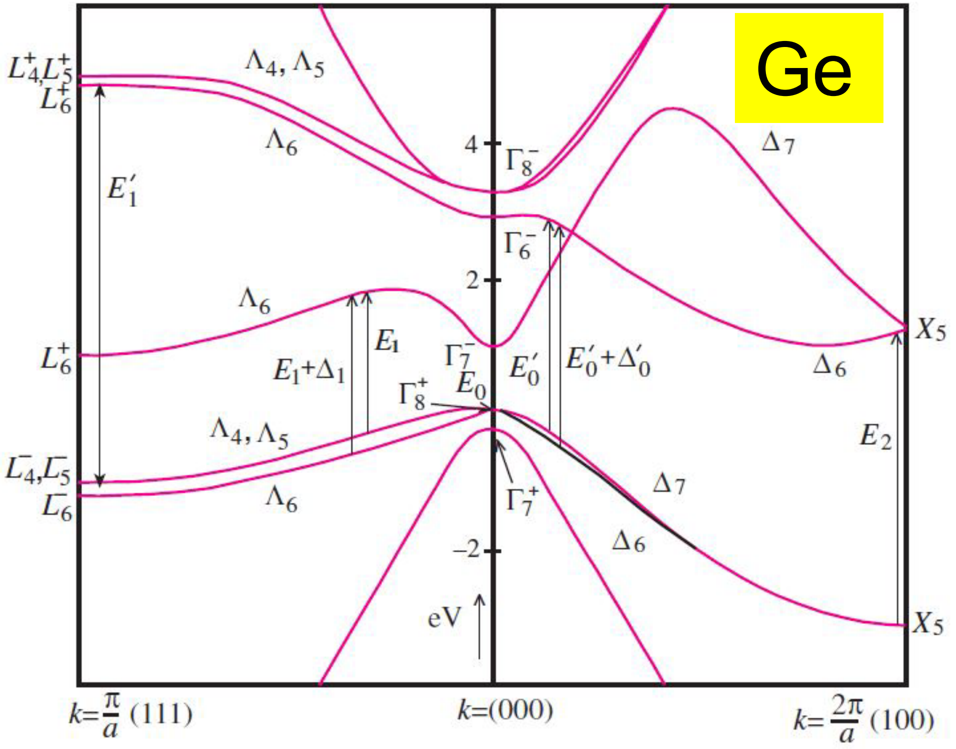

- Γ_7^- CB moves downward between Γ_8^+ and Γ_7^+ (split-off) VBs.
    - Γ_7^-→VB (negative curvature)
    - Γ_8^+(heavy hole)→Top VB
    - Γ_8^+(light hole)→Lowest CB (positive curvature)

Optical constants of Ge versus α-Sn

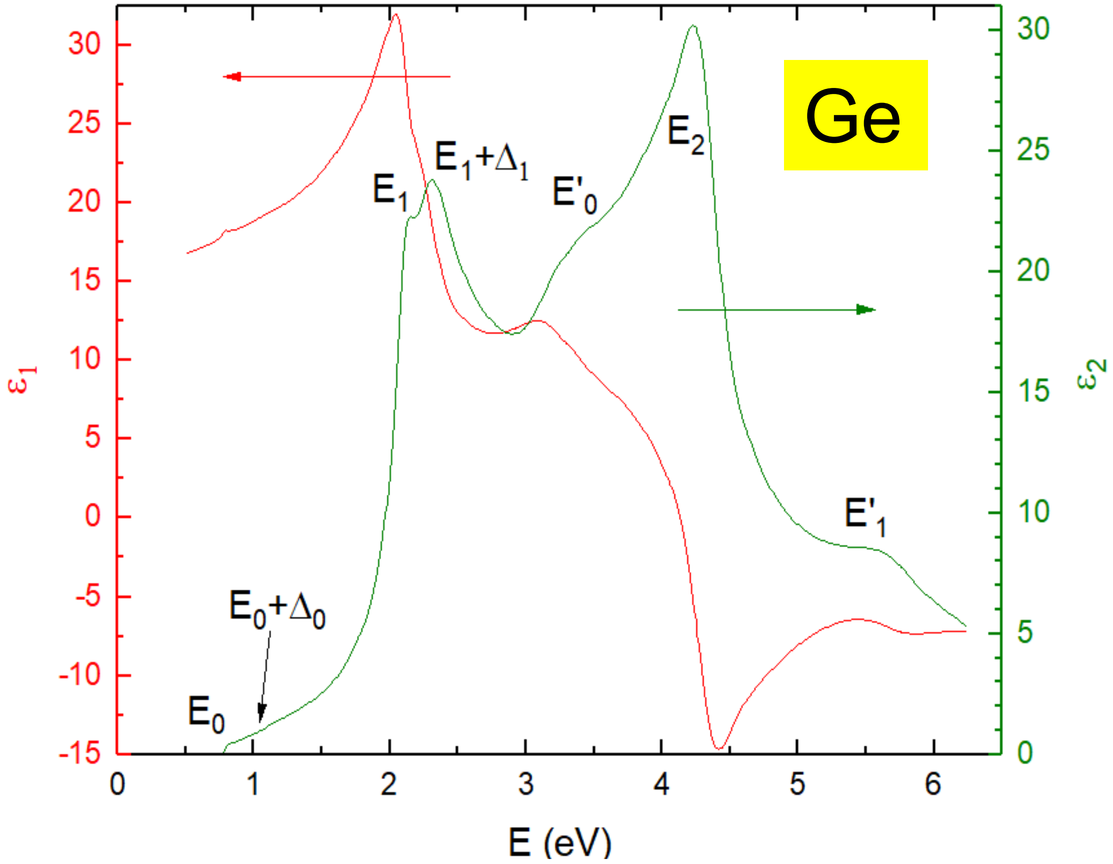

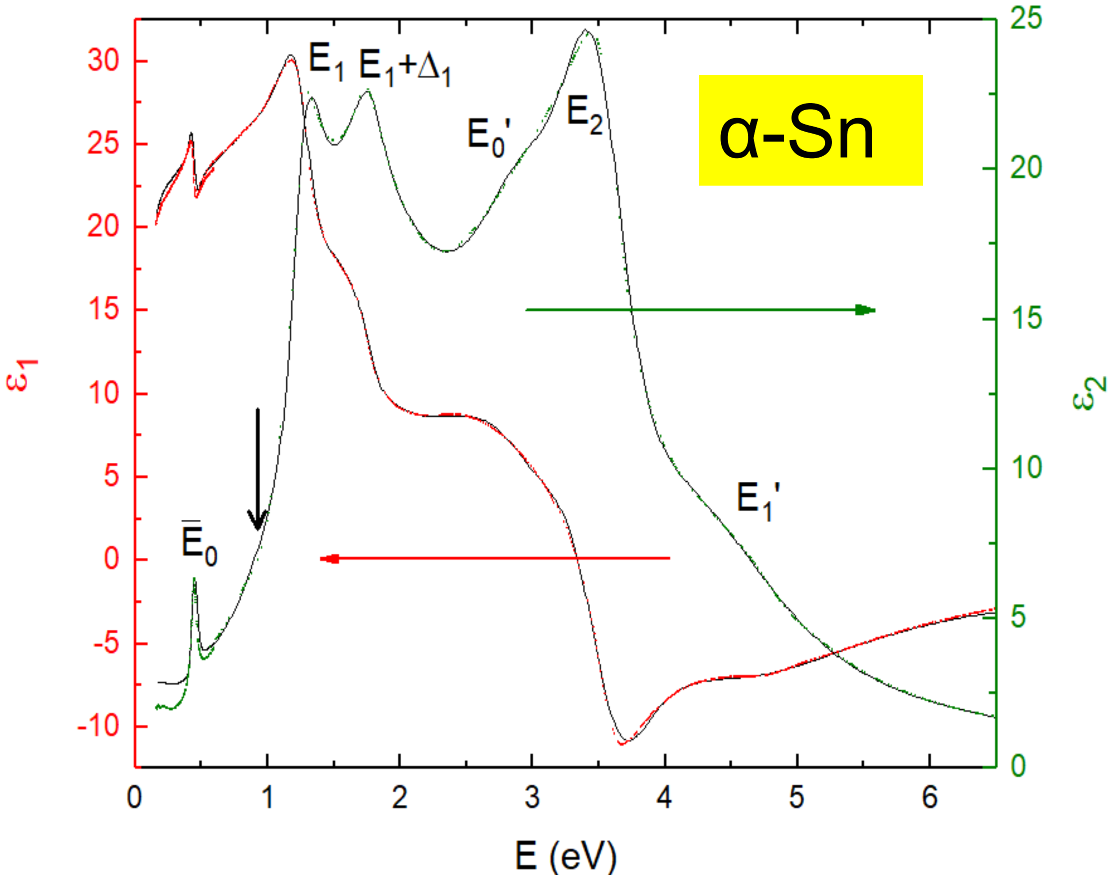

- Critical point line shapes with energies ≥ 1 eV are identical in both α-Sn and Ge $\rightarrow \epsilon(\omega)=B-A(\omega-E-i\Gamma)^{-\mu}e^{i\varphi}$ (consistent with historical results)
- But $\bar{E}_0$ in α-Sn has a completely different line shape in comparison to E_0 in Ge

Viña *et al.*, Phys. Rev. B **31**, 958 (1985)
Viña *et al.*, Phys. Rev. B **30**, 1979 (1984)
Carrasco *et al.*, Appl. Phys. Lett. **113**, 232104 (2018)

Direct bandgap of Ge versus α-Sn

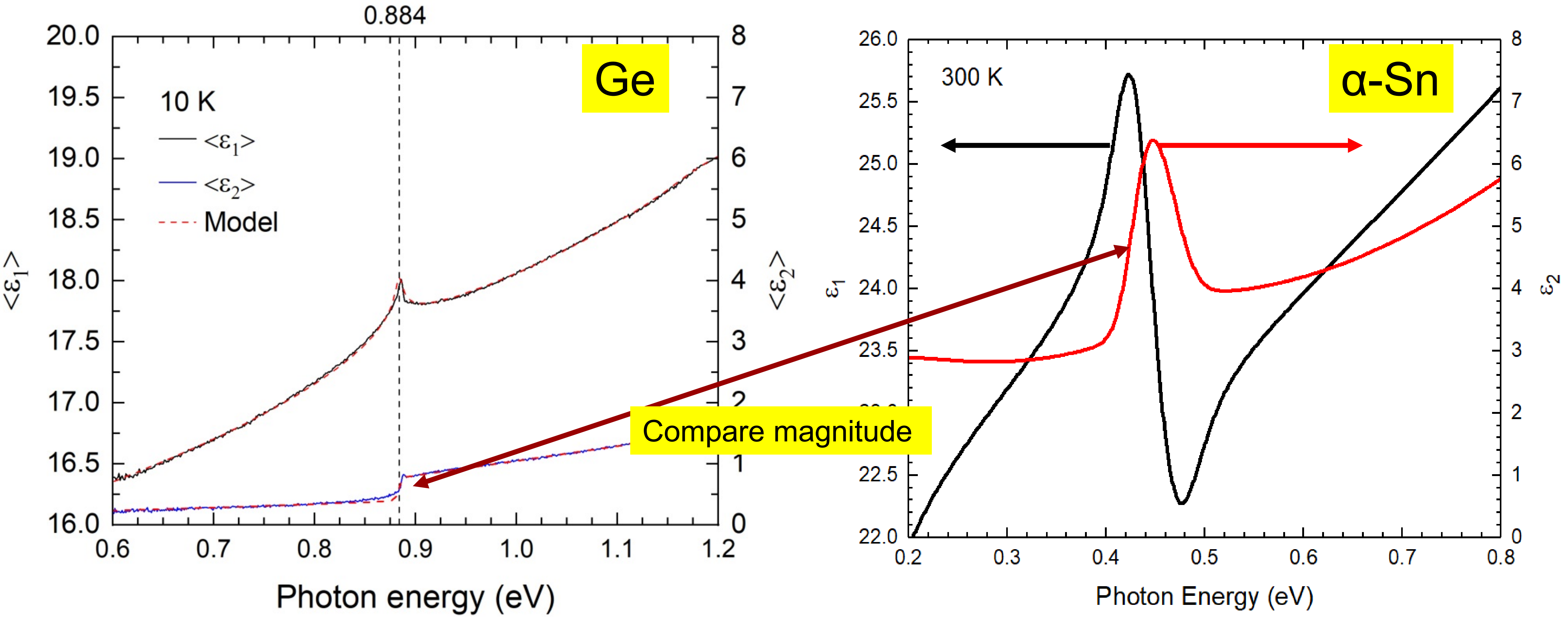

- What does α-Sn have that Ge doesn't?

α-Sn band diagram

- ○ Intravalence band transitions.
  - $\Gamma_7^- \rightarrow \Gamma_8^{+v}$ (light hole)
  - $\Gamma_7^- \rightarrow \Gamma_8^{+c}$ (heavy hole)
- ○ Suggests high hole concentration.
  - L-Valley may be lower than valence band maximum
  - OR doping from substrate

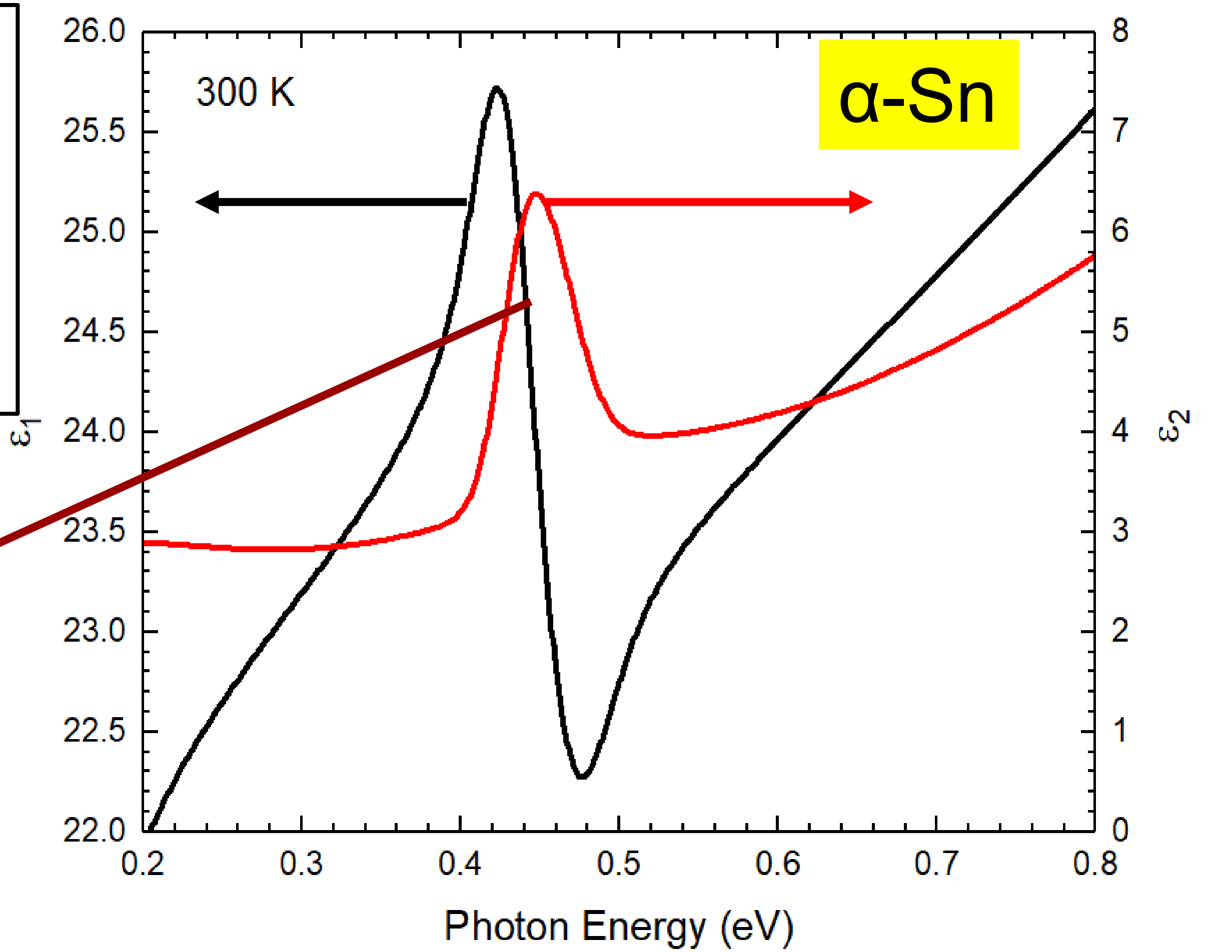

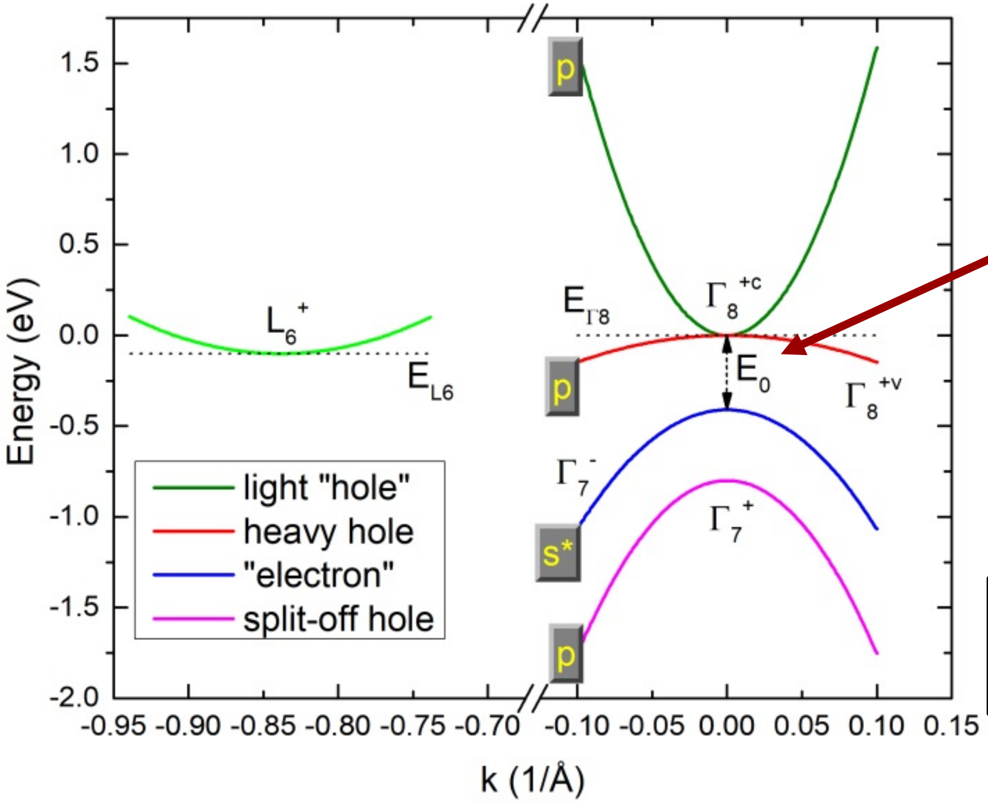

- What does α-Sn have that Ge doesn't?
  - **Negative Band Gap**

Ge E_0 temperature dependence

- Ge E_0 energy red shifts with increasing temperature.
  - Energies extracted by reciprocal space analysis.
  - Can be described by Bose-Einstein factor.

$$E(T) = a - b\left[\frac{2}{e^{\frac{\theta_B}{T}}-1}+1\right]$$

a - unrenormalized transition energy

b - electron-phonon coupling strength

$k\theta_B$ - effective phonon energy

Fitting parameters	a (meV)	b (meV)	θ_B (K)
Parametric Oscillator fit	945 ± 3	65 ± 5	280 ± 20
Reciprocal space analysis	945 ± 3	65 ± 4	280 ± 20
Second derivative analysis	937 ± 5	47 ± 9	210 ± 40

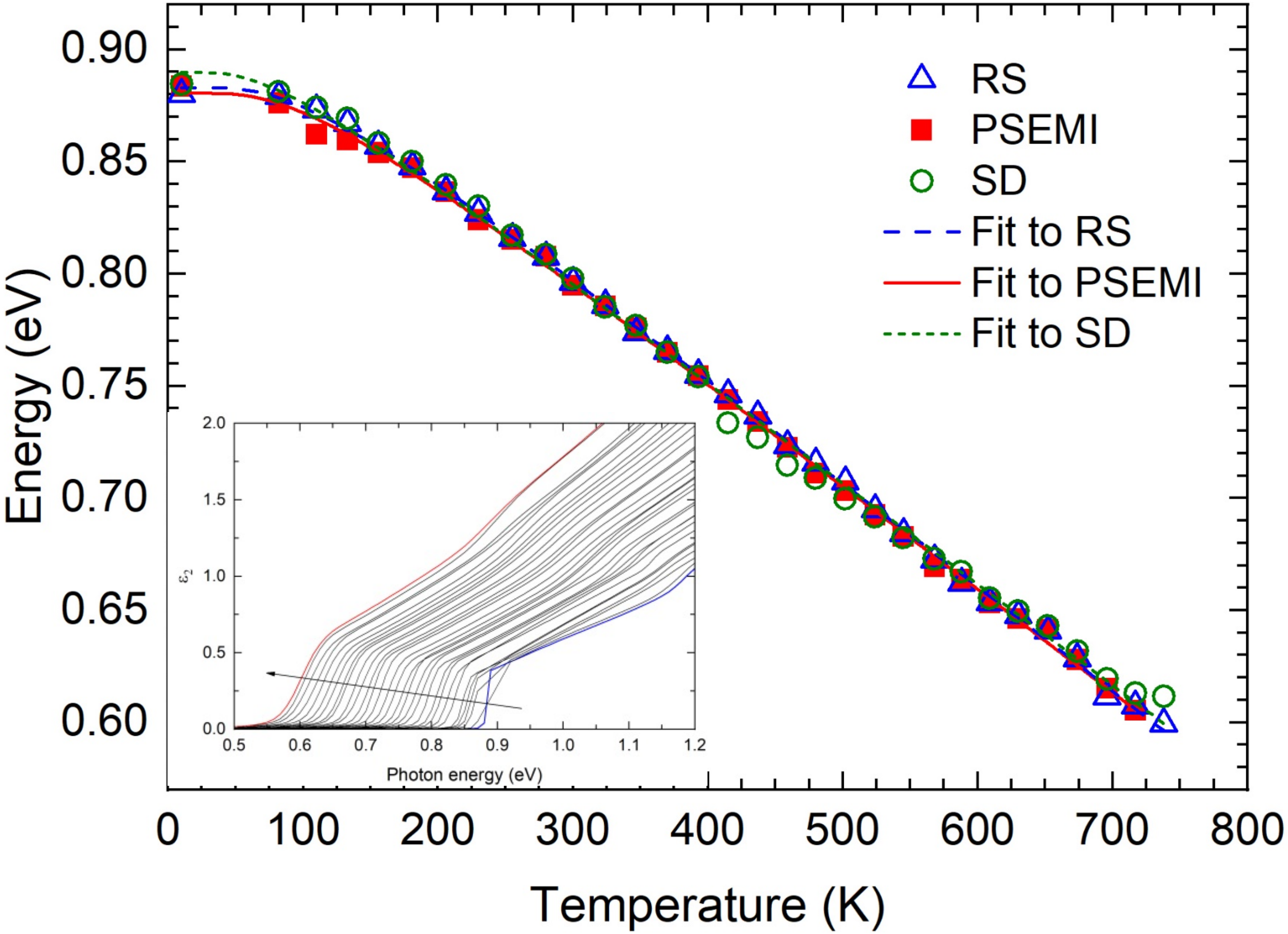

Emminger *et al.*, JVST B. **38**, 012202 (2020).

α-Sn $\bar{E}_0$ temperature dependence

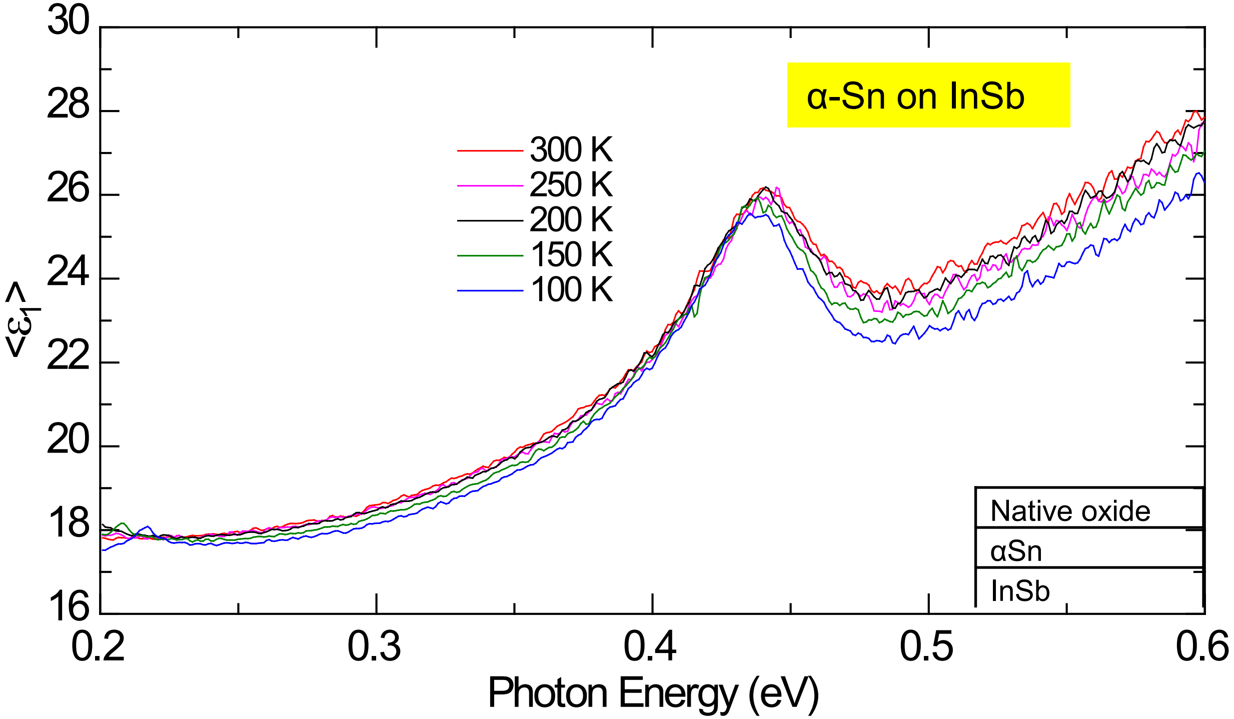

- Temperature *independent* energy
- Temperature *independent* amplitude
- Suggesting p-doping from substrate

α-Sn $\bar{E}_0$ temperature dependence

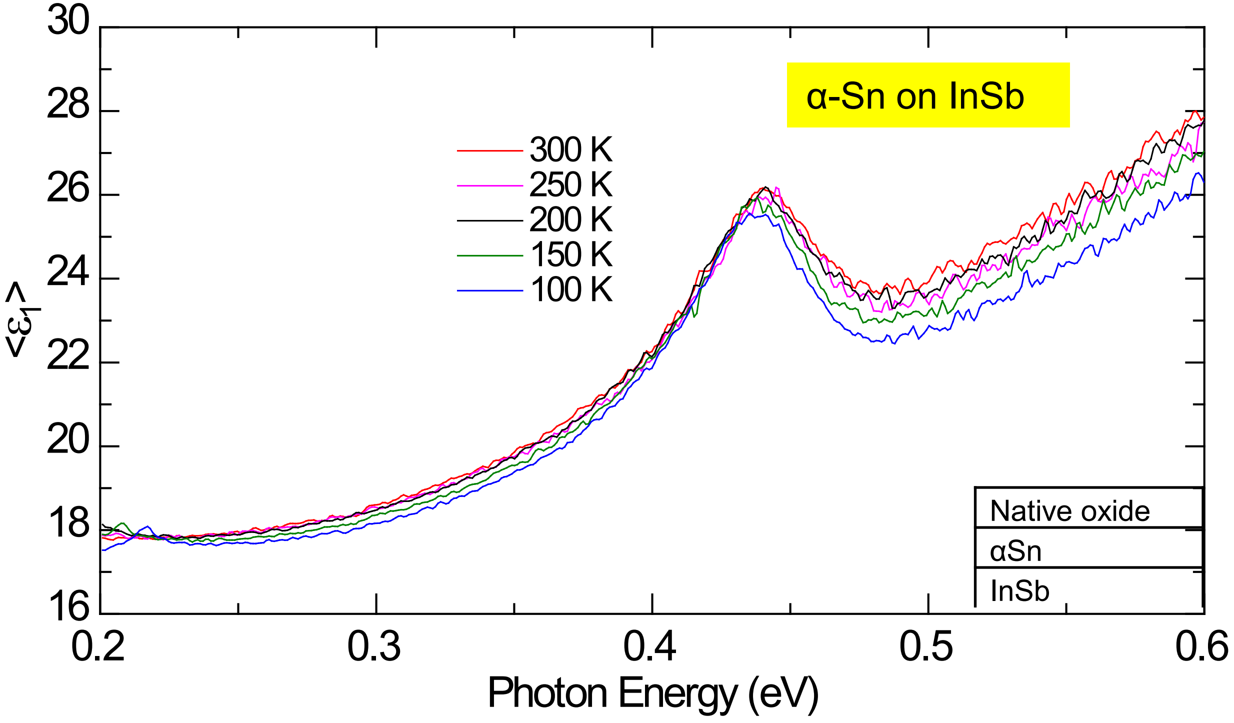

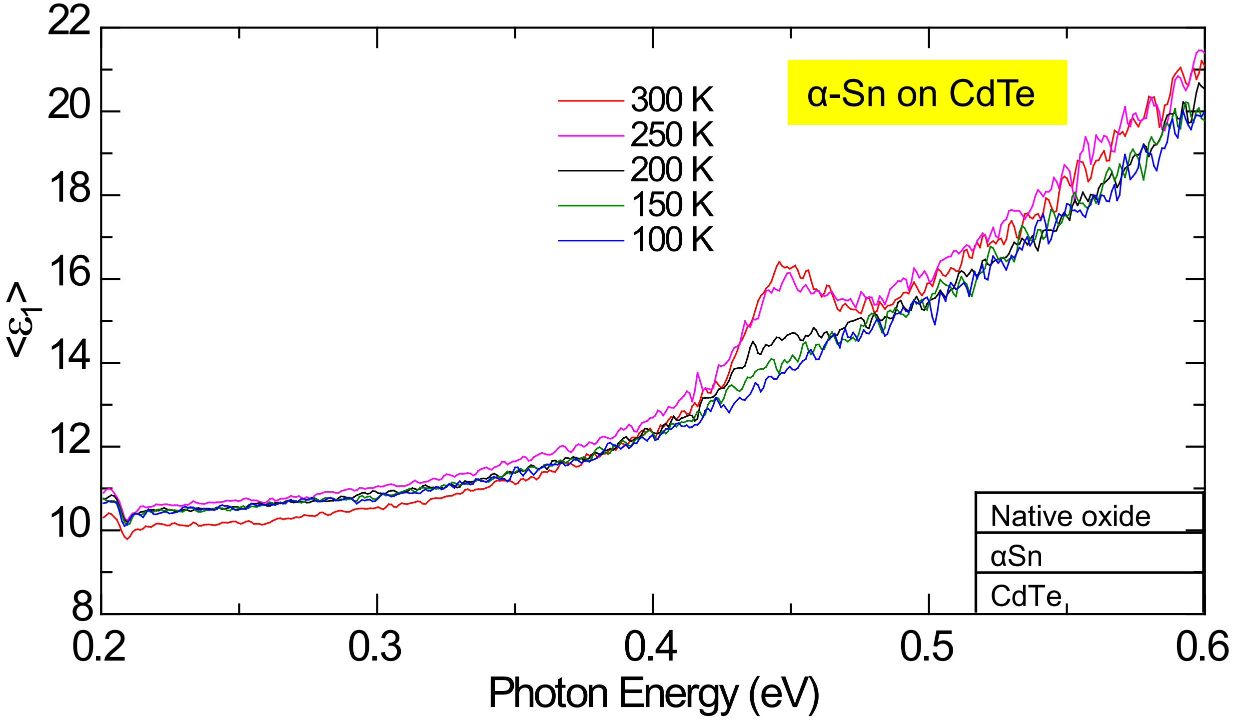

- Temperature *independent* energy
- Temperature *independent* amplitude
- Suggesting p-doping from substrate

- Temperature *independent energy*
- Temperature *dependent* amplitude
- Suggesting hole carriers from thermal excitations

Optical constants of $Sn_{1-x}Ge_x$ alloys

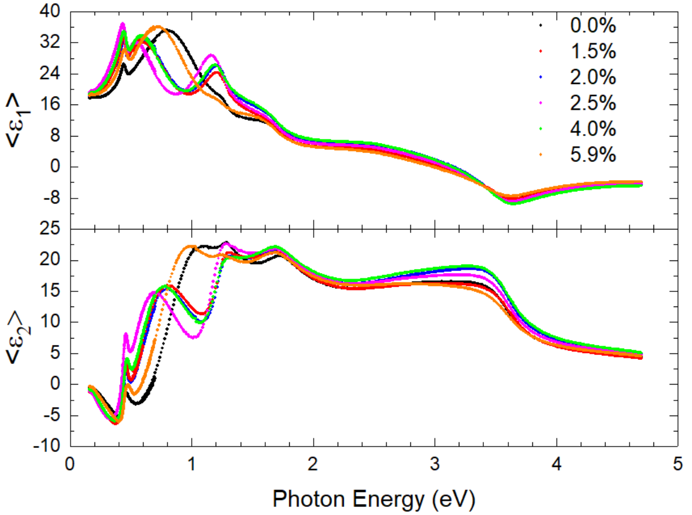

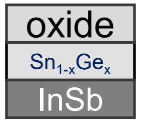
oxide

$Sn_{1-x}Ge_x$

InSb

- E_1 and $E_1 + \Delta_1$ red shift with increasing Ge content
  - Expected from deformation potential theory
- $\bar{E}_0$ blue shifts with increasing Ge content

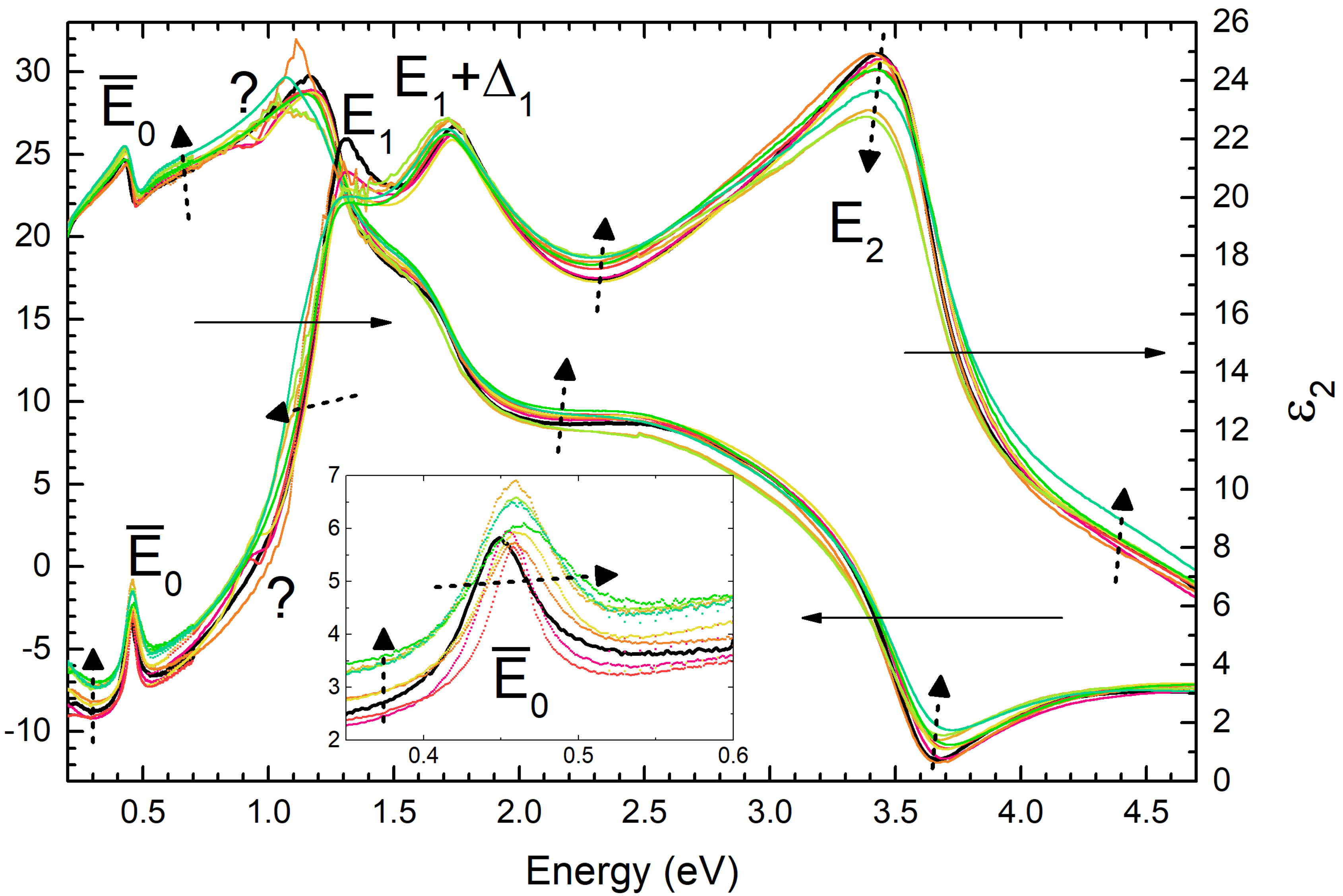

E_1 and $E_1+\Delta_1$ transitions in $Sn_{1-x}Ge_x$ alloys

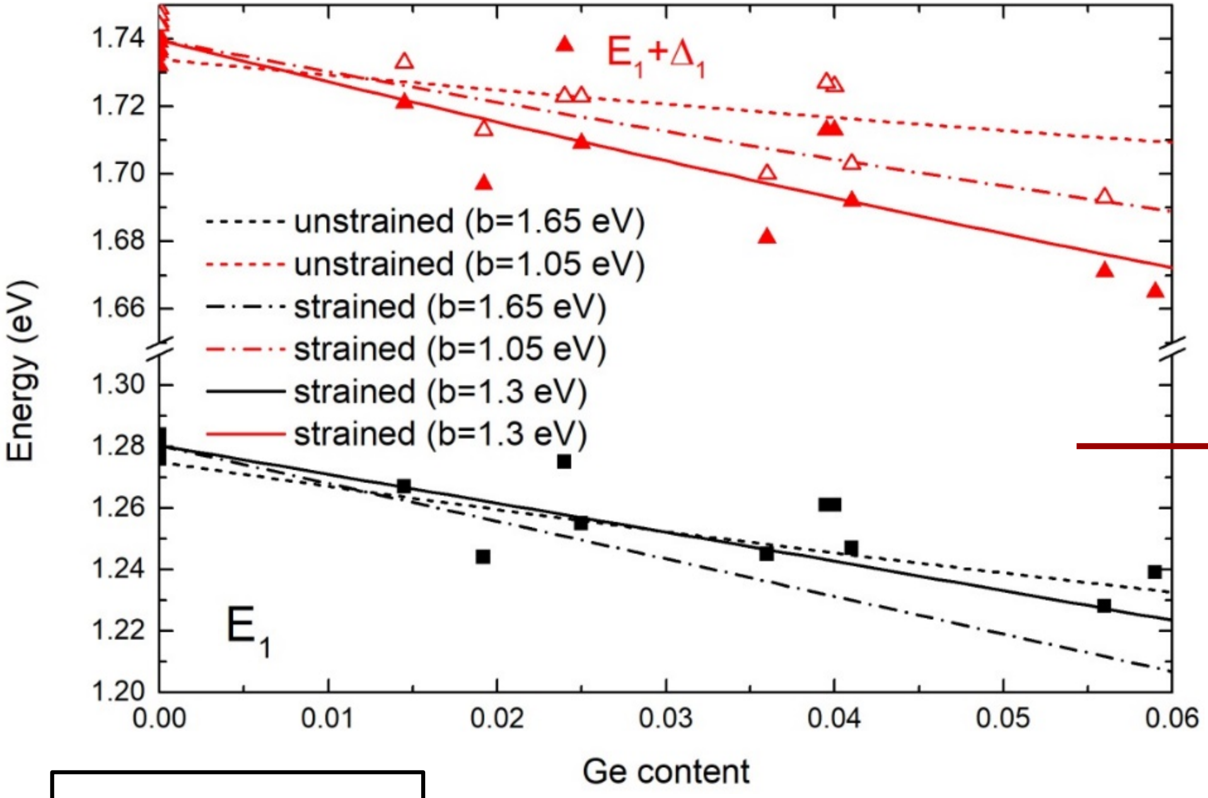

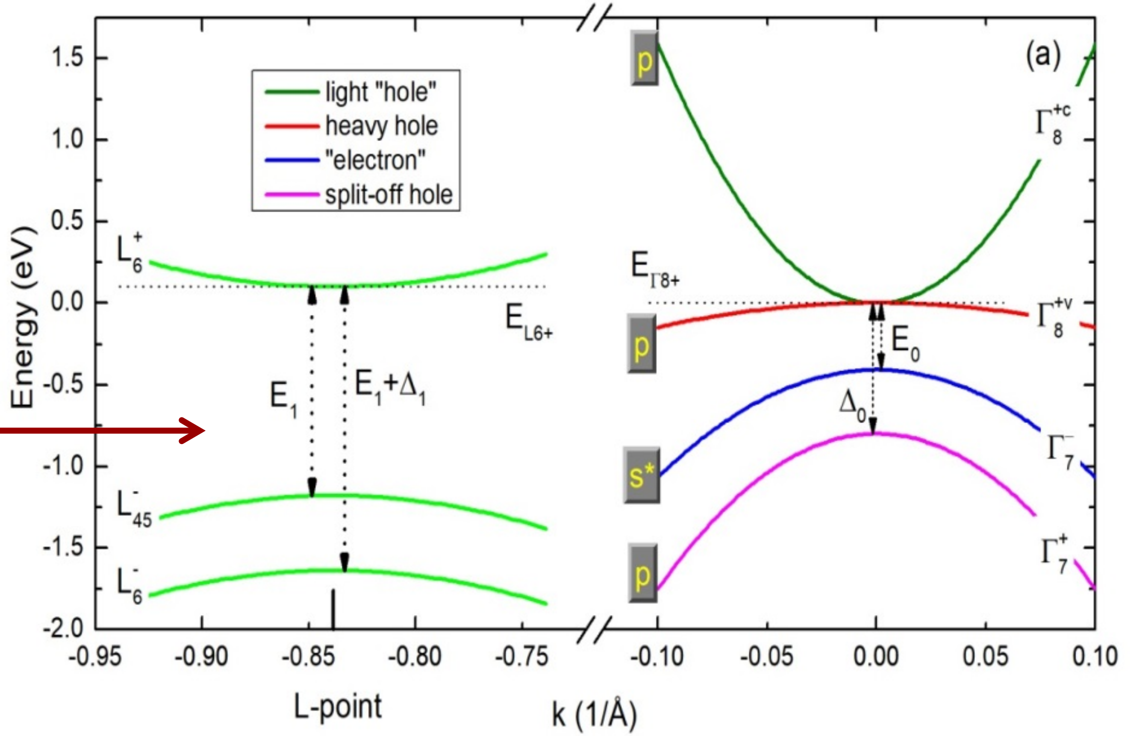

A … amplitude
E … CP energy
Γ … broadening
φ … phase angle
μ ... ”dimension”

μ = 1	0D
μ = 1/2	1D
μ = 0	2D
μ = -1/2	3D

$$\epsilon(\omega) = B - A(\omega - E - i\Gamma)^{-\mu} e^{i\varphi}$$

- Numerical second derivative of complex dielectric function performed.
    - Allows determination of critical point parameters

Carrasco *et al*. Appl. Phys. Lett. **114**, 062102 (2019)

$\bar{E}_0$ transitions in $Sn_{1-x}Ge_x$ alloys

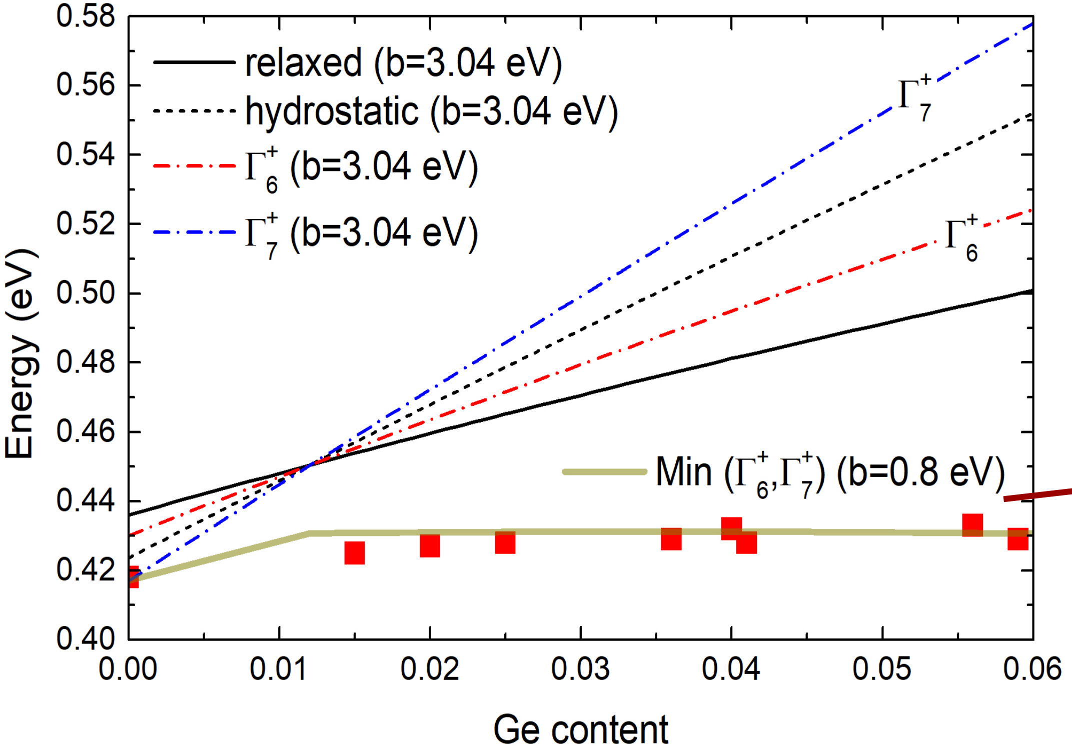

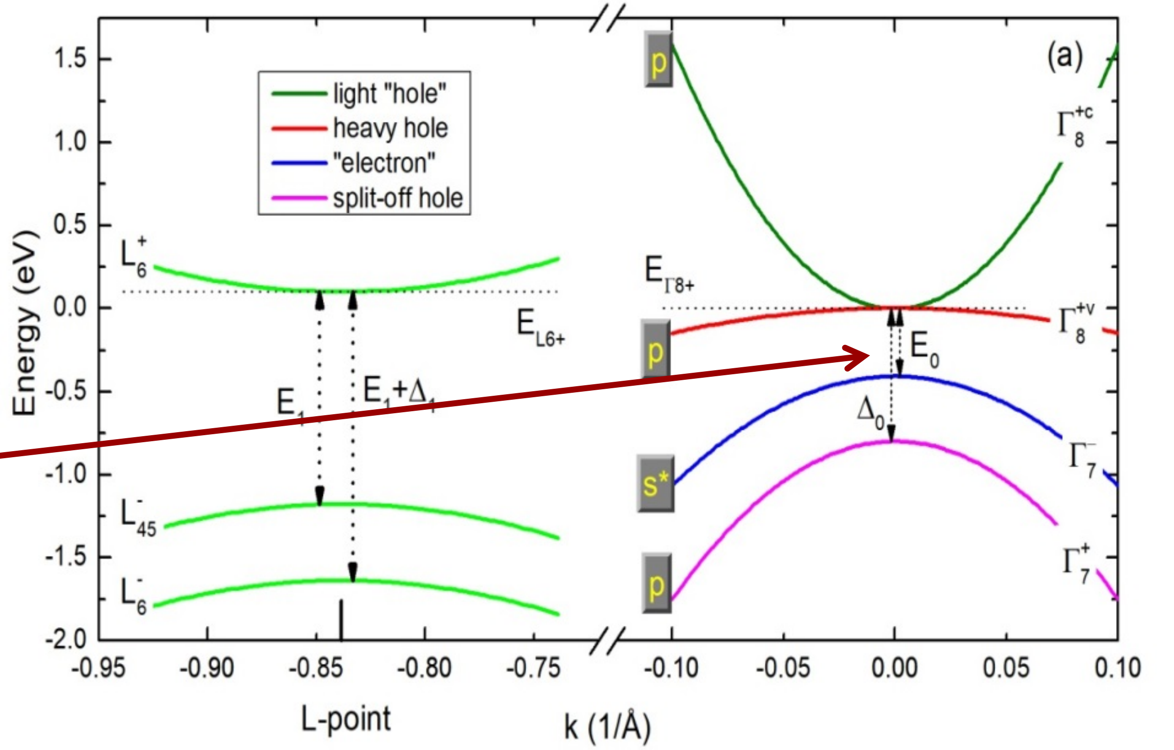

- What is the dimensionality of $\bar{E}_0$ transitions?
- Why is $\bar{E}_0$ nearly independent of Ge content?
  - Need theory that considers band warping and non-parabolicity

Carrasco *et al*. Appl. Phys. Lett. **114**, 062102 (2019)

Conclusions part IV

- α-Sn has similar dielectric function to Ge in UV-VIS.
- However, in IR, α-Sn has a **negative** band gap at 0.41 eV.
- Need comprehensive theory including quantum statistics, non-parabolicity, and band warping due to strain to describe $\bar{E}_0$ peak.

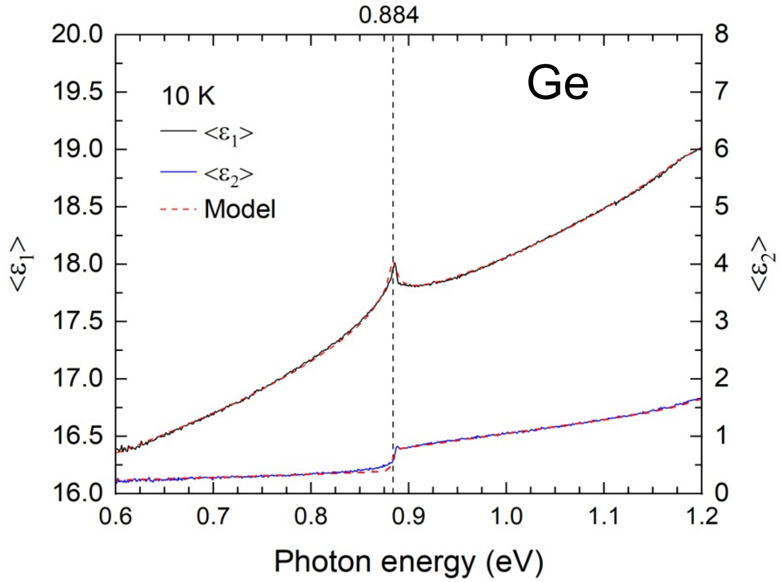

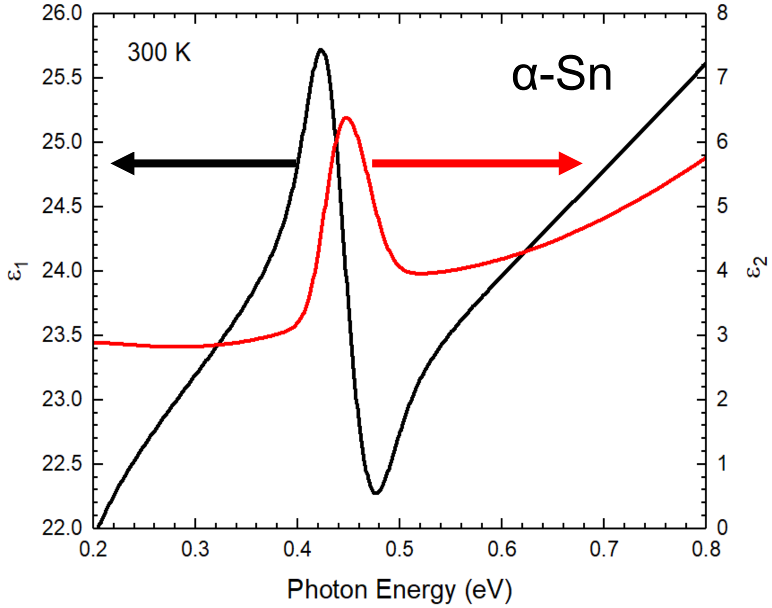

Grand canonical conclusion

Low-cost, high yield material solutions needed to satisfy satellite-based sensing

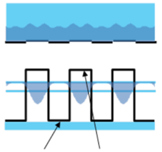

- **A III-V superlattice solution to mid-wave infrared sensing**
    - ➢ Mature and developed solution to mid-wave sensing
    - ➢ Wavefunction overlap is a concern

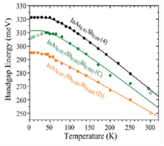

- **A bulk III-V solution to mid-wave infrared sensing**
    - ➢ Bulk III-V alloys is less developed but provides promise of satisfying mid-wave sensing without concern for wavefunction overlap

- **A group IV solution to mid-wave sensing**
    - ➢ Absorption beyond 6 μm observed, requires investigation and discovery of higher-level material performance

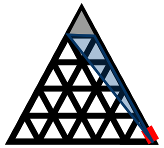

- **Beyond mid-wave materials and toward topological quantum materials**
    - ➢ Strong absorption observed, requires discovery of fundamental band structure behavior

Future work

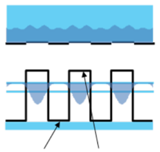

- **Group III-V superlattices front**
  - ➢ Explore doping profiles to lower tunnelling dark current and improve InGaAs/InAsSb superlattice device performance

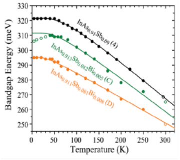

- **Group III-V quinary front**
  - ➢ Explore wide design space for maximum Bi incorporation and improve the minority carrier lifetime of the quinary material system
  - ➢ Explore absorption of the alloy

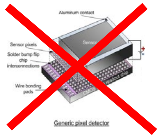

- **Group IV GeSn mid-wave front**
  - ➢ Determine minority carrier lifetime and create relations between growth parameters and optical performance

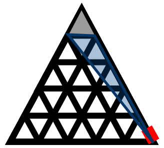

- **Group IV α-Sn front**
  - ➢ Perform a doping study of α-Sn and determine $\bar{E}_0$ dependence on doping
  - ➢ Perform $\vec{k} \cdot \vec{p}$ band structure calculations that take into account band nonparabolicity to accurately model $\bar{E}_0$ peak

Thank you!

Many thanks to:

- Dr. Preston T. Webster, Dr. Perry C. Grant, Dr. Christian P. Morath, and RVSU AEOSS team at KAFB
- Dr. Arnold M. Kiefer, and RYDH team at Wright-Patterson AFB
- Dr. Kolodzey, Dominic Imbrenda, University of Delaware team
- Dr. Stefan Zollner, Cesy Zamarripa, Carola Emminger, Farzin Abadizaman, Nuwanjula Samarasingha, and Pablo Paradis
- Dr. Vassili Papavassiliou, Dr. Igor Vasiliev, and Dr. David Voelz

Ellipsometry group with Dr. John Woollam at 2017 AVS 64th International Symposium and Exhibition, Tampa, Florida

Extra slides

Superlattices

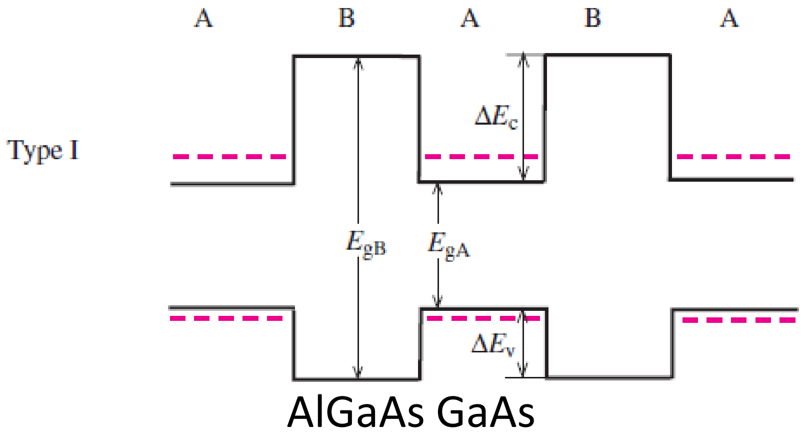

Type I: Electrons and holes are both confined in the same layer

ex: GaAs/AlGaAs

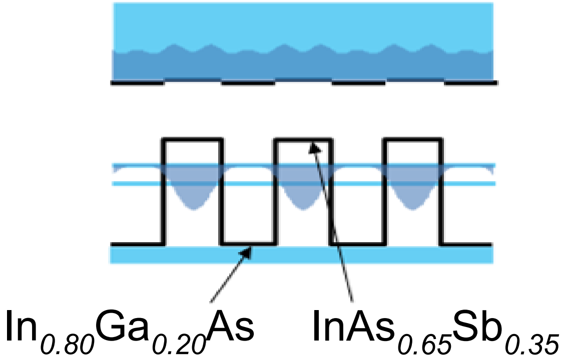

Type IIA: Electrons and holes are confined in different layers (staggered)

ex: In(Ga)As/InAsSb

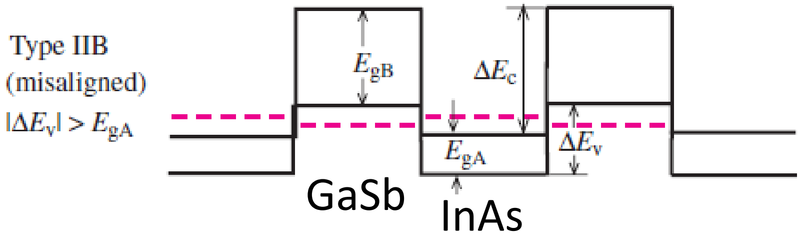

Type IIB: small energy gap between electrons in layer A and small/no energy gap in holes in layer B (misaligned).

ex: InAs/GaSb

Kronig penney model

- Imagine an electron in a one-dimensional periodic square-well potential with wells and barriers with widths a and b, barrier height V_0, transcendental equations:
- $\cos(kd) = \cos(k_1 a)\cos(k_2 b) - \frac{k_1+k_2^2}{2k_1 k_2}\sin(k_1 a)\sin(k_2 b)$ for E > V_0
- $\cos(kd) = \cos(k_1 a)\cosh(\kappa b) - \frac{k_1^2-\kappa^2}{2k_1 \kappa}\sin(k_1 a)\sinh(\kappa b)$ for E< V_0
- $E = \frac{\hbar^2 k_1^2}{2m_A^*}$
- $E - V_0 = \hbar^2 k_2^2/(2m_A^*)\ for\ E > V_0$
- $V_0 - E = \hbar^2 \kappa^2/(2m_A^*)\ for\ E < V_0$

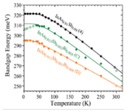

Calibrations necessary for quinary growth

1. Calibrate In, Ga growth rates
2. Calibrate InAs RHEED to As/In = 1
3. Lattice matched InAsSb @ 440C

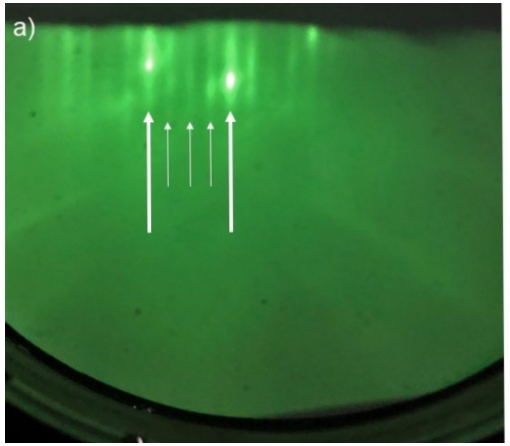

As-rich

Same Azimuth

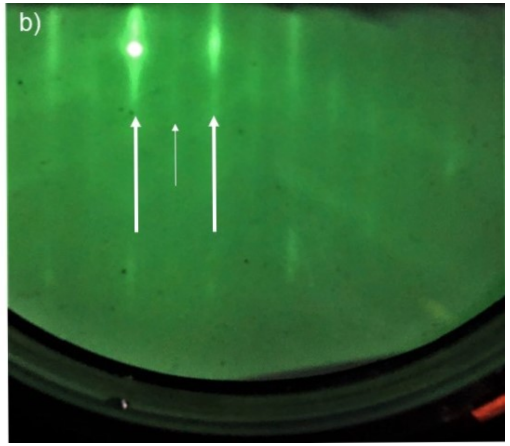

As-lean

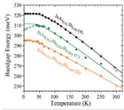

Calibrations necessary for quinary growth

Run number	Sample	In growth rate (µm/hr)	Ga growth rate (µm/hr)	As/III	Sb/III	Bi/III	XRD strain (arcseconds)
1	InAsSb	1.008	0.0	0.953	0.110	0.0	-462

1. Calibrate In, Ga growth rates
2. Calibrate InAs RHEED to As/In = 1
3. Lattice matched InAsSb @ 440C
4. Compressive InAsSb @ 400 C (unity As flux ratio)

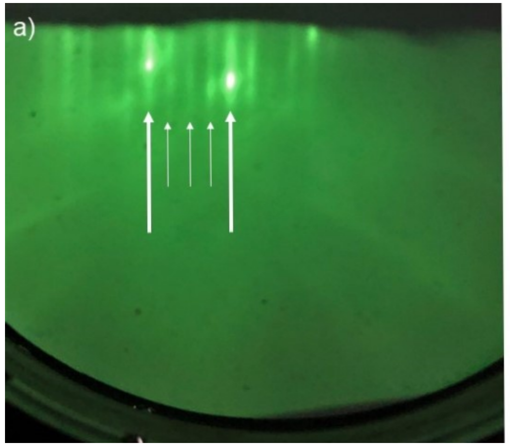

As-rich

Same Azimuth

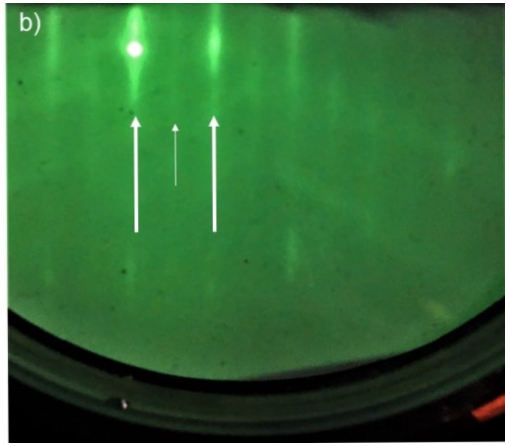

As-lean

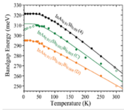

Calibrations necessary for quinary growth

Run number	Sample	In growth rate (µm/hr)	Ga growth rate (µm/hr)	As/III	Sb/III	Bi/III	XRD strain (arcseconds)
1	InAsSb	1.008	0.0	0.953	0.110	0.0	-462
2	GaInAsSb	0.969	0.029	0.963	0.112	0.0	-43

1. Calibrate In, Ga growth rates
2. Calibrate InAs RHEED to As/In = 1
3. Lattice matched InAsSb @ 440C
4. Compressive InAsSb @ 400 C (unity As flux ratio)
5. Lattice matched GaInAsSb on GaSb @ 400 C

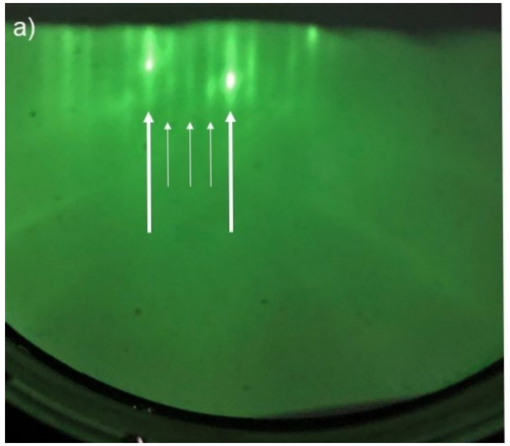

As-rich

Same Azimuth

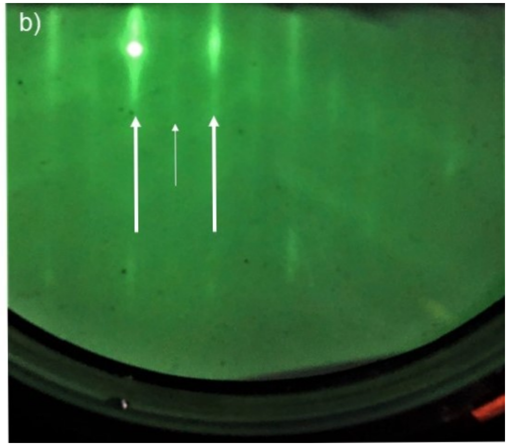

As-lean

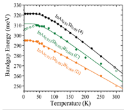

Calibrations necessary for quinary growth

Run number	Sample	In growth rate (µm/hr)	Ga growth rate (µm/hr)	As/III	Sb/III	Bi/III	XRD strain (arcseconds)
1	InAsSb	1.008	0.0	0.953	0.110	0.0	-462
2	GaInAsSb	0.969	0.029	0.963	0.112	0.0	-43
3	GaInAsSbBi	0.985	0.029	0.966	0.108	≈0.02	-55

1. Calibrate In, Ga growth rates
2. Calibrate InAs RHEED to As/In = 1
3. Lattice matched InAsSb @ 440C
4. Compressive InAsSb @ 400 C (unity As flux ratio)
5. Lattice matched GaInAsSb on GaSb @ 400 C
6. Using same conditions as 2), grow GaInAsSbBi @ 400 C

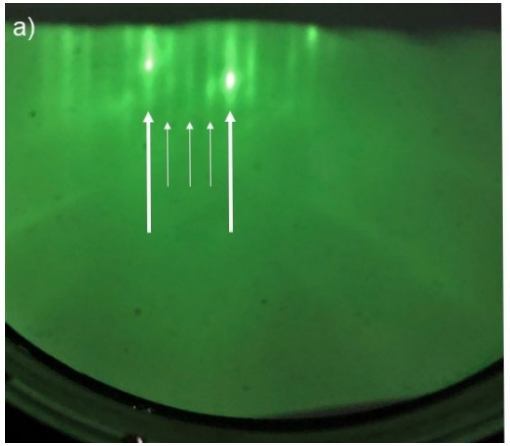

As-rich

Same Azimuth

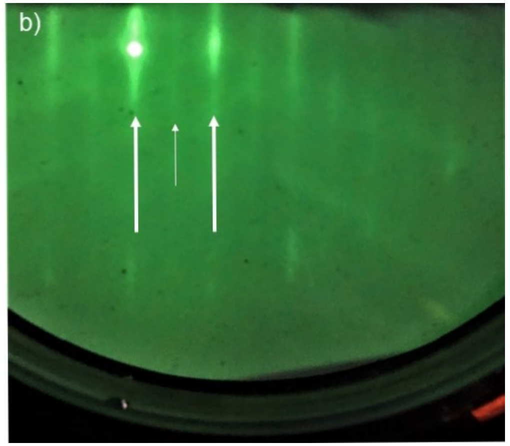

As-lean

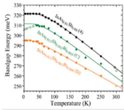

Calibrations necessary for quinary growth

Run number	Sample	In growth rate (µm/hr)	Ga growth rate (µm/hr)	As/III	Sb/III	Bi/III	XRD strain (arcseconds)
1	InAsSb	1.008	0.0	0.953	0.110	0.0	-462
2	GaInAsSb	0.969	0.029	0.963	0.112	0.0	-43
3	GaInAsSbBi	0.985	0.029	0.966	0.108	≈0.02	-55

1. Calibrate In, Ga growth rates
2. Calibrate InAs RHEED to As/In = 1
3. Lattice matched InAsSb @ 440C
4. Compressive InAsSb @ 400 C (unity As flux ratio)
5. Lattice matched GaInAsSb on GaSb @ 400 C
6. Using same conditions as 2), grow GaInAsSbBi @ 400 C

- ➢ Keep V/III flux ratios consistent
- ➢ Keep total group III growth rate consistent
- ➢ Any changes will be due to Bi incorporation

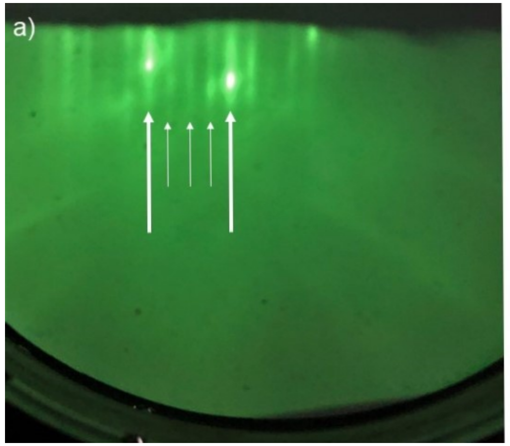

As-rich

Same Azimuth

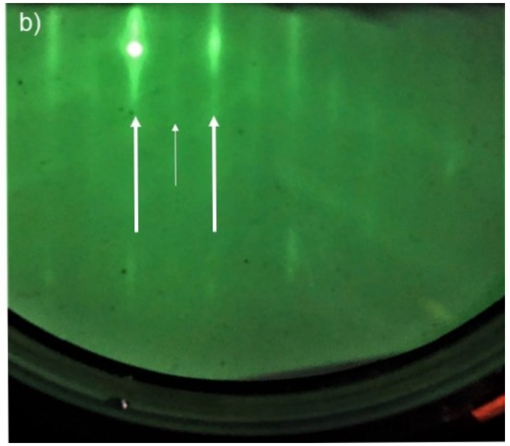

As-lean

Physics behind PL and dielectric function

- Electric transition probability R for photon absorption per unit time (Cardona eq 6.43b) (Fermi's golden rule for electron transition rate)
- $R = \frac{2\pi}{\hbar}\left(\frac{e}{m\omega}\right)^2 \left|\frac{E(\omega)}{2}\right|^2 \sum_k |P_{cv}|^2 \delta\left(E_c\left(\vec{k}\right) - E_v\left(\vec{k}\right) - \hbar\omega\right)$
- Power loss per unit volume

$$power\ loss = R\hbar\omega$$

$$-\frac{dI}{dt} = \frac{c}{n}\alpha I = \frac{\epsilon_2 \omega I}{n^2}$$

$$-\frac{dI}{dt} = R\hbar\omega$$

$$I = \frac{n^2}{8\pi}|E(\omega)|^2 - Intensity$$

- Photoluminescence is

$$PL = \frac{8\pi\epsilon_\infty}{h^3c^2}\frac{\alpha(hv)(hv)^2 d(hv)}{exp(hv/k_BT)} - Spontaneous\ emission\ transition\ rate\ per\ unit\ volume$$

$$\epsilon_1(\omega) - 1 \ = \frac{2}{\pi}\mathcal{P}\int_0^\infty \frac{\omega' \epsilon_2(\omega')d\omega'}{\omega'^2 - \omega^2} - kramers - kronig\ relations$$

Biasing a device

- Reverse biasing a device acts to increase size of depletion region

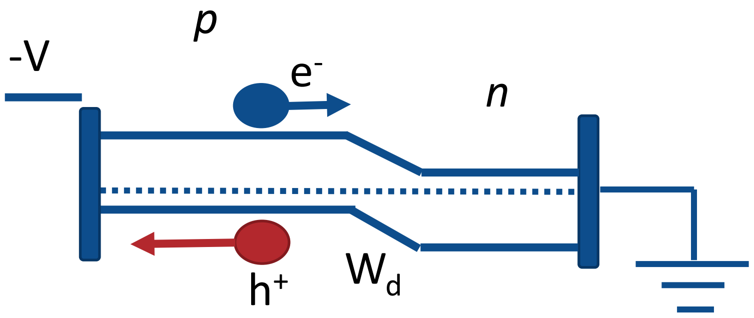

pn-reverse bias

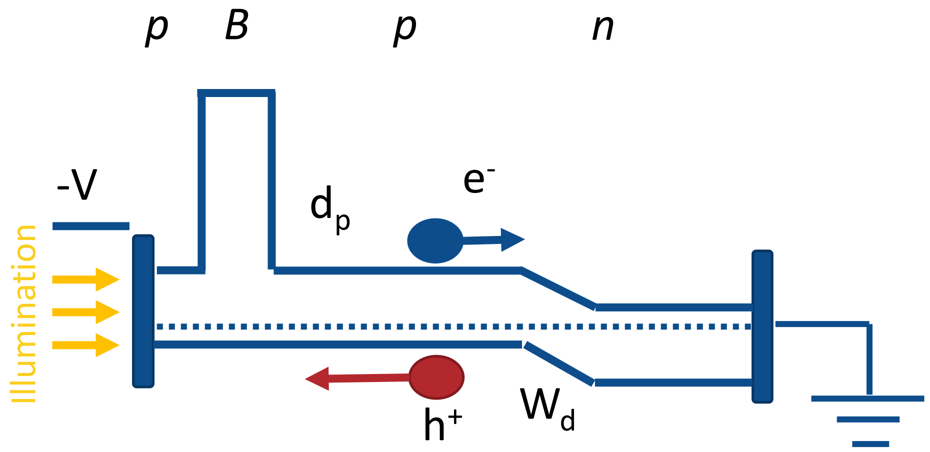

pBpn-reverse bias

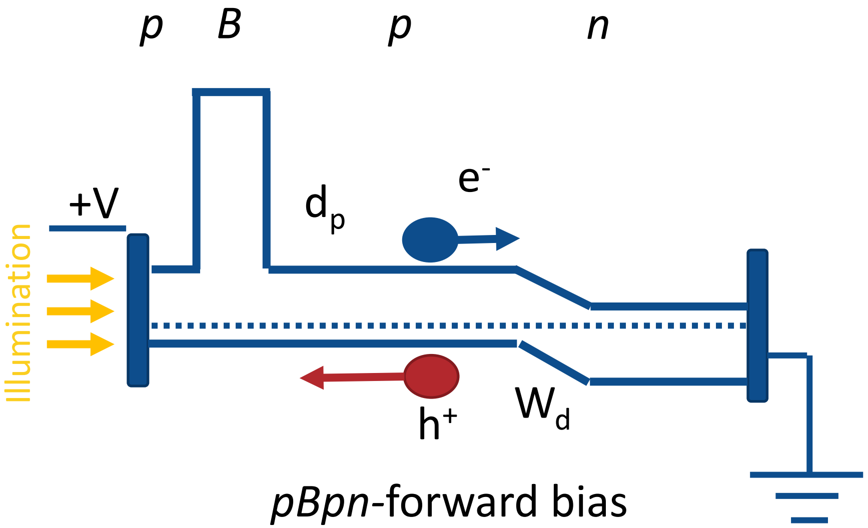

pBpn-forward bias

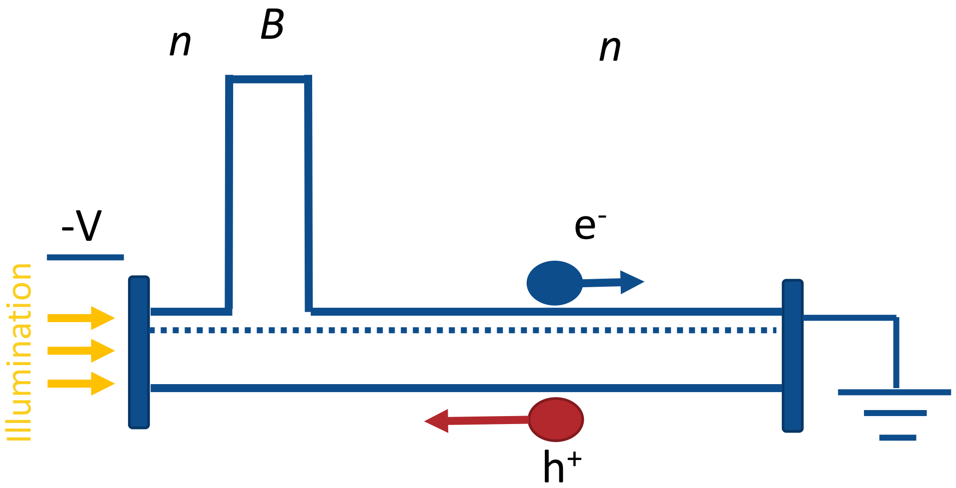

nBn-reverse bias

Free Carrier Response

α-Sn optical constants expressed as a sum of electronic transitions and free carriers

$$\varepsilon(\omega)=1-\sum_k \frac{\omega_{P,k}^2}{\omega^2+i\gamma_{D,k}\omega}+\sum_j g_j(\omega)$$

Drude electronic

2	tin-oxide	34.80 Å
1	sum_eps-rc (tin_p)/100% (tindrude)	686.62 Å
0	insb	1 mm
-1	tin_p	0.00 Å
-2	tindrude	0.00 Å

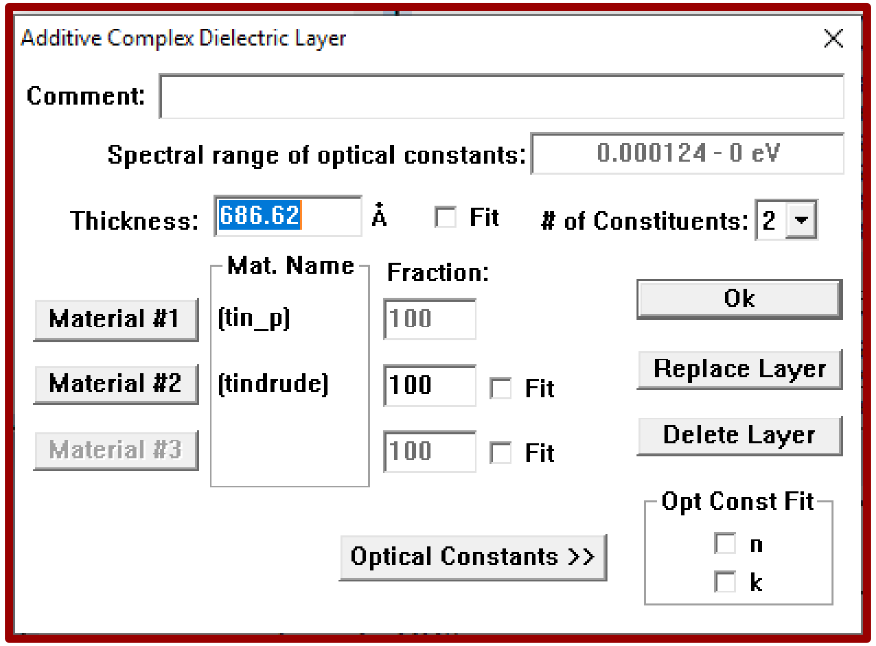

Additive Complex Dielectric Layer

Comment:

Spectral range of optical constants: 0.000124 - 0 eV

Thickness: 686.62 Å ☐ Fit # of Constituents: 2

	Mat. Name	Fraction:	
Material #1	(tin_p)	100	
Material #2	(tindrude)	100	☐ Fit
Material #3		100	☐ Fit

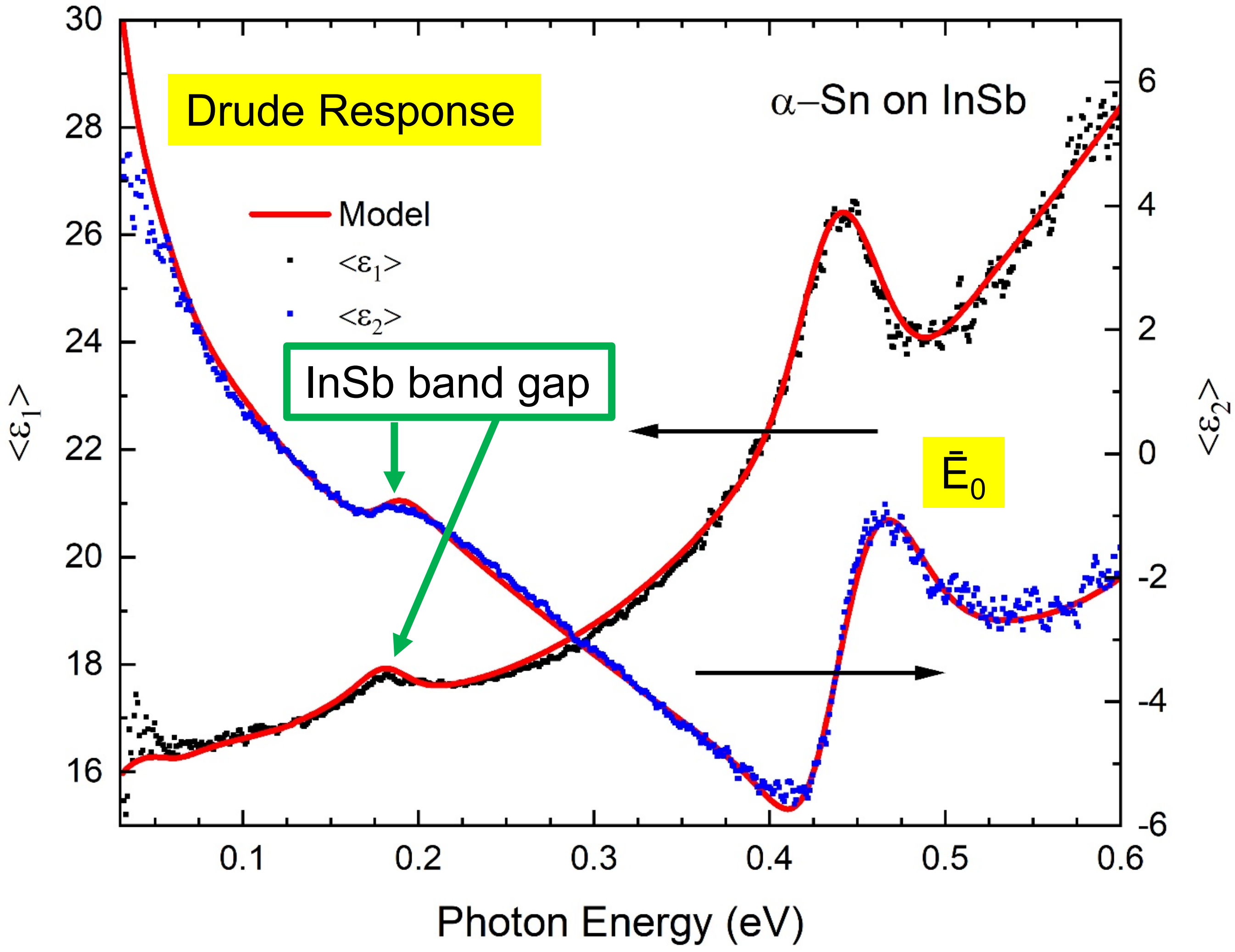

Free Carrier Response

α-Sn optical constants expressed as a sum of electronic transitions and free carriers

$$\varepsilon(\omega)=1-\sum_k \frac{\omega_{P,k}^2}{\omega^2+i\gamma_{D,k}\omega}+\sum_j g_j(\omega)$$

Drude electronic

2	tin-oxide	34.80 Å
1	sum_eps-rc (tin_p)/100% (tindrude)	686.62 Å
0	insb	1 mm
-1	tin_p	0.00 Å
-2	tindrude	0.00 Å

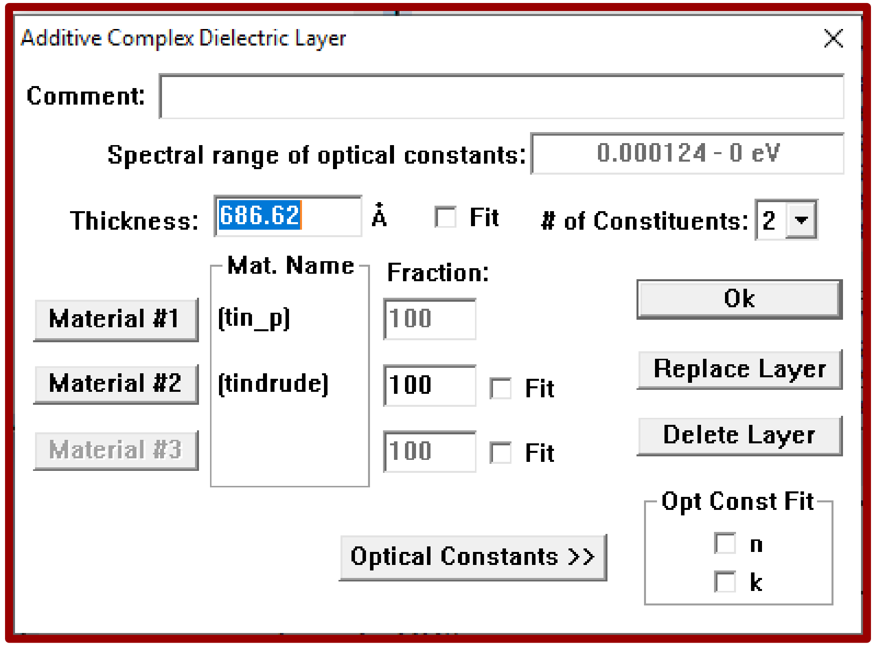

Comment:

Spectral range of optical constants: 0.000124 - 0 eV

Thickness: 686.62 Å ☐ Fit # of Constituents: 2

Mat. Name	Fraction:	
(tin_p)	100	
(tindrude)	100	☐ Fit
	100	☐ Fit

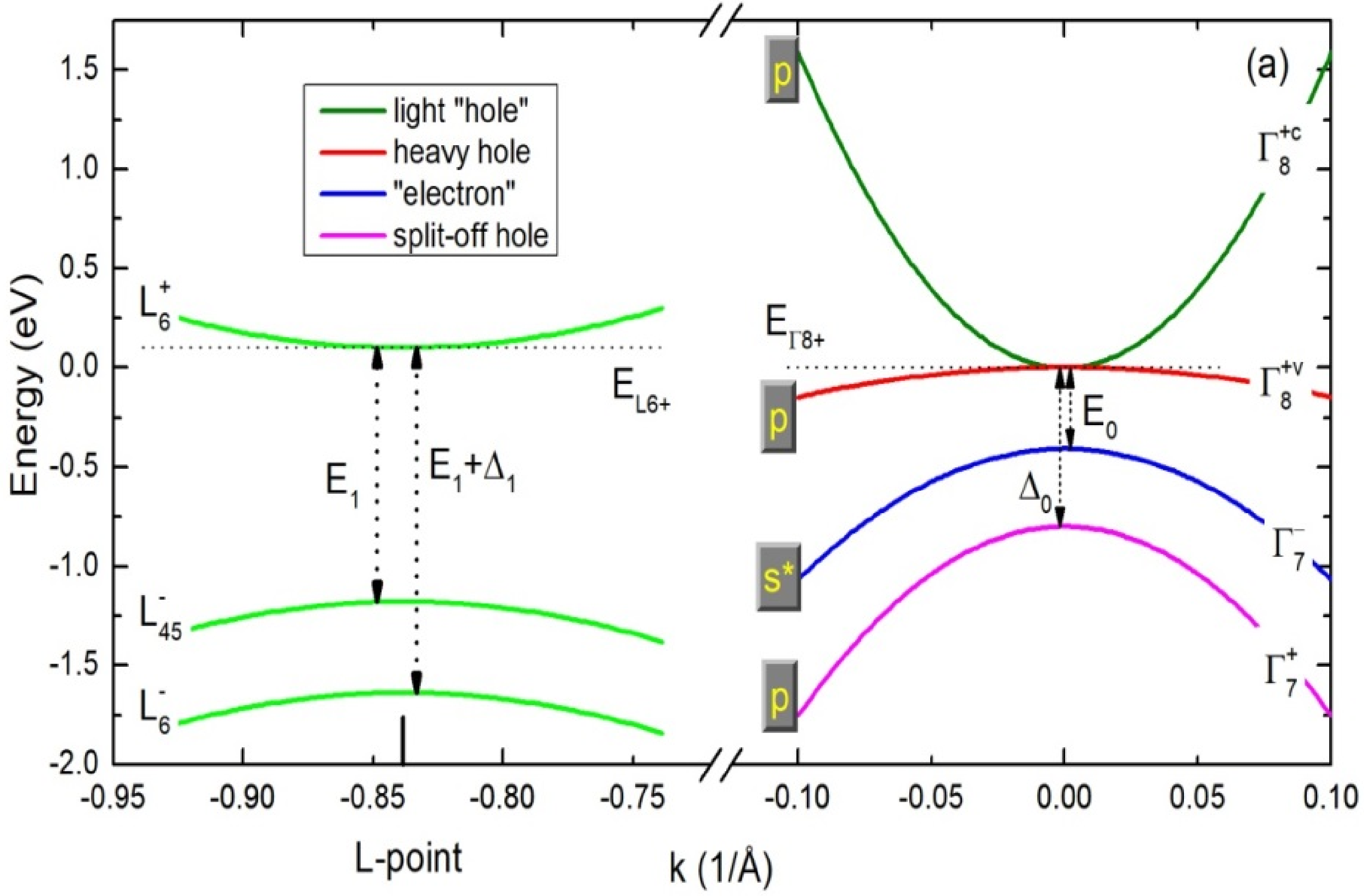

- 3 carriers species, 2 Drude contributions

Free Carrier Response

α-Sn optical constants expressed as a sum of electronic transitions and free carriers

$$\varepsilon(\omega)=1-\sum_k \frac{\omega_{P,k}^2}{\omega^2+i\gamma_{D,k}\omega}+\sum_j g_j(\omega)$$

Drude electronic

$$\boxed{\omega_{u,i}^2=\frac{n_i e^2}{\epsilon_0 m_i^* m_0}}$$

$$\mu_i=\frac{e}{m_i^* m_0 \gamma_{D,i}}$$

- Two Drude terms were used
  - Light and heavy free carriers

Carrier Concentrations		
substrate	heavy hole or L-electrons ($m^* \sim 0.20m_0$)	light hole ($m^* = 0.024m_0$)
i-InSb	$2.87(2)\mathrm{X}10^{19}$ cm^{-3}	$1.38(1)\mathrm{X}10^{18}$ cm^{-3}
n-InSb	$3.32(1)\mathrm{X}10^{19}$ cm^{-3}	$1.04(1)\mathrm{X}10^{18}$ cm^{-3}
p-InSb	$4.00(1)\mathrm{X}10^{19}$ cm^{-3}	$1.366(4)\mathrm{X}10^{18}$ cm^{-3}
Hoffman	$\sim 4.00\mathrm{X}10^{18}$ cm^{-3}	$\sim 6.00\mathrm{X}10^{17}$ cm^{-3}

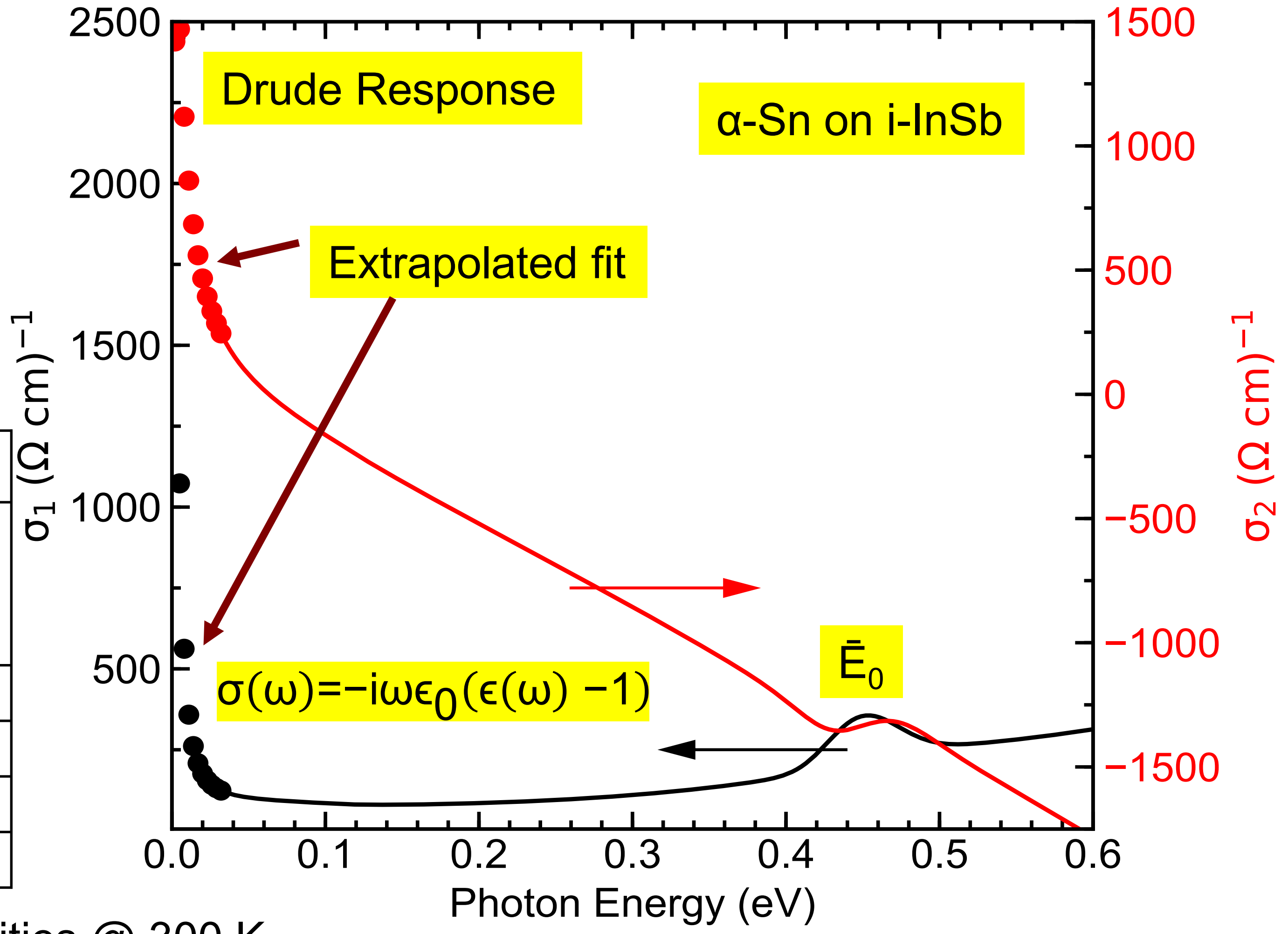

Drude Response

α-Sn on i-InSb

Extrapolated fit

$\bar{E}_0$

$\sigma(\omega)=-i\omega\epsilon_0(\epsilon(\omega)-1)$

➢ Substrate doping has a small effect on carrier densities @ 300 K

C. A. Hoffman, *et al* Phys. Rev. B., **40**, 11693 (1989)

Free Carrier Response

α-Sn optical constants expressed as a sum of electronic transitions and free carriers

$$\varepsilon(\omega) = 1 - \underbrace{\sum_k \frac{\omega_{P,k}^2}{\omega^2 + i\gamma_{D,k}\omega}}_{\text{Drude}} + \underbrace{\sum_j g_j(\omega)}_{\text{electronic}}$$

$$\omega_{u,i}^2 = \frac{n_i e^2}{\epsilon_0 m_i^* m_0}$$

$$\boxed{\mu_i = \frac{e}{m_i^* m_0 \gamma_{D,i}}}$$

- Two Drude terms were used
  - Light and heavy free carriers

Carrier Mobilities		
substrate	heavy hole or L-electrons ($m^* \sim 0.20m_0$)	light hole ($m^* = 0.024m_0$)
i-InSb	19.8(2) cm^2/Vs	1.45(30)X10^4 cm^2/Vs
n-InSb	19.2(1) cm^2/Vs	1.66(31)X10^4 cm^2/Vs
p-InSb	15.2(1) cm^2/Vs	9.52(57)X10^3 cm^2/Vs
Hoffman	~1000 cm^2/Vs	~4.00X10^3 cm^2/Vs

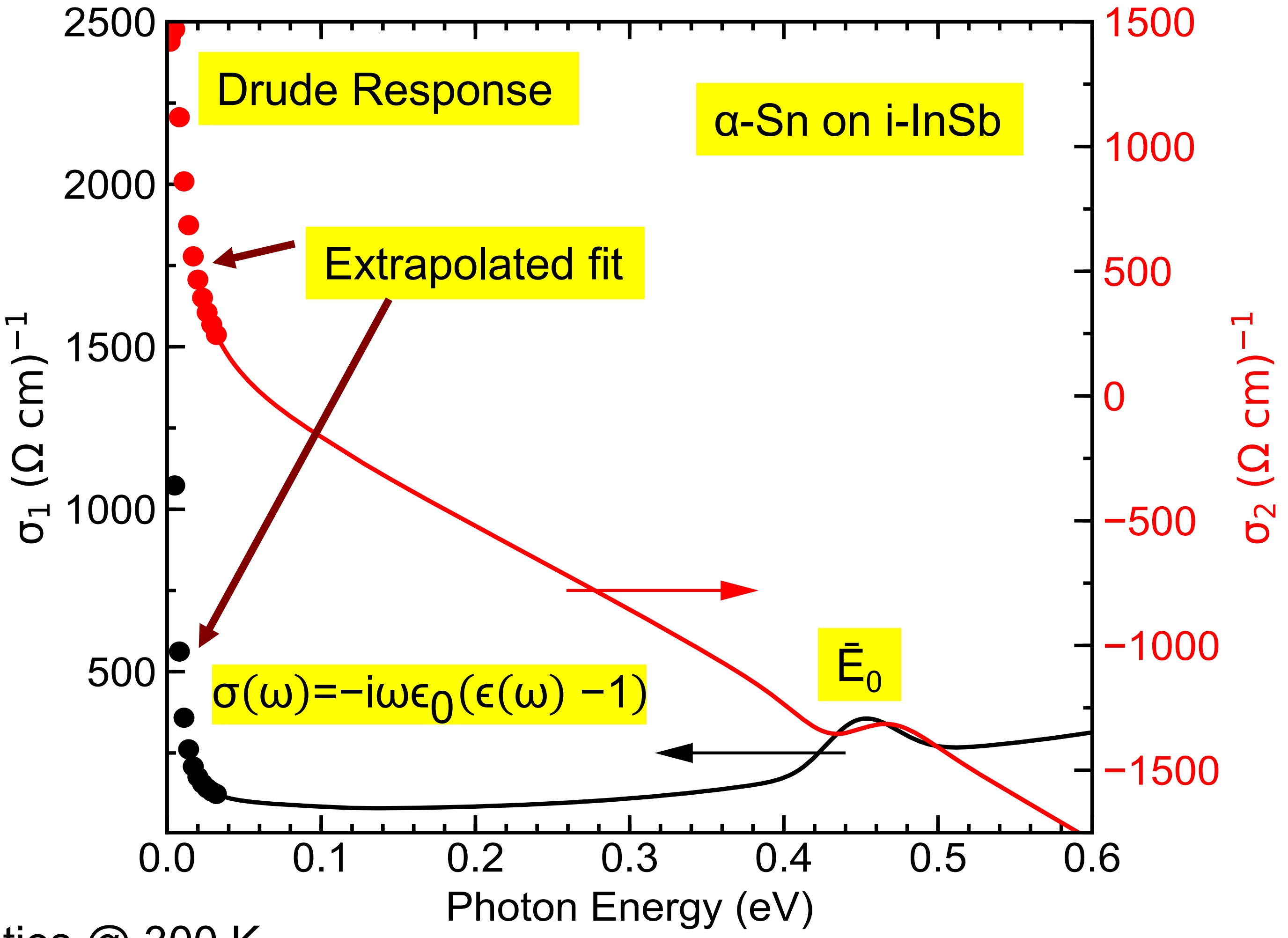

➢ Substrate doping has a small effect on carrier densities @ 300 K

C. A. Hoffman, *et al* Phys. Rev. B., **40**, 11693 (1989)